PHOTON-ASSISTED ELECTRON TUNNELING IN METAL-BARRIER-METAL JUNCTIONS

by

Ravinder K. Jain

Memorandum No. ERL-M522

June 1975

ELECTRONICS RESEARCH LABORATORY

College of Engineering
University of California, Berkeley
94720

ACKNOWLEDGMENTS

I am indebted to Professor T. Ken Gustafson for his guidance and enthusiastic support of this and the rest of my graduate research. I am also grateful to Professor L. M. Falicov for reading this manuscript, and for providing useful suggestions and hearty encouragement. I would also like to thank Professor J. R. Whinnery for his advice and assistance throughout my graduate years.

This work has also derived much from the continual interaction provided by several of my colleagues at Berkeley. These include Jon Heritage, T. R. Ranganath, Sadeg Faris, Shihyuan Wang, Daniel Siu, Tatsuo Izawa and Mike Farrier. Particular thanks go to Tim Ryan and V. T. Rajan who seemed to be always available for critical hints and suggestions,

I would also like to thank Paula Bjork for the excellent typing and Barbara Kerekes for her craftsmanship with the figures.

This research has been possible due to National Science Foundation Grant GK-33939, and National Aeronautics and Space Administrations Grant NGR-05-003-559, and I am grateful for this assistance.

TABLE OF CONTENTS

III. OPTICAL EXCITATION OF ELECTRON TUNNELING CURRENTS IN METAL-BARRIER-METAL JUNCTIONS

A. INTRODUCTION

B. NOTATION AND CONVENTIONS

C. TUNNELING MODEL - PRINCIPAL ASSUMPTIONS

1. Electron excitation due to absorption of light

a. Single electron excitations

b. Collective electron excitations

2. Geometry and transport considerations

3. Potential barrier and transmission probability

4. Miscellaneous details

D. EXPRESSIONS FOR THE TUNNELING CURRENT

1. Single electron excitations, normal incidence

2. Collective electron excitations, oblique incidence

E. EXPERIMENTAL DETAILS AND CONCLUSIONS

1. The source of ultraviolet radiation

2. The metal-barrier-metal structure

3. The experimental set-up

F. CONCLUSIONS

I. INTRODUCTION

Point contact metal-barrier-metal (MBM) junctions have recently been used extensively in mixing experiments[1-3] from submillimeter wavelengths to the infra-red, and in room-temperature detection[4-9] of electromagnetic radiation from the microwave to the visible. While the responsivity of MBM diodes is generally small compared to most other radio-frequency and infrared detectors (except in the negative resistance case observed recently,[9] and under feedback-stabilized conditions[10]), they have the great advantage of a large bandwidth[1,11] and of a response time shorter than that of any other detector yet conceived. Presumably the high speed of response is due to the extremely small RC time[6,7] ($< 10^{-12}$ sec) inherent in the geometry, and the extreme speed[12] ($\sim 10^{-16}$ sec) of the actual tunneling mechanism that is generally believed to be responsible for the detection and other nonlinear[1,2,6-8,13] characteristics up to the visible frequencies.

Previous theoretical analyses of the MBM detector have generally been restricted to photon energies much lower than the work function of the two metals. Except for Lucas and Cutler's analysis,[13] the theoretical approach has been to assume rectification due to the nonlinearity of the tunneling I-V characteristics[6-8], and the main difference in the various results are contained in the theoretical approximations used for the determination of the nonlinear I-V characteristics. With such an approach, the radiation incident upon the junction causes an effective modulation of the Fermi-levels on the two sides of the barrier; and the detected

signal is essentially due to the difference in the number of electrons tunneling in the two directions under the influence of such a modulation. This difference in the electron currents is partly due to the asymmetry of the barrier,[14] caused either by the difference in the work function of the two metals or by an external bias voltage. The exact geometry of the whisker[15] and the absorptivities or densities of states of the metals do not form part of this theoretical model.

The purpose of the present work is to investigate the response of the MBM diode at photon energies that are comparable to or greater than the work functions of the metals used. At these visible and ultra-violet frequencies,[16] direct excitations of the electrons[17] within the two metals by the incident radiation should be important in the evaluation of the tunneling current, as elaborated below.

For single electron excitations,[18] the photon-induced tunneling across the barrier might occur as a direct (one-step) process or an indirect (two-step) process as shown in the schematic energy level diagrams of Fig. 1, where 1 and 2 represent the two metals separated by a trapezoidal barrier. In the indirect or two-step process illustrated in Fig. 1(a), the incident photons excite electrons from initial states like E_o to higher states $E = E_o + \hbar\omega$ in <u>each</u> metal, with subsequent tunneling across the barrier with a much higher transmission probability. For the direct or one-step process shown in Fig. 1(b), the incident photons cause direct tunneling from states like E_o^2 in metal 2, to states E in metal 1 such that $E^1 = E_o^2 + \hbar\omega$. For normal (non-superconducting) metals,

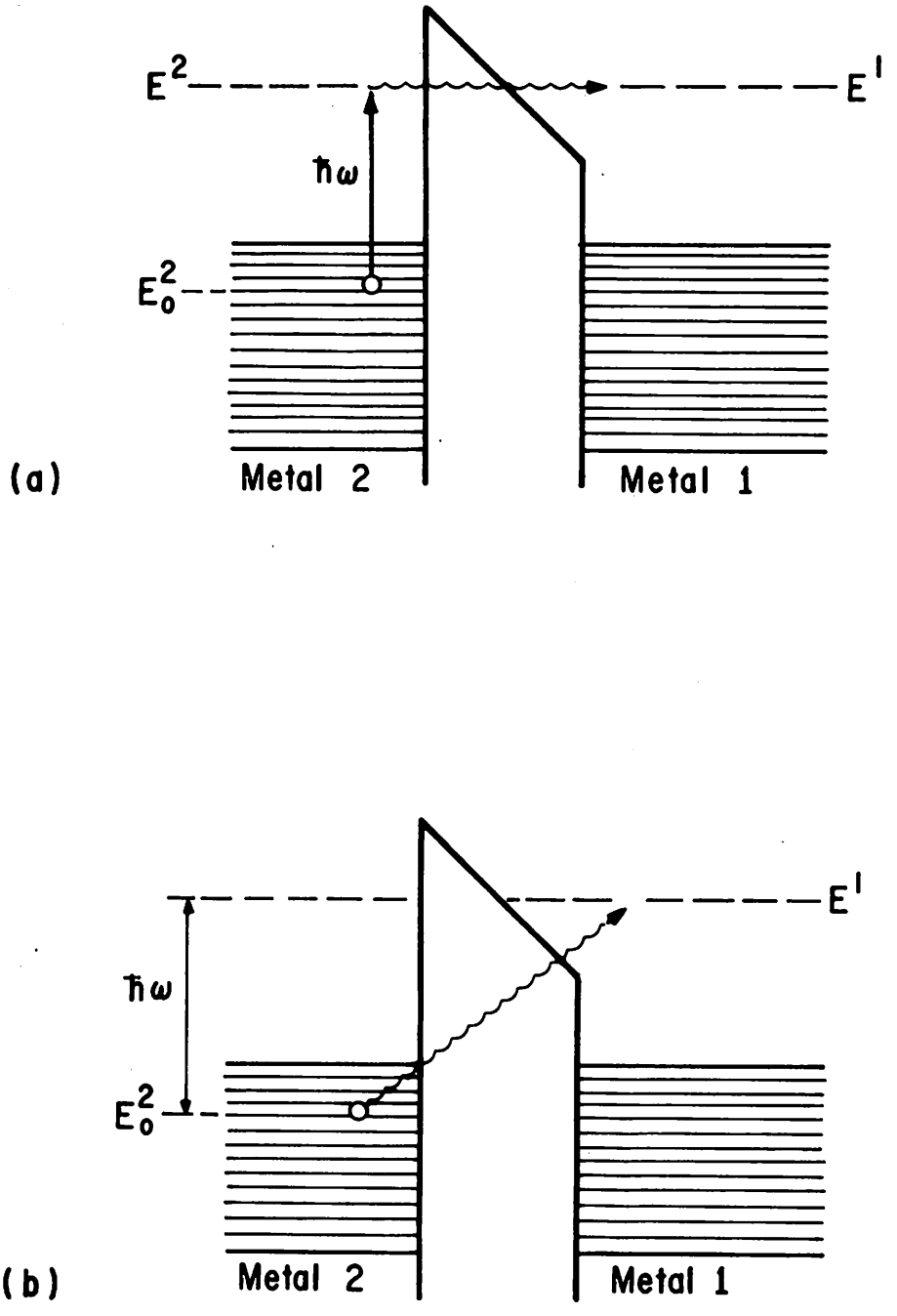

Fig. I-1 : (a) Photon-assisted tunneling via an indirect or two-step process

(b) Direct or one-step photon-assisted tunneling

this contribution should be negligible due to the relative weakness of the corresponding tunneling matrix element.[19]

At this point it might be appropriate to mention that if one considers the two-step process of Fig. 1(a) in terms of the time-resolved optical frequency oscillations of the photo-electrons (and thus also of the absorption and emission) as suggested by Mandel and Meltzer,[20] then one essentially has optical frequency tunneling currents. Assuming that such optical frequency currents experience the same I-V characteristics as dc currents results in the "rectification due to nonlinearities" type of analyses referred to earlier.[13]

The rest of this work is basically organized as follows. In the next section (II), we will discuss the optical properties of metals, with special consideration to the electronic interband transitions and the possibility of exciting collective electron or plasmon modes in appropriately chosen thin films. Besides, reflectivity data of specific metals is examined to ascertain a high-frequency limit for the induction of the "optical voltage" that is intrinsic to the above-mentioned Fermi-level-modulation type of analysis of the MBM detection characteristics. In section III, we give two different approaches (corresponding essentially to the two different electron excitations discussed) for the determination of the photon-assisted tunneling current. Of particular interest is the expected enhancement of this current in a Ag-Al_2O_3-Al structure, due to the excitation of plasmon modes in a thin film of Ag by p-polarized radiation. The final section proposes an experimental set-up for the verification of these resonantly enhanced tunneling currents.

I. References

1. B. Fan, S. M. Faris, T. K. Gustafson, T. Izawa, D. P. Siu and S. Y. Wang, presented at the 1974 International Electron Devices Meeting, Washington, D.C.
2. S. M. Faris and T. K. Gustafson, Appl. Phys. Lett. 25, 544 (1974).
3. E. Sakuma and K. M. Evenson, IEEE J. Quantum Electron. QE-10, 599 (1974).
4. T. K. Gustafson, R. V. Schmidt and J. R. Perucca, Appl. Phys. Lett. 24, 620 (1974).
5. T. G. Small, G. M. Elchinger, A. Javan, A. Sanchez, F. J. Bachner and D. L. Smythe, Appl. Phys. Lett. 24, 275 (1974).
6. S. M. Faris, T. K. Gustafson and J. C. Wiesner, IEEE J. Quantum Electron. QE-9, 737 (1973).
7. S. P. Kwok, G. I. Haddad and G. Lobov, J. Appl. Phys. 42, 554 (1971).
8. (a) S. I. Green, Journ. Appl. Phys. 42, 1166 (1971).
   (b) S. I. Green, P. D. Coleman and J. R. Baird, presented at the 1970 Symposium on Submm. Waves, Brooklyn, N. Y.
9. S. Y. Wang, S. M. Faris, D. P. Siu, R. K. Jain and T. K. Gustafson, Appl. Phys. Lett. 25, 493 (1974).
10. When high impedance (10K and greater) diodes are stabilized by means of an electronic feedback loop, signals as large as 20 mV/100 mW of radiated power have been measured: H. Gee and R. K. Jain, unpublished result.
11. A. Sanchez, S. K. Singh and A. Javan, Appl. Phys. Lett., 21, 240 (1972).

I. References

12. T. E. Hartman, J. Appl. Phys. 33, 3427 (1962).

13. Recently, Lucas and Cutler [Solid State Comm. 13, 361 (1973)] have proposed a thermal field emission (TFE) analysis in which the non-linearity responsible for the detection of infrared laser light is assumed to be due to the extreme directionality of the emission process in contrast to the "weak" non-linearity of the tunneling I-V characteristic.

14. The difference in the Fermi energies of the two metals also contributes to differences in these currents. Also, if one tries to neutralize the barrier asymmetry with an external bias $V_b = \Delta\phi/e$.g., one changes the kinetic energies of the electrons on either side, causing preferential tunneling.

15. In the TFE explanation mentioned above (Ref. 13), this asymmetry in the geometry is considered crucial for rectification, electron emission (tunneling) being assumed to occur only from the conical tip to the base plate thus resulting in an extremely nonlinear I-V characteristic.

16. Clearly since $\omega >> kT/\hbar$, the quantum character of the radiation should become important at these higher frequencies.

17. These may be collective or single electron excitations. The collective excitations may generally be assumed to decay into single electron excitations before tunneling, or to cause an effective perturbation of the barrier similar to a Fermi-level modulation.

18. The effect of collective excitations is to introduce a sharp resonance in the frequency dependence of the tunneling characteristics. This resonant enhancement is discussed in detail in Section III.

I. References

19. Note that in superconducting metals with energy gap Δ_i, the corresponding matrix element is important for $\hbar\omega \simeq (\Delta_1 + \Delta_2)/2$, primarily due to the extremely large density of states at both the initial and final energies. However, even in superconductors these matrix elements are negligible at optical frequencies.

20. L. Mandel and D. Meltzer, Phys. Rev. 188, 198 (1969).

II. OPTICAL PROPERTIES OF METALS

A. INTRODUCTION

As is well known,[1] the optical properties of metals can be completely specified by the two propagation constants: the index of refraction n, and the extinction coefficient k (these are often lumped together to form the complex refractive index $\mathcal{N} \equiv n+ik$); and all the other important optical properties[2] can be easily expressed in terms of these two constants. For instance, the intensity absorption coefficient α at frequency ω is given by[3]

$$\alpha(\omega) = \frac{2k(\omega)\omega}{c} \tag{1}$$

and the intensity reflection coefficient R at normal incidence is

$$R(\omega) = |r(\omega)|^2 = \frac{\{n(\omega)-1\}^2 + k^2(\omega)}{\{n(\omega)+1\}^2 + k^2(\omega)} \tag{2}$$

where $r(\omega) = \frac{\mathcal{N}-1}{\mathcal{N}+1}$ is the complex reflection coefficient for the electric field.

For many phenomena, the complex refractive index $\mathcal{N}$ is the simplest way of describing a solid.[4] However, from the theoretical point of view, the frequency and wave-number (q) dependent complex dielectric constant (or its inverse ε^{-1}, the dielectric response function) represents the most natural way of specifying the optical properties of a solid, since it lends physical insight to the elementary excitations caused in the solid by an external disturbance. Thus for instance, $\varepsilon(q,\omega)$ describes almost directly the excitations produced by

electromagnetic waves (transverse disturbance), and also those produced by fast electrons (longitudinal disturbance). Although there are generally two dielectric functions,[5] ε_T and ε_L respectively, describing the response of a cubic crystal or an isotropic solid to these two different types of disturbances, in the present context of the long-wavelength limit ($q \to 0$ for $\hbar\omega \lesssim 10$ eV)[6] these reduce to the same function $\varepsilon(0,\omega)$ denoted here by $\varepsilon(\omega)$ for brevity.

This complex dielectric constant $\varepsilon(\omega) = \varepsilon_1(\omega) + i\,\varepsilon_2(\omega)$ must obviously be compatible with the phenomenological Maxwell's equations, in which the material properties[7] are typically described by a real dielectric constant $\varepsilon_1(\omega)$ and a real conductivity $\sigma(\omega)$. For this compatibility we require $\varepsilon_2(\omega) = \frac{4\pi\sigma(\omega)}{\omega}$ and that $\varepsilon(\omega)$ and $\mathcal{N}(\omega)$ be related by $\mathcal{N}(\omega) = \sqrt{\varepsilon}(\omega)$. Thus one has[8]

$$\varepsilon_1(\omega) = n^2(\omega) - k^2(\omega) \tag{3}$$

$$\text{and} \quad \varepsilon_2(\omega) = \frac{4\pi\sigma(\omega)}{\omega} = 2n(\omega)\,k(\omega) = \frac{\alpha(\omega)n(\omega)c}{\omega} \tag{4}$$

Using $\nu = \frac{\omega}{2\pi}$ and $\lambda = \frac{c}{n\nu}$, Eq.(4) yields the often-used expressions for absorptivity and conductivity, viz.

$$\alpha(\lambda) = 4\pi k/\lambda \tag{5a}$$

$$\sigma(\nu) = n(\nu)k(\nu)\nu \tag{5b}$$

B. SINGLE ELECTRON EXCITATIONS AND DERIVATIONS FOR $\varepsilon(\omega)$:

Several expressions have been derived for $\varepsilon(\omega)$, using both classical[9-11] and quantum mechanical[11-16] approaches. Two of the most useful results are the classical expressions derived for metals and insulators respectively by Drude[9] and Lorentz[10], under the assumption of electrons as completely free particles (Drude), or as particles bound to ionic sites as harmonic oscillators (Lorentz). Thus, neglecting local field corrections[17] we have

$$\varepsilon^f(\omega) = 1 - \frac{\omega_p^2}{\omega^2+i\omega\gamma} = 1 - \frac{\omega_p^2}{\omega^2+i\omega/\tau} \tag{6}$$

and

$$\varepsilon^b(\omega) = 1+\sum_\ell \frac{\omega_{p\ell}^2}{\omega_\ell^2-\omega^2+i\gamma_\ell\omega} \tag{7}$$

in the Drude and Lorentz pictures respectively.[18] In the above expressions, ω_p is called the plasma frequency, and is given by

$\omega_p^2 = \frac{4\pi n_e e^2}{m_e}$, where n_e is the density of (free) electrons

e is the electronic charge

m_e is the mass of a free electron.*

γ, the free electron damping rate or the mean collisional frequency of the electrons.

$\tau = 1/\gamma$ is the mean time between collisions,

ω_ℓ are the natural frequencies of the harmonic oscillators,

*When the distinction between free electron mass and effective mass is not of concern, the subscript e will be dropped for simplicity.

γ_ℓ are the damping rates of these oscillations,

$\omega_{p\ell}^2 = \frac{4\pi n_\ell e^2}{m_e}$, where n_ℓ represents the number of oscillators of characteristic frequency ω_ℓ. Thus, $\omega_{p\ell}^2 = \omega_{pt}^2 f_\ell$, where f_ℓ represents the "oscillator strength" of the ω_ℓ resonance. Clearly $\sum_{\ell=0} f_\ell = 1$, since $\sum_{\ell=0} n_\ell$ = total number of electrons, n_{et}.

Direct quantum mechanical analogs[11] to the above classical pictures exist for systems with perfect "free electron" parabolic energy bands or for systems of isolated atoms with discrete energy levels. Thus, an expression identical to Eq.(7) is obtained for $\varepsilon(\omega)$ in the quantum mechanical picture for a system of isolated atoms. Here ω_ℓ are the allowed electronic transition frequencies, γ_ℓ are the linewidths of these transitions and f_ℓ the quantum-mechanical oscillator strengths of these transitions.

For a solid, more sophisticated approaches must be used.[12-16] For instance, Ehrenreich[13] has derived a relatively rigorous expression for $\varepsilon(\omega)$ using a form of electromagnetic theory for electrons in the band approximation. This involves averaging microscopic equations over regions large compared to the interparticle separation, but small compared to λ, the wavelength of the disturbance. The averaging procedure includes a physical distinction between the local field producing charge polarization and the macroscopic field. The microscopic description involves beginning with a Hamiltonian for an n-body system, and determining the expectation values for local charge and current distributions in the interaction picture from which the averaged complex susceptibility, or the "response function"

is eventually determined by means of the random phase approximation.[13,15] When the final expression for $\varepsilon(\omega)$ is written in a way[13,19] that separates intraband (corresponding to "free" electrons if bands are parabolic) and interband ("bound" electron) terms, we have

$$\varepsilon(\omega) = 1 - \frac{\omega_{pc}^2}{\omega^2 + i\,\omega\gamma_c} + \frac{e^2}{\pi^2 m_e}\int d^3\bar{k} \sum_{\ell,\ell'} \frac{f_{\ell\ell'}(\bar{k})}{[\omega_{\ell\ell'}^2 - (\omega + i\gamma_{\ell\ell'})^2]} \qquad (8)$$

whose terms show strong resemblance to the free electron and bound electron terms obtained in the simple Drude and Lorentz classical pictures. In the above equation

$$\omega_{pc}^2 = \frac{4\pi n_c e^2}{m_a} \qquad (9a)$$

is the square of the conduction band plasma frequency, n_c is the conduction electron density, and

$$m_a^{-1} = (4\pi^3 n_c \hbar^2)^{-1} \int d^3k \left(\frac{1}{3}\right) \nabla_k^2 E_c(k) \qquad (9b)$$

is the average inverse effective mass of the conduction electrons, the so-called "optical" mass defined by Cohen.[20] γ_c is the mean collisional rate of the conduction band electrons ($\gamma_c = 1/\tau_c$, the relaxation time). Further, ℓ and ℓ' are band indices, $\gamma_{\ell\ell'} = 1/\tau_{\ell\ell'}$, where $\tau_{\ell\ell'}$ is the average interband relaxation time between the distinct states of transition frequencies $\omega_{\ell\ell'}$. $f_{\ell\ell'}(\bar{k})$ are the transition

matrix elements or oscillator strengths for states between the two bands, and are given by[21]

$$f_{\ell\ell'}(\bar{k}) = \frac{2}{\hbar\, \omega_{\ell\ell'}(\bar{k}) m_e} \left| P_{\ell\ell'}(k) \right|^2 \tag{10}$$

where $P_{\ell\ell'}(\bar{k})$ is the momentum matrix element.

Thus it is seen that for a solid, one can generally write

$$\varepsilon(\omega) = 1 - \delta\varepsilon^f + \delta\varepsilon^b = \varepsilon^f + \delta\varepsilon^b = \varepsilon^b - \delta\varepsilon^f \tag{11}$$

where ε^f and ε^b are "free-electron" and "bound-electron" contributions which are essentially modified forms of the classical equations [Eq.(6) and (7)], and correspond in effect to intraband and interband electron behavior. Thus for ideal "free electron" behavior, as occurs at infrared and lower frequencies for some metals: $\delta\varepsilon^b = 0$, and for an ideal insulator: $\delta\varepsilon^f = 0$.

However, $\delta\varepsilon^b$ contributions occur in all solids and even the simplified expressions for $\delta\varepsilon^b$ in Eq. (8) must usually be modified. For instance when a crystal, such as one of the noble metals,[19] contains a set of partly filled conduction bands (c), a lower completely filled d-band (d) as well as filled core states and empty excited bands, $\delta\varepsilon^b$ may be written at 0^oK as

$$\delta\epsilon^b = \frac{e^2}{\pi^2 m_e} \left[\sum_{l \le d} \int_{k>k_F} d^3k \, f_{cl}(k) g_{lc} \right.$$

$$\left. + \sum_{l>c} \int_{k<k_F} d^3k \, f_{lc}(k) g_{lc} + \sum_{\substack{l \le d, \\ l'>c}} \int d^3k \, f_{l'l}(\bar{k}) \, g_{l'l} \right] \quad (12)$$

Here k_F denotes the wave number at the Fermi surface and $g_{\ell\ell'} = [\omega_{\ell\ell'}^2 - (\omega + i\gamma_{\ell\ell'})^2]$, as in Eq. (8). The form of this equation indicates that the interband terms associated with the conduction electrons are part of the bound-electron contribution to the dielectric constant. It should also be noted that $\delta\epsilon^b(\omega)$ satisfies the Kramers-Kronig relations[38] since both $\epsilon(\omega)$ and $\epsilon^f(\omega)$ do.

B.1. INTRABAND BEHAVIOR

B.1.a. Free electron picture and range of validity

For most metals $\omega_{pc} >> \gamma_c$ and interband behavior is negligible below a certain critical frequency ω_i, which is easily identified by a sharp increase in the absorption ϵ_2 or the optical conductivity σ. Below ω_i, ϵ_2 shows a monotonic decrease corresponding to $\epsilon_2^f \simeq \frac{\omega_{pc}^2 \gamma_c}{\omega^3}$, as expected for the case when $\delta\epsilon^b \simeq 0$ and $\omega_{pc} >> \gamma_c$. Figure 1 shows the behavior of ϵ_2^b for the noble metals, as obtained from Nillson[22], clearly illustrating that $\hbar\omega_i \approx$ 2eV for Cu and Au, and is approximately 4eV for Ag. Thus, for the noble metals at frequencies below 2eV, the modified Drude equation:

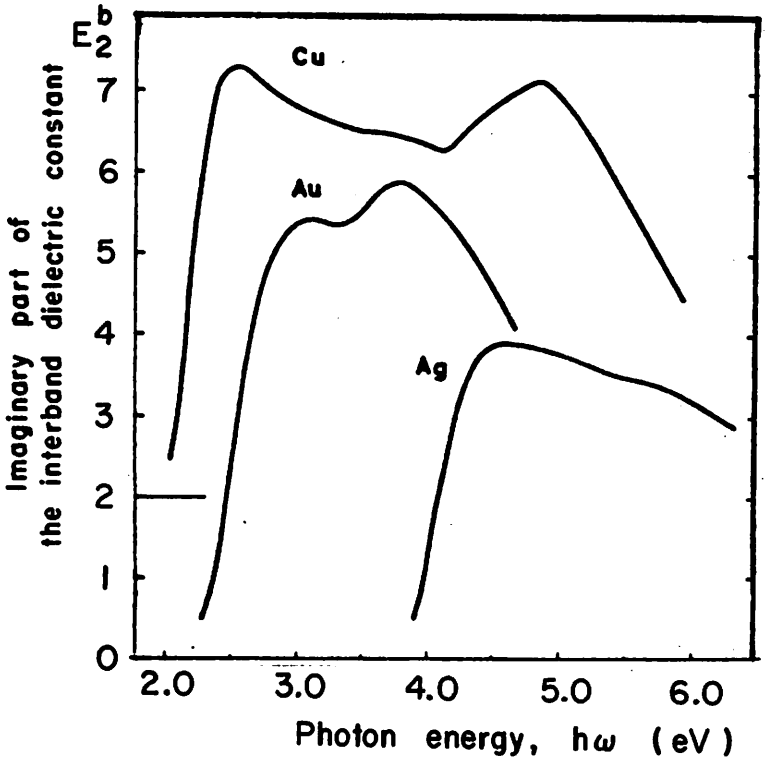

Fig. II-1 : The imaginary part of the dielectric constant for the noble metals Cu, Ag and Au. Note that the intraband part has been subtracted and the Cu-curve has been shifted two units upwards for clarity (Reprinted from Nillson, Ref. 22)

$$\varepsilon^f(\omega) = 1 - \frac{\omega_{pc}^2}{\omega^2+i\omega\gamma_c}$$

is very accurately valid.[23] Thus, the Drude theory is very useful for studying the low-frequency behavior of these metals.

For simplicity, consider the case where the plasma frequency $\omega_{pc} \triangleq \omega_p$ lies well below ω_i (as is true for the alkali metals). Thus, we have a nearly-free electron metal in which $\delta\varepsilon^b$ may be neglected up to frequencies well above ω_p. Then, dropping the conduction band subscript c in the above equation for simplicity, we have the usual Drude equations:

$$\varepsilon^f(\omega) = 1 - \frac{\omega_p^2}{\omega(\omega+i\gamma)} = 1 - \frac{\omega_p^2}{\omega(\omega+i/\tau)} \tag{13a}$$

yielding

$$\varepsilon_1^f(\omega) = n^2-k^2 = 1 - \frac{\omega_p^2\tau^2}{(1+\omega^2\tau^2)} . \tag{13b}$$

$$\varepsilon_2^f(\omega) = 2nk = \frac{\omega_p^2}{\omega\tau(\omega^2+1/\tau^2)} \tag{13c}$$

and[24]

$$\sigma(\omega) = \frac{\omega_p^2}{4\pi\ \tau\ (\omega^2+1/\tau^2)} . \tag{14}$$

Also, the penetration depth $\delta = \frac{1}{\alpha} = \frac{c}{2\omega k}$ (provided that it is much longer than the mean free path of the electrons $L \simeq v_F\tau$), is given by[23]

$$\delta = \frac{c}{\omega\sqrt{2}}\left[\left(1 - \frac{2(\omega_p\tau)^2}{1+(\omega\tau)^2} + \frac{\omega_p^4\tau^2}{\omega^2[1+(\omega\tau)^2]}\right)^{1/2} - 1 + \frac{(\omega_p\tau)^2}{1+(\omega\tau)^2}\right]^{-1/2} \quad (15)$$

Since $\omega_p >> 1/\tau$, [ω_p is typically around 10 eV (2.4×10^{15}Hz) and $1/\tau$ is typically of the order of 10^{13} Hz], the Drude equations can be considered separately for three frequency regions:

(i) $0 << \omega^2 << 1/\tau^2$, (Hagen -Rubens or "absorbing & reflecting" region)

(ii) $1/\tau^2 << \omega^2 << \omega_p^2$ (Relaxation or "strongly reflecting" region)

(iii) $\omega^2 >> \omega_p^2$ (Ultra-violet transparency region).

The behavior of the optical constants in each of the above three regions is derived below and shown schematically in Fig. 2. We will shortly examine how the inclusion of $\delta\varepsilon^b$ affects this qualitative behavior.

(i) $0 << \omega^2 << 1/\tau^2$ (Hagen-Rubens region):

In this region, $\varepsilon_1^f(\omega) \simeq 1 - \omega_p^2\tau^2 < 0$ and $\varepsilon_2^f(\omega) \simeq \frac{\omega_p^2\tau}{\omega}$.

Thus, ε_1^f is large and negative,

and ε_2^f is positive but <u>much</u> larger in magnitude than ε_1^f

since $|\frac{\omega_p^2\tau}{\omega}| >> |\omega_p^2\tau^2| >> 1$

Thus, $\varepsilon^f(\omega) \simeq i\,\varepsilon_2^f(\omega) \simeq i\left(\frac{\omega_p^2\tau}{\omega}\right) \simeq (n^2-k^2) + i(2nk)$

$\Rightarrow n^2 \simeq k^2 \simeq \frac{\omega_p^2\tau}{2\omega} >> 1$

---

* Note that the penetration depth given here refers to the light intensity. This is obviously half as small as the field penetration depth, which is usually referred to in the classical skin depth formula.

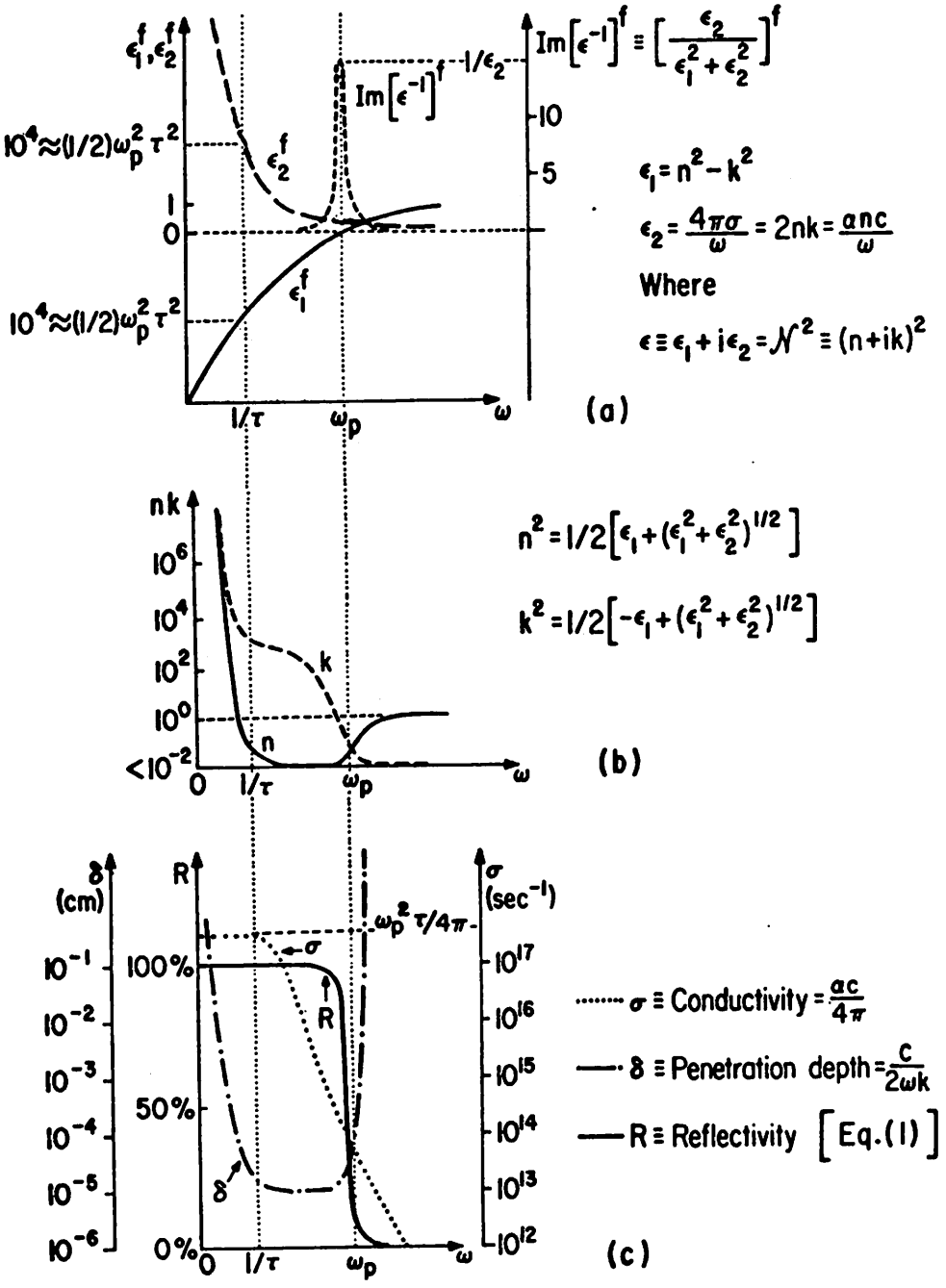

Fig. II-2 : Schematic behavior of the frequency dependence of the optical properties of a free-electron (Drude) metal with $\omega_p\tau = 100$: (a) Dielectric constants; (b) Propagation constants; (c) Usual experimental constants (Absorption α ∼ 1/δ) coefficient

Thus both n and k are very large, and so the reflectivity $R(\omega)$ must be very high. Thus from Eq. (2),

$$R(\omega) = \frac{1 - 2n/(n^2+k^2+1)}{1 + 2n/(n^2+k^2+1)}$$

$$\approx 1 - 4n/(n^2+k^2) \approx 1 - 2/n = 1 - 2\left(\frac{2\omega}{\omega_p^2\tau}\right)^{1/2} ,$$

yielding the celebrated Hagen -Rubens relationship.[25]

$R(\omega) = 1 - 2\left(\frac{\omega}{2\pi\sigma_o}\right)^{1/2}$, where σ_o is the d.c. conductivity. Thus, the metal is <u>both strongly reflecting and strongly absorbing</u>, and the absorption coefficient $\alpha(\omega) \approx \frac{2\omega_p}{c}\left(\frac{\omega\tau}{2}\right)^{1/2}$ i.e. it varies as $\omega^{1/2}$. Also, it may be noted that the skin depth $\delta = \frac{c}{2\omega_p}\left(\frac{2}{\omega\tau}\right)^{1/2}$ varies as $\omega^{-1/2}$.

(ii) <u>$1/\tau^2 << \omega^2 << \omega_p^2$ (Relaxation region):</u>

Here we have $\varepsilon_1^f(\omega) \approx 1 - \frac{\omega_p^2}{\omega^2} \approx -\frac{\omega_p^2}{\omega^2} < 0$

and $\varepsilon_2^f(\omega) \approx \frac{\omega_p^2}{\omega^3\tau}$, which is the characteristic free-electron ω^{-3} dependence often noted at frequencies below the onset of interband behavior.[22] Also, since $|\varepsilon_2^f| \Big/ |\varepsilon_1^f| \approx 1/\omega\tau << 1$, we have $n(\omega) \approx \omega_p/2\omega^2\tau << 1$ and $k(\omega) \approx \left[(\omega_p/\omega)^2 - 1\right]^{1/2} \approx (\omega_p/\omega) >> 1$. Thus, $R(\omega) \approx 1 - 2/\omega_p\tau$; and $\alpha(\omega) = 2\omega_p/c$.

We note that the metal is still strongly reflecting; however, this time the high reflectivity is due to the extremely small value of $n(\omega)$. Also $\sigma(\omega) \approx \frac{\omega_p^2}{4\pi\omega^2\tau}$ falls rapidly with increasing frequency $(1/\omega^2)$ and is interestingly inversely proportional to τ or the d.c. conductivity σ_o. Thus the reflectivity is very high and independent of frequency. Likewise, the total fractional power absorbed, $A = 1-R \approx \frac{2}{\omega_p\tau}$ is very small and independent of frequency. It can also be seen that the penetration depth $\delta \approx c/2\omega_p$ is small and independent of frequency. For most metals, $\omega_p \approx 10.0$ eV, yielding δ of the order of 600 Å. Thus for Al, $\omega_p \sim 15\text{eV} \Rightarrow \delta \approx 400$ Å.

(iii) $\omega^2 >> \omega_p^2$ (Transparent region):

Here we have $\varepsilon_1^f(\omega) = 1 - \left(\frac{\omega_p}{\omega}\right)^2 \approx 1$

and $\varepsilon_2^f \approx \frac{\omega_p^2}{\omega^3\tau} << 1$

Thus, obviously ε_1^f is positive and ε_2^f negligible.

$$\therefore\ n \approx \sqrt{\varepsilon_1} \approx \left[1-(\omega_p/\omega)^2\right]^{1/2} \approx 1$$

and, $k \approx \omega_p^2/2\omega^3\tau \approx 0$.

Thus both the reflection and the absorption coefficient are very low, with $\alpha(\omega) \approx \frac{\omega_p^2}{\omega^2\tau c}$. The penetration depth, $\delta \approx \frac{\omega^2\tau c}{\omega_p^2}$ increases with

ω, implying that the medium becomes increasingly transparent with an increase in frequency. Also, $\sigma(\omega) \approx \omega_p^2/4\pi\omega^2\tau$, exactly as in (ii).

Figure 2 displays schematically the above-mentioned characteristics of a Drude metal (assuming $\omega_p\tau = 100$) in a composite plot of all three spectral regions. Also plotted in Fig. 2 is the quantity $\mathrm{Im}[\varepsilon^{-1}]$. This important quantity, called the "energy loss function", is proportional to the spectral energy loss experienced by fast electrons (or other charged particles) traversing the metal.[13,42] The sharp maximum seen at ω_p is indicative of an efficient transfer of energy at this frequency to longitudinal modes of collective electron oscillations. These collective excitations, called plasmons, will be discussed again in a subsequent section.

With appropriate assumptions on the averaged values of τ (for instance, neglecting its anisotropy over the Fermi surface) and on the interpretation of ω_p, the above Drude picture has been experimentally shown to be fairly accurate for most of the alkali metals, for Al, and in the infrared region for the noble metals (Ag, Au and Cu). Thus for instance, plots of ε_1^f and ε_2^f/λ versus λ^2 for the relaxation region should be linear: $\varepsilon_2^f/\lambda = A\lambda^2$, where $A = \dfrac{\omega_p^2}{\tau 8\pi^3 c^3}$. Such plots[29] for Au, Ag and Cu in the region $1\mu \lesssim \lambda \lesssim 2\mu$ are shown in Fig. 3. Except for the small intercept, which is usually attributed to electron-electron interactions,[23] the data indicates the strong validity* of the Drude picture for the noble metals. Also the value of τ deduced from such low-temperature measurements[26] is typically around 10^{-12} sec and larger, although for Au at room temperature, τ is of the order of 10^{-14} sec. (Note that we have neglected discussions of the anisotropy in the measurement of τ, which occurs in practice).

* This data essentially helps ascertain the upper limit for the frequency range at which the Drude picture is still valid.

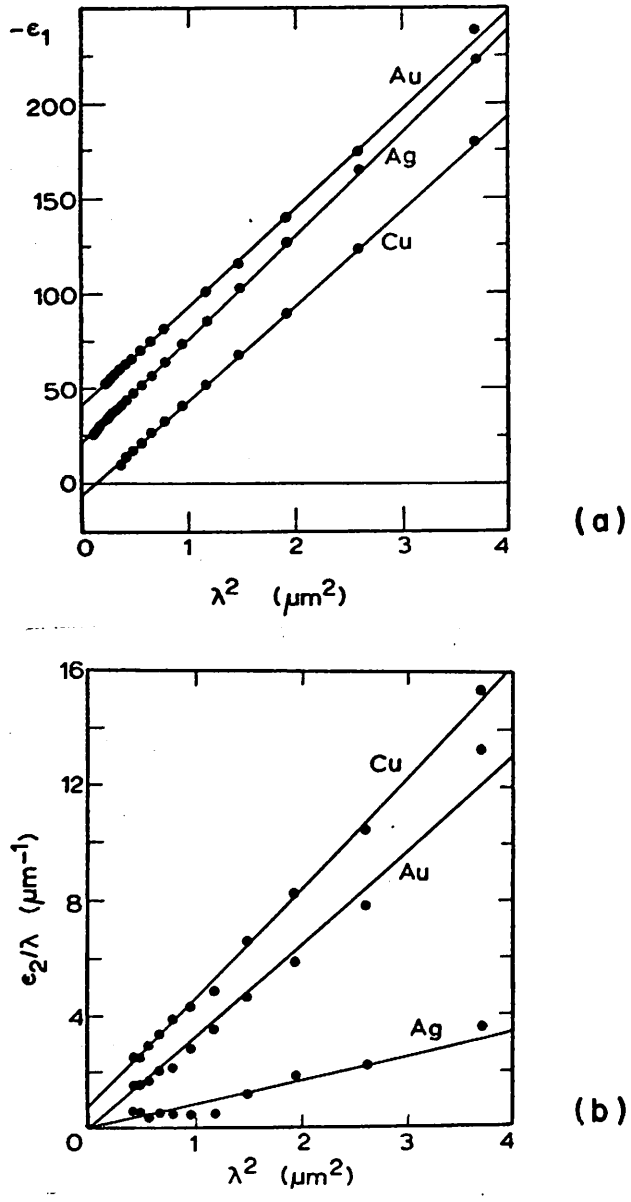

Fig. II-3: Plot of the dielectric constants (Reprinted from Ref. 29) of the noble metals (Cu, Ag, Au) versus the square of the wavelength for the region $1\mu \lesssim \lambda \lesssim 2\mu$ indicating the validity of the nearly free-electron picture in these regions: (a) $-\varepsilon_1$ vs. λ^2 ; (b) ε_2/λ vs. λ^2.

A simpler (though not as rigorous) experimental method for determining the relative validity of the free electron model and the frequency range of this validity is the examination of the reflectance spectrum. Assuming carefully polished clean surfaces, the free electron model predicts reflection coefficients $R(\omega)$ higher than 99% for $\omega << \omega_p$, and the effect of introducing a small $\delta\varepsilon^b$ in the Drude Eqs. (13) and (14) is easily seen to result in a relatively sharp drop in the reflectivity.* Thus a drop in $R(\omega)$ usually determines the practical upper limit of validity of the Drude model. Reflectivity data[19,27-31] for several metals is given in Fig. 4. Neglecting details in structure, one can tabulate the values of ω_i from this data. These are shown in Table 1. Also one should note that the high reflectivity (> 99%) of the noble metals and Al indicates the greater accuracy of the free electron picture for these metals. Our interest in determining the region of validity of the free-electron model is partly to specify the spectral region over which these metals display the conventional (low-frequency) metallic behavior, as evidenced by the induction of oscillatory surface currents and consequent antenna properties. The presence of high reflectivity is generally consistent with the notion of setting up surface currents and subsequent re-radiation at the appropriate frequency.

B.1.b. Anomalous skin effect

When the mean free path of the electrons L is not small[32] in comparison with either the penetration depth δ or the wavelengths in the metal, then some of the above-mentioned considerations are only weakly valid.[33,34] In this case, the current density at any

* This is discussed in a little more detail in section B.2.a.

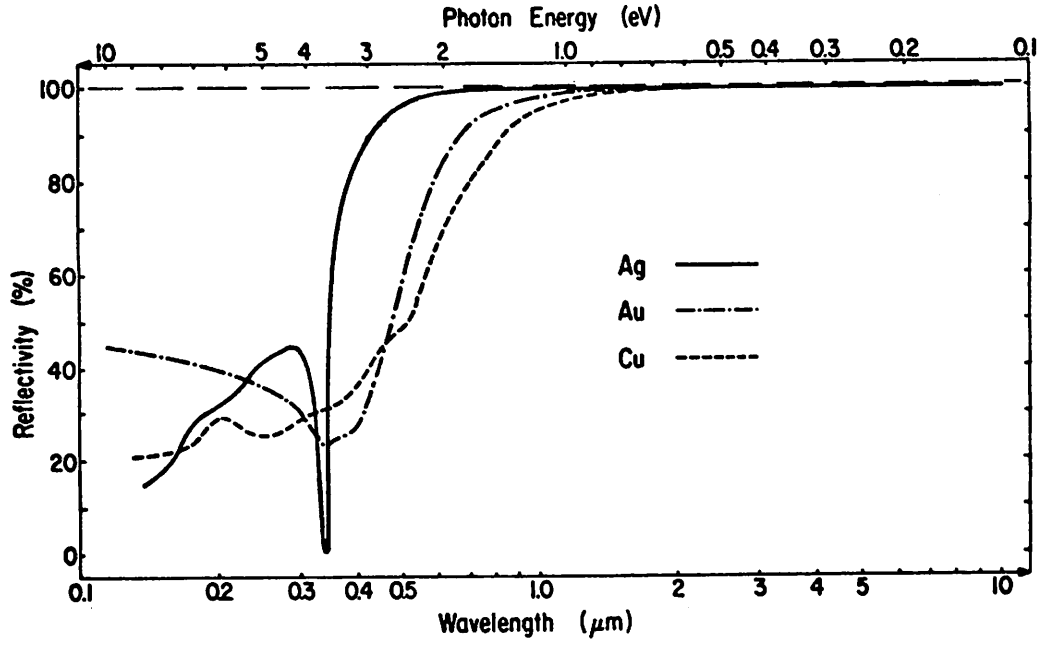

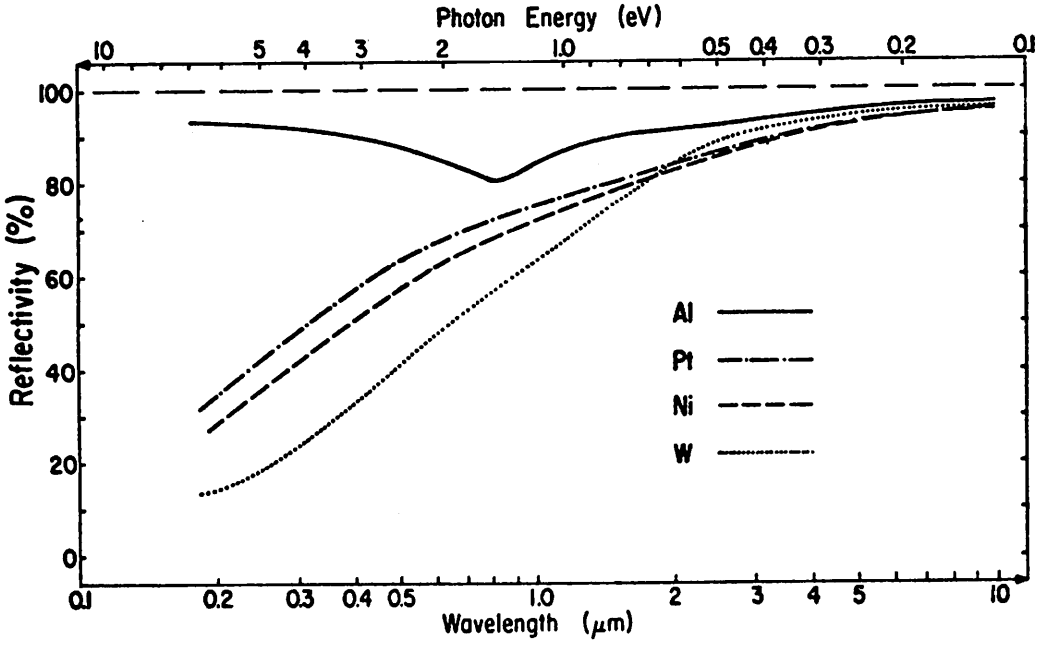

Fig. II-4: Intensity reflectance spectrum at normal incidence for several metals:

(a) The noble metals (from Ref. 27 to 29)
(b) Aℓ, Pt, Ni, W (from Ref. 30 and 31)

TABLE 1

METAL	$\hbar\omega_i$	λ_i, μ	$\tau_{300^oK,Sec}$*	$\tau_{4^oK,Sec}$††
Ag	3.85eV	0.33μ	$\sim 3\times10^{-14}$	-
Aℓ	<1•6eV>**	<0•78μ>**	-	-
Au	2.45eV	0.5μ	$\sim 9.3\times10^{-15}$	-
Cu	2.08eV	0.6μ	$\sim 7\times10^{-15}$	$\sim 7\times10^{-10}$
Ni	(~0.15)†	(~8μ)†	-	-
Pt	(~0.2)†	(~6μ)†	-	-
W	(~0.31)†	(~4μ)†	-	-

† Only weakly free electron metal, $R_{|max} \sim 95\%$

* From Ref. 29 (Johnson and Christy)

†† Estimated from data in Ref. 17 (Kittel)

** Weak interband absorption peak

point is determined not only by the electric field at that point but also by the motion of electrons which arrive there from other places at a distance greater than δ but less than or comparable to the mean free path. Thus the ordinary concept of conductivity, which implies an instantaneous relationship between induced current and the total electric field is no longer valid. Since a fewer number of electrons interact with the field one effectively has a reduction in both the conductivity and the penetration depth. This causes a reduction in reflectivity and an increase in the absorptivity A = 1-R. Besides the proximity of the surface in these small δ conditions typically causes a further increase in the absorptivity due to the scattering of the electrons at the surface. The increase in the absorptivity due to the anomalous skin effect over that of the classical Hagens-Rubens absorptivity A_{H-R} is given by the factor[33]

$$\frac{A_{anom}}{A_{H-R}} \simeq 1 + \frac{\sqrt{3}}{4} \frac{\tau v_F}{c} \sqrt{\frac{3\pi\mu\, n_e e^2}{m^*}}$$

where m^* is the effective mass of the electrons, and it has been assumed that the reflection of electrons at the surface is diffuse. For noble metals in the near infra-red, this ratio is only slightly larger than unity at room temperature, although it may be as high as 10^3 at liquid He temperatures. Since we are presently concerned only with room temperature behavior, the anomalous skin effect is not important for the rest of our discussion. In particular

for Ag up to ultra-violet wavelengths of 0.3 μ, the absorption at room temperature is described first by the relaxation region [$v_F/\omega << L << \delta$] and at higher frequencies by interband absorption (See Table 1). However, at much lower temperatures, the free electron (interband) absorption would have to be described by the extreme anomalous skin effect[34] [$v_F/\omega << \delta << L$].

B.2. Interband Behavior

B.2.a. General features. Let us first examine how $\delta\varepsilon^b$ modifies the behavior of the optical constants expected from the Drude picture. In particular it is interesting to consider why a low frequency interband absorption usually causes a decrease in reflectivity, whereas at higher frequencies, interband transitions are often accompanied by an increase in reflectivity.

The onset of interband absorption ω_i usually occurs in the relaxation region (i.e. $1/\tau < \omega_i < \omega_p$). For this region $n \simeq 0$ in the Drude picture, which accounts for the high reflectivity ($R \simeq 1$), as can be seen from Eq. (1). Also at such frequencies $\varepsilon_2^f \gtrsim 0$, and $\varepsilon_1^f \lesssim 0$, and $|\varepsilon_2^f| << |\varepsilon_1^f|$ in the Drude picture.

Since the onset of interband behavior is physically associated with transitions (usually direct/vertical) from the Fermi surface (F.S.) to the next higher band, or from a lower lying band to the Fermi surface, it is accompanied by an increase in the absorption coefficient α. This often manifests itself by a series of distinct peaks in the absorption spectrum, as in the case of noble metals; each peak corresponding to a distinct interband transition that is easily identifiable from (and in turn helps accurately modify) their energy band diagrams.[35,36,37]

This is illustrated for Ag and Cu. in Figs. (5) and (6),where the first three peaks correspond to the L_3 to F.S., $X_5 \rightarrow X_4$, and $L_2, \rightarrow L_1$ transitions and are labelled as 1, 2, and 3 respectively. As seen from Eq. (4), an increase in α results in an increase in both σ and ε_2. One important consequence of the increase in ε_2 due to $\varepsilon_2{}^b$ is a sharp increase in n from its usual infinitesimal value in the relaxation region, as would be generally expected from[8] $n = \frac{1}{2}[\varepsilon_1 + (\varepsilon_1{}^2 + \varepsilon_2{}^2)^{1/2}]$. This in turn results in a decrease in reflectivity as clearly seen from Eq. (1). Thus the initial interband absorption is accompanied by a drop in the reflectivity R as well as an increase in the values of n, k, α and σ . However, once both n and R have changed considerably from their normal relaxation region values, the above-mentioned limiting approximations no longer hold, and it is clear that a new peak in the interband absorption might result in a peak in the reflectivity. This is usually true for higher frequency interband transitions. A summary of the typical qualitative behavior discussed above is portrayed in Fig. 7.

Another important consequence of interband absorption is that sharp absorption ($\delta\varepsilon_2{}^b$) peaks often result in sharp peaks in $\delta\varepsilon_1{}^b$, as can be deduced from Kramers-Kronig relations[38] and simple sum rules. This may result in unusual optical characteristics as in the special case of Ag, which is discussed below in great detail.

B. 2.b. Specific Metals: Experimental Data on Optical Constants and Discussion

(i) Experimental Methods

Before discussing the data, it is probably useful to summarize briefly how such data on optical constants is typically obtained.

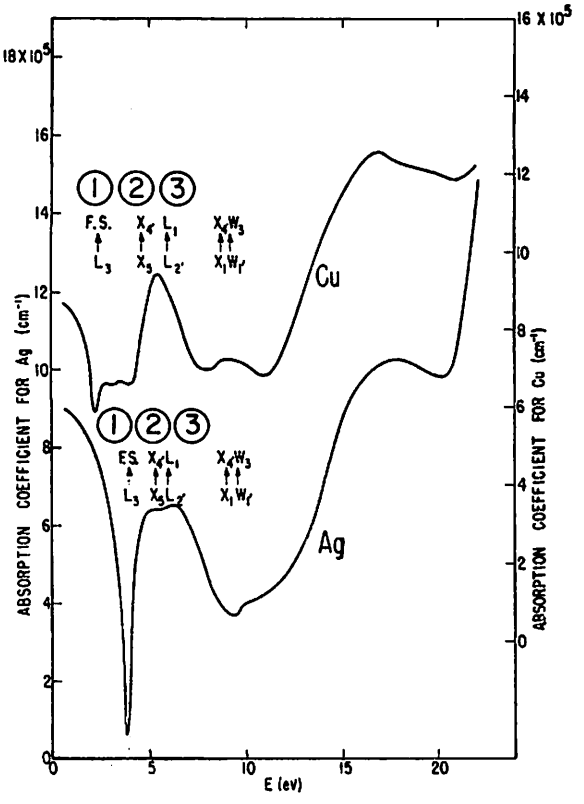

Fig. II-5:

(a) Spectral dependence of the absorption coefficient of Ag and Cu (Reprinted from Ref. 19). The arrows correspond to interband transitions at symmetry points in the band structure, which is detailed in Fig. II-6.

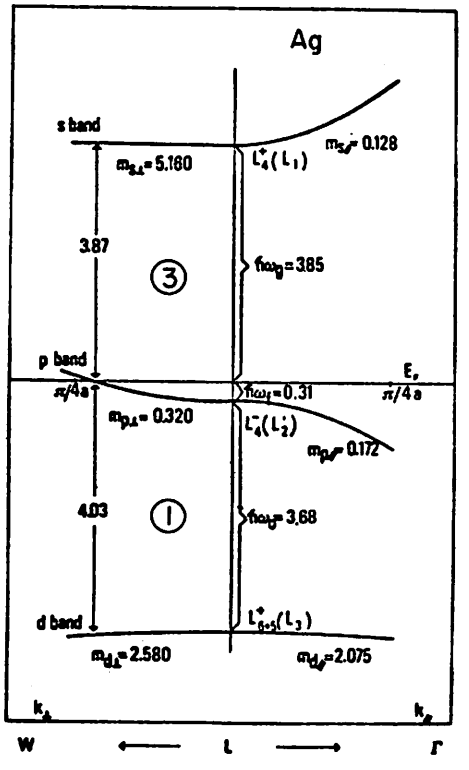

(b) See Fig. II-6. This Figure shows the detail of the band structure of Ag near the L-symmetry point. (Reprinted from Ref. 36(d)) (1) and (3) mark the $L_3 \rightarrow F \cdot S.$ and $L_2' \rightarrow L_1$ transitions seen in the absorption coefficient data of Fig. II-5.

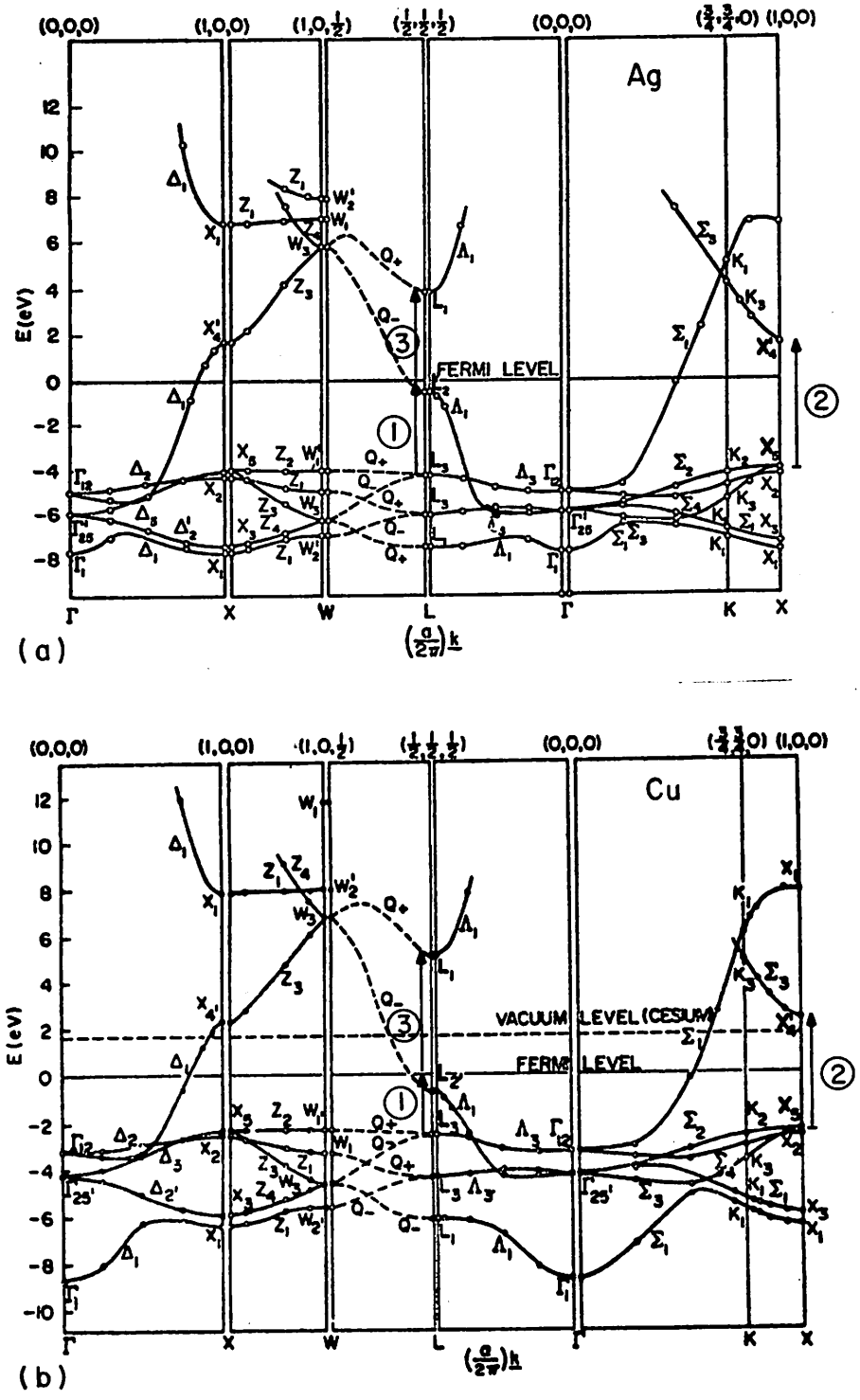

Fig. II-6: Band structure for (a) Silver and (b) Copper as calculated by Segall (Reprinted from Berglund and Spicer, Ref. 35(b)).

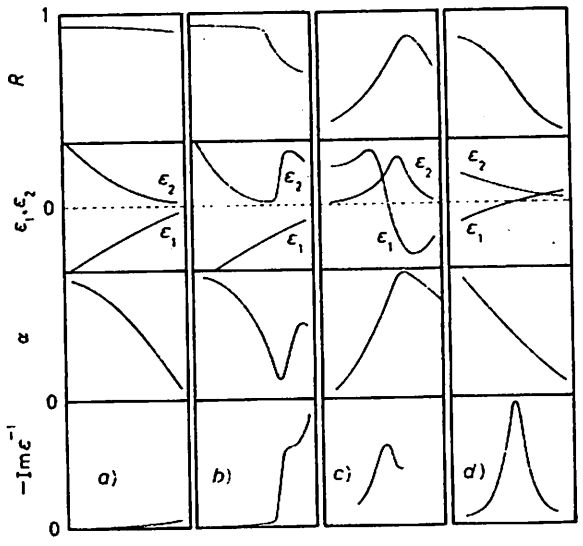

Fig. II-7: Typical behavior of optical constants associated with various excitation processes in metals (a) free-electron range; (b) low-energy interband transitions; (c) interband transitions; (d) plasma region. (Reprinted from Ehrenreich, Ref. 13).

For metals, the most convenient starting point is usually the measurement of reflectivity at normal incidence.[2a] The procedure is basically as follows. The Fresnel equation for the reflection coefficient $r(\omega)$ at normal incidence is:

$$r = \frac{n+ik-1}{n+ik+1} = |r|e^{i\theta} \tag{16}$$

and $R = |r|^2$ is the measured reflectance (i.e. the square of the amplitude of the field reflection coefficient). The phase θ at any frequency ν_o is computed from this data by using Kramers-Kronig relations between the real and imaginary parts of the complex function $\ln r = \ln|r| + i\theta$. This relation may be written as:[39]

$$\theta(\nu_o) = \frac{1}{\pi}\int_o^\infty \frac{d\ell n|r(\nu)|}{d\nu} \ell n \left|\frac{\nu + \nu_o}{\nu - \nu_o}\right| d\nu,$$

and can be integrated by computer techniques. Since contributions to $\theta(\nu_o)$ from ν far away from ν_o is usually small, a finite range of integration will suffice, although this range should be as wide as possible. Once θ has been calculated, relatively accurate values of n and k may be obtained using the above-mentioned Fresnel equation for $r(\omega)$. Values of ε_1, ε_2, α, σ, etc. are then usually deduced from these by using Eqs. (3) to (5).

(ii) Alkali Metals

For completeness it is useful to mention here that the optical properties of the alkali metals agree remarkably well with those deduced for free electron behavior. However, the practical difficulty of working with these metals due to their extreme reactivity

make them uninteresting in the present context.

(iii) Aluminum

The reflectivity of Al was shown in Fig. 4 and is repeated in Fig.8(a) over an extended range,[40] along with the absorption coefficient obtained by Kramers-Kronig analysis of the reflectivity data. Also shown in Fig. 8 is the frequency dependence of the dielectric constants (ε_1 and ε_2), the optical conductivity (σ) and Im $[\varepsilon^{-1}]$, as obtained from optical reflectance data. Except for the interband structure at 0.5 eV and 1.6 eV as seen in the absorptance data[41] of Fig. 9, the optical behavior of Al agrees well with the Drude picture. Since the 0.5 eV peak is very weak it hardly shows itself in the reflectance data, but the 1.6 eV peak causes a dip in reflectivity, as expected from our earlier discussion. Also the sharp drop in the reflectivity near 15 eV indicates that the plasma frequency is approximately 15 eV. This is confirmed by the plot of the energy loss function,[42-44] whose sharp peak at 15.8 eV is "the hallmark of a plasma resonance."[13] Thus Al is a particularly useful metal for our experiments due to its conformity to Drude behavior, and uniformly high (> 95%) reflectivity over the entire range of interest.

(iv) Noble metals

Ag: As mentioned earlier the optical properties of Ag exhibit rather unusual behavior. Figure 10 shows experimental data[19] for the normal reflectance as a function of photon energy. The reflectance of Ag remains as high as 99.3% up to nearly 3 eV[28,29] and then near 3.8 eV, it drops dramatically in a fraction of an eV from ~ 90% to less than 1% and then rises rapidly again to an appreciable value.

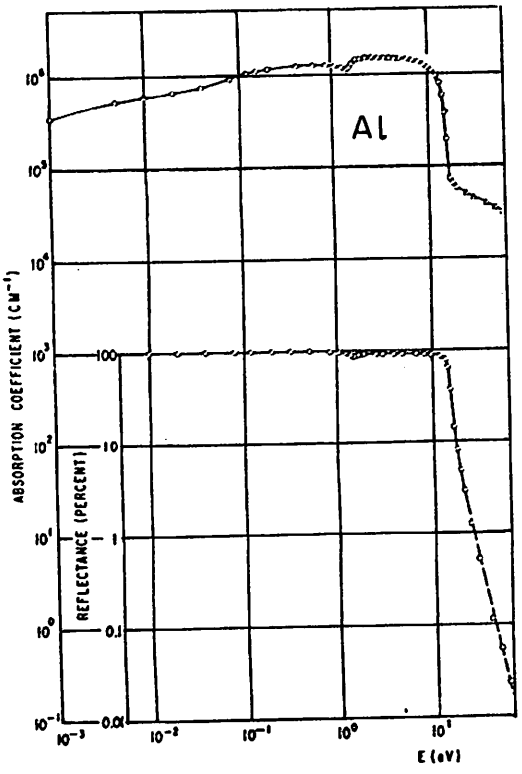

Fig. II-8: Optical properties of Aluminum: (a) Reflectivity and absorption coefficient data over an extended range (Reprinted from Ref. 40)

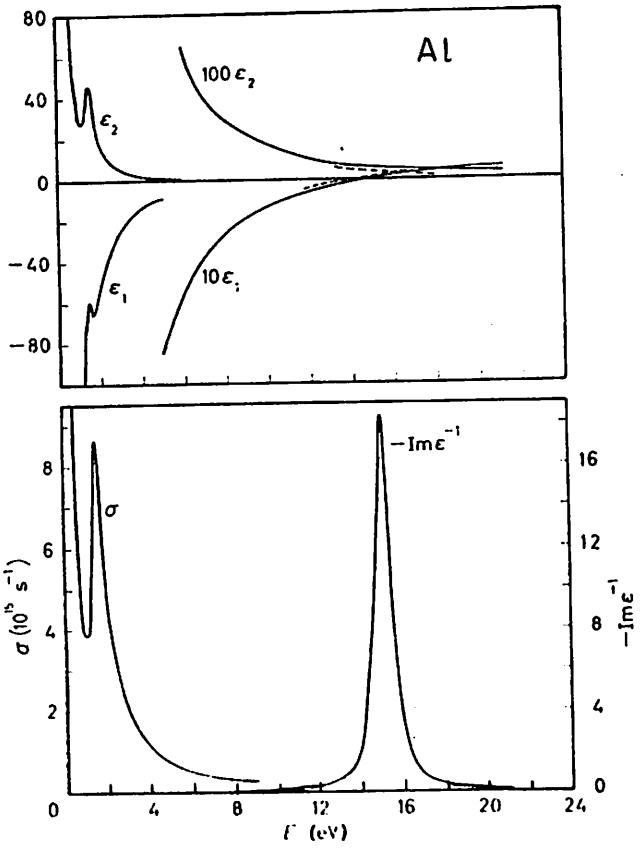

(b) Frequency dependence of ε_1, ε_2, conductivity σ and the energy loss function - Im ε^{-1}. The effect of the 1.6 eV interband peak on ε_1, ε_2 and σ is obvious. (Reprinted from Ref. 13).

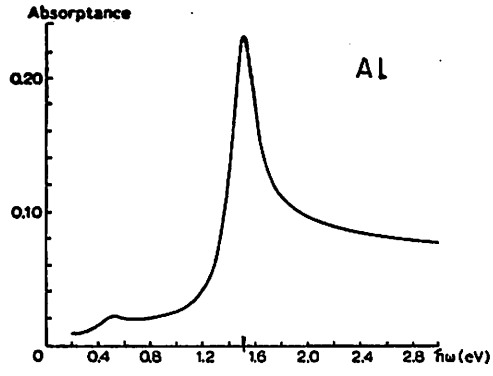

Fig. II-9: Absorptance spectrum for pure Aℓ at 4^{o}K, showing the strong 1.6 eV band and another weak band at 0.5 eV. (Due to Bos and Lynch, reprinted from Ref. 23).

(a)

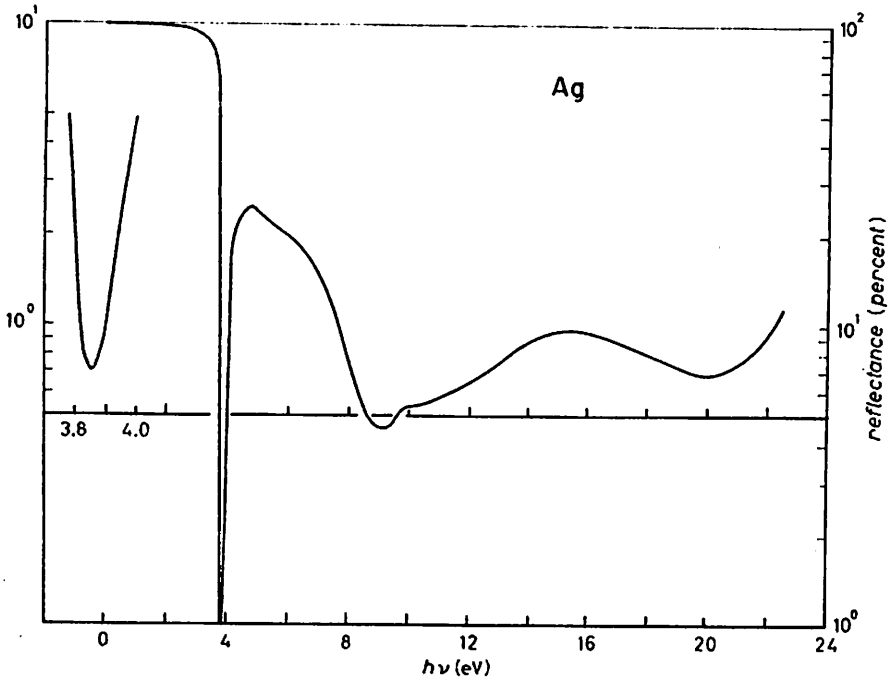

(b)

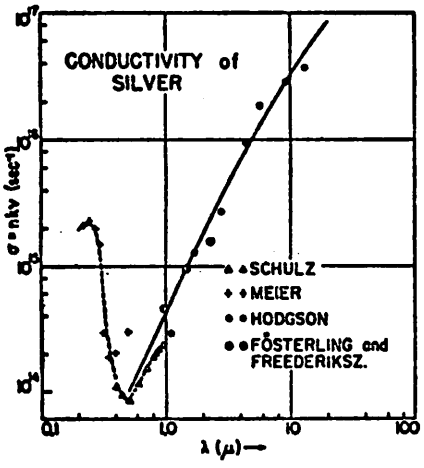

(c)

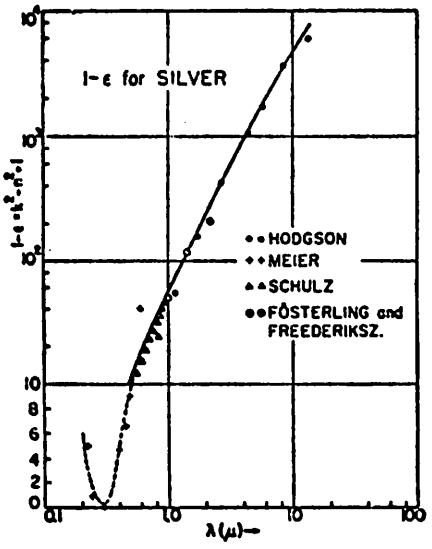

Fig. II-10:

Optical data for Silver:

(a) Reflectance, R

(b) Conductivity, σ

(c) Dispersion, $1-\varepsilon_1$

The reflectance data is from Ehrenreich (Ref. 13) and (b) and (c) are reprinted from M. P. Givens (Ref. 1(c)).

This unusual behavior which also reveals itself in the energy loss function (Fig. 11b), can be understood by a careful examination of the dielectric constants[45] shown in Fig. 11a and in Fig. 12 on an expanded scale. The figure indicates that Kramers-Kronig relations may be used to separate the dielectric constants into intra- and inter-band contributions. As was shown in Sec. II.B.1a, for the relaxation region the intra-band contributions fall off rapidly with increasing frequency viz. $\varepsilon_2^f \approx \frac{\omega_p^2}{\omega^3\tau}$ and $\varepsilon_1^f \approx 1 - \frac{\omega_p^2}{\omega^2}$. Thus in Fig. 12, ε_2 can be easily divided into two distinct regions in which respectively the inter- and intra-band contributions vanish. Because of linearity and the fact that the Kramers-Kronig relations apply separately to $\varepsilon(\omega)$ and $\varepsilon^f(\omega)$, they must also apply separately to $\delta\varepsilon^b(\omega)$. Thus, since $\varepsilon_2(\omega) \approx \delta\varepsilon_2^b$ above ω_i, we can calculate $\delta\varepsilon_1^b$ for all frequencies, especially for frequencies $\omega<\omega_i$ by using the appropriate Kramers-Kronig relationship:

$$\delta\varepsilon_1^b = \frac{2}{\pi} \int_{\omega_i}^{\infty} d\omega' \, \delta\varepsilon^b{}_2 \, (\omega') \, \frac{\omega'}{\left(\omega'^2 - \omega^2\right)}$$

Then by subtracting $\delta\varepsilon_1^b$ from ε_1^{exp}, one can determine the intra-band part of ε_1, i.e. ε_1^f over the same frequency range. (It should be noted that because of the excellent agreement of the behavior of the thus-determined ε_1^f with the Drude formula, and because ε_1^f is independent of τ in this region ($\omega\tau>>1$), this analysis of experimental data is used to determine the optical mass m_a[29]).

Figure 13 shows such a decomposition of ε_1. It should be noted that the results for large frequencies were obtained by extrapolating ε_1^f

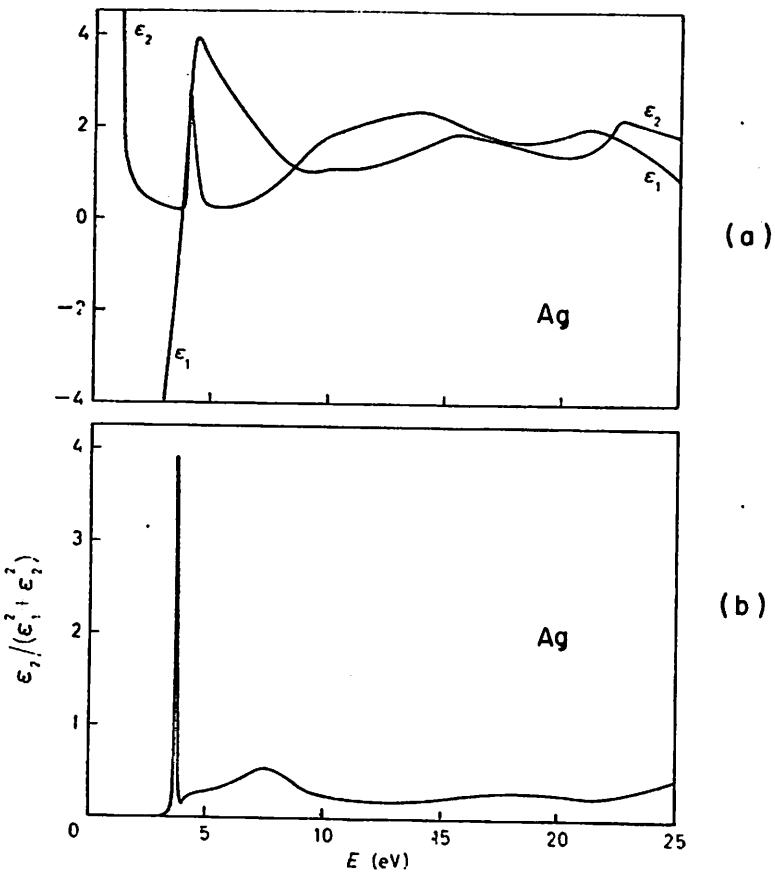

Fig. II-11 : Optical data for Silver (Reprinted from Ref. 13):

(a) Dielectric constants ε_1, ε_2

(b) Energy loss function - Im ε^{-1} for Ag clearly indicating a plasma resonance near 4 eV.

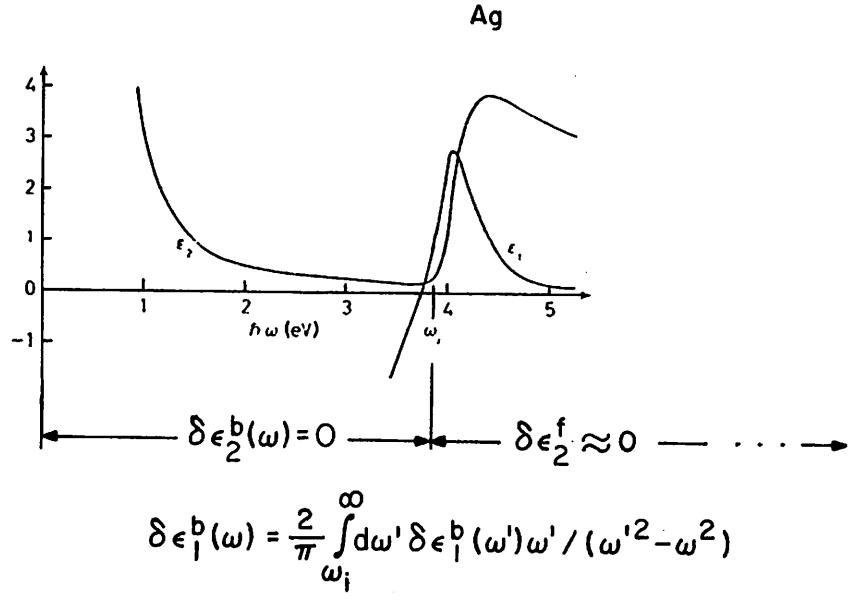

Fig. II-12 : Detail of Fig. II-11(a) (Reprinted from Ref. 13) useful in separating "free" (intraband) and "bound" (interband) contributions to ε in Ag. The threshold for interband transitions is indicated by ω_i (see text).

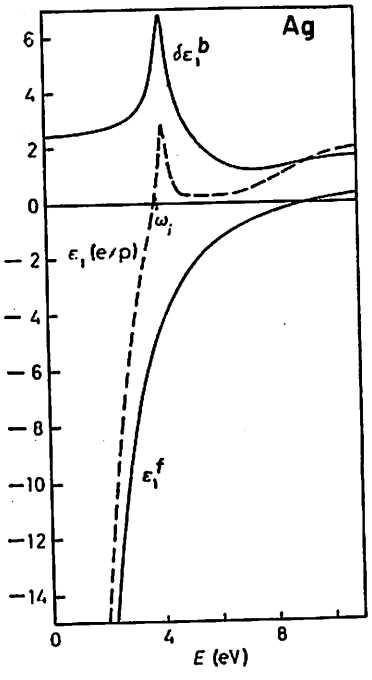

Fig. II-13: Decomposition of experimental values of ε_1 for Ag into free and bound contributions ε_1^f and $\delta\varepsilon_1^b$. (Reprinted from Ref. 13)

(as described by the Drude formula) into this region and then subtracting the experimental value of ε_1 to obtain $\delta\varepsilon_1^{\,b}$. [This peak in $\delta\varepsilon_1^{\,b}$ corresponds closely to the peak in $\varepsilon_2^{\,b}$, and these help explain the characteristic colors of the noble metals. For Ag, $\omega_i \simeq 3.87$ eV, for Au, $\omega_i \sim 2.45$ eV and for Cu it is ~ 2.08 eV]. An important consequence in Ag is that ε_1 gets effectively "pulled" through zero by the strong $L_3 \rightarrow L_2$, interband transition. This helps meet the conditions $\varepsilon_1 = 0$ and $\varepsilon_2 \simeq 0$, which typify a sharp plasma resonance. The onset of this plasma resonance is signalled not only by a sharp drop in reflectivity but also by a sharp peak in the Im $[\varepsilon^{-1}]$ spectrum. Physically, the effect of the interband transition may be understood as being caused by the screening effect of the highly polarizable d electrons. (This will be elaborated on in the subsequent section.) It may also be noted that the subsequent rapid increase in the reflectivity of Ag is rather interestingly due to the continued sharp rise in both ε_1 and ε_2, caused once again by the $L_3 \rightarrow L_2$, interband transition.

Au and Cu : Au and Cu do not show the dramatic behavior seen in Ag, as seen in the optical data in Fig. 14. While the peaks in $\delta\varepsilon_1^{\,b}$ have almost the same magnitude in both Au and Cu as in Ag, the fact that they occur at lower energies, where $\varepsilon_1^{\,f}$ is much more negative means that ε_1 does not increase sufficiently to pass through zero as a result of the interband transition, as it did in the case of Ag.

In the following sections we will explore consequences of the relatively low-frequency plasma resonance of Ag, its optical

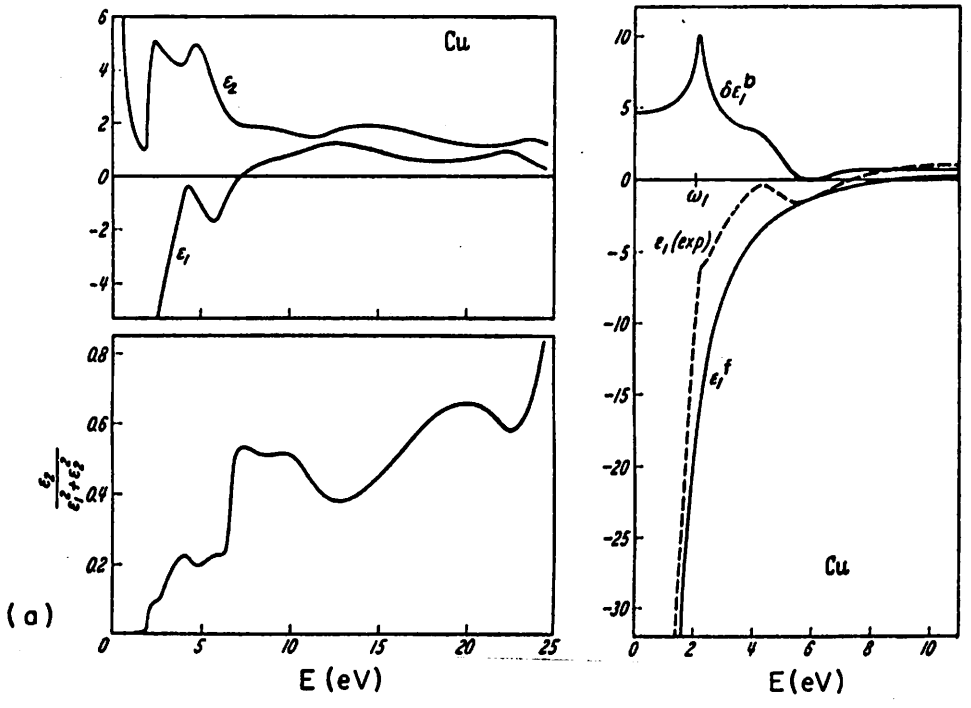

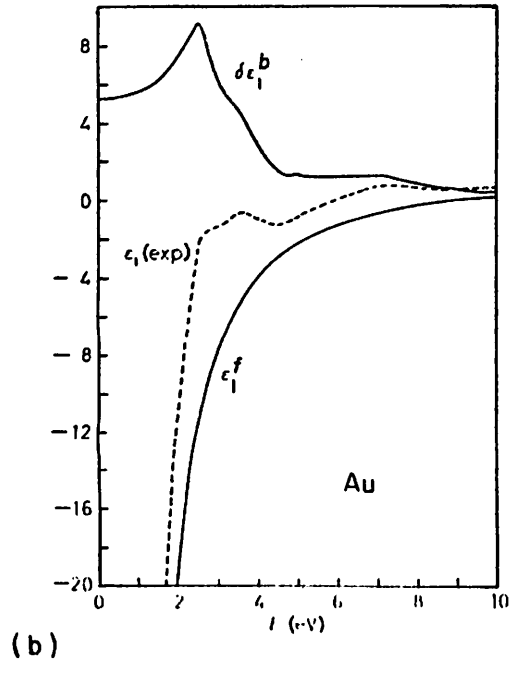

Fig. II-14:

Data for Cu and Au similar to that of Ag in Fig. II-11 to Fig. II-13.

(a) Cu (Reprinted from Ref. 86)

(b) Au (Reprinted from Ref. 13)

excitation and direct observation via electron tunneling into an adjacent Al electrode.

C. COLLECTIVE ELECTRON EXCITATIONS (PLASMONS)

C.1. General description and specification of observed metallic plasma frequencies.

As mentioned briefly in Section II, the conduction electrons and the ionic cores of a metal comprise a stable plasma which is capable of collective longitudinal oscillations, called plasma oscillations.[43] The condition for such longitudinal oscillations is simply: $\varepsilon(\omega) = 0$, as can be seen by inserting plane waves containing the factor $\exp\left[i\ (\bar{k}\cdot\bar{r} - \omega t)\right]$ in Maxwell's equations. For a free electron metal in which screening effects due to the polarizability of the core electrons are negligible (as in Lithium), the frequency of plasma oscillations is given precisely by the constant $\omega_p \triangleq \omega_{pc} = \dfrac{4\pi n_c e^2}{m_a}$ (already defined as "the plasma frequency") in the Drude equations. However, for most free electron metals, the Drude dielectric constant of Eq. (13) should be modified[46] to

$$\varepsilon(\omega) = \varepsilon_{core} - \left(\frac{\omega_p}{\omega}\right)^2 + i\left(\frac{\omega_p}{\omega}\right)^2 \frac{\gamma}{\omega} \qquad (17)$$

where ε_{core} accounts for the polarizability of the ion core. Since $\gamma << \omega \approx \omega_p$, $\varepsilon_2 << 1$ and the plasma resonance frequency gets shifted to $(\varepsilon_{core}^{-1/2})\ \omega_p$. The value of ε_{core} is usually small, and so for most metals $\omega_{po} \approx \omega_p = \dfrac{4\pi n_c e^2}{m_a}$. Except for the alkali metals, which have

generally lower values of n_c the values of ω_{po} are in the far ultraviolet (typically 10 to 15 eV). However, in the special case of Ag the plasma frequency gets shifted dramatically, from $\hbar\omega_p \approx 9$ eV to $\hbar\omega_{po} = 3.78$ eV, due to the high polarizability of the d-electrons in the core. As discussed briefly in Section B.2.b, this is because of the unusually strong influence of an interband (inner d-band to conduction sp-band) transition, which in itself is nearly resonant with the shifted plasma frequency. Because of its unusual character, the plasma resonance of Ag is often called a "hybrid" resonance, resulting from the cooperative behavior of both the d- and the conduction electrons.[19] In practice however, the character of the plasma resonance in Ag is seen to be essentially similar to that of other free electron metals (the alkalis and Al) in its sharp energy loss function[42-44] and in the characteristic energy loss experiments.[43,47] In the latter, a longitudinal disturbance (typically electrons in the keV range traversing the metal) couples with the plasma oscillations, thereby losing energy in quantized units of $\hbar\omega_p$, called plasmons. Because it combines the general features of well-defined plasma oscillations at a relatively accessible plasma frequency with convenience of handling (in contrast with the alkalis), Ag has become a popular representative for the experimental study[48-62] of plasmons in metals, and will be of particular interest to us for the remainder of this discussion.

For reference, the experimentally observed plasma frequencies $\hbar\omega_{po}$ for several metals are tabulated in Table 2, along with their relative linewidths $\Delta E_{po}/E_{po}$, where $\Delta E_{po} = \hbar(\Delta\omega_{po})$ and $E_{po} = \hbar\omega_{po}$.

TABLE 2

METAL	Special Comments	Plasmon energy: $\hbar\omega_{po}$, in eV	Vacuum wavelength λ_{po}, in Å	Linewidth of resonance, $\Delta E_{po}/E_{po}$	$\Delta\lambda_{po}$, in Å	References	χ, in eV†	E_f, in eV*
Ag	Narrowest resonance	3.784±.018	3275±15Å	~ 0.025 (ΔE_{po} ~ 90meV)	~ 80Å	47a 54 56	4.31-4.81 (4.73)	5.48
K	<— Nearly free-electron metals —> (well-defined plasma resonances)	3.785±0.01	3270±10Å	~ 0.07 (ΔE_{po} ~ 250meV)	~220Å	63 64	2.0-2.26 (2.24)	2.12
Na		5.71-5.85	~ 2100 Å	-	-	64 65	2.06-2.47 (2.28)	3.23
Li		~ 7.12 eV	~ 1550 Å	-	-	64	2.28-2.49 (2.42)	4.72
Rb		~ 3.65 eV	~ 3400 Å	-	-	66	(2.09)	1.85
Aℓ		~14.97	~ 830 Å	~0.04 (ΔE_{po}~590 meV)	-	67 68	4.08-4.25 (4.20)	13.44
Mg	Relatively poor plasma oscillations	8.9 - 10.6 (10.21)	~ 1200 Å	~ 0.059	-	68 69	3.59-3.79 (3.68)	7.13
Zn		8.6 - 9.6 (9.46)	~ 1320 Å	~ 0.061	-	69	3.32-4.31 (4.24)	9.39
Cd		7.8 - 8.7 (8.68)	~ 1430 Å	~ 0.092	-	69	3.68-4.49 (4.07)	7.46

† Values of the electron work functions are obtained from the "CRC Handbook of Chemistry and Physics", 51st Edition (1970-1971). The values in parentheses are the typical "preferred" values of the photoelectric work function.

* Free electron Fermi energy values from reference 17.

The linewidths $\Delta\omega_{po}$ are given approximately by $2\varepsilon_2/\varepsilon_1'$, and are of the order of $\gamma_d = \frac{1}{\tau} << \omega_p$ for the free-electron-like metals ($\varepsilon_1' \equiv d\varepsilon_1/d\nu$). Also tabulated here are the approximate vacuum work functions χ and Fermi Energies E_F of the chosen metals.

C.2. Optical excitation of plasmons in thin films

Due to their longitudinal character, plasmons* are very easily excited by fast electrons traversing the metal. However, the possibility of exciting plasmons optically is not as obvious, because of the transverse character of the electromagnetic field. Although p-polarized light of frequency ω_p at oblique incidence will create a small longitudinal disturbance near the surface of the bulk metal, coherent excitation of the collective electron oscillations cannot occur, and thus the net photon $\leftrightarrow$ plasmon coupling is weak. This is indicated clearly by Forstmann's calculation,[71] where modification of the usual Fresnel boundary conditions to include the possibility of a longitudinal wave excitation resulted in only an insignificant decrease in the value of the reflectance.

However the situation is quite different for metallic films whose thickness t is much less than $\lambda_p = 2\pi c/\omega_p$ (i.e., the free-space wavelength corresponding to ω_p). Ferrell[72] first predicted an enhancement in photon $\leftrightarrow$ plasmon coupling in thin films due to the excitation of an antisymmetric surface plasmon mode normal to the foil. This mode (corresponding to a vibrating "double layer" dipole) is essentially transverse in character and leads to an easily observed peak in the absorptance[44,53,61,73] at ω_p. More recently, several workers[74,75] have predicted an additional set of resonances in the absorptance spectrum near ω_p which appear as narrow peaks superimposed on the relatively broad ω_p peak caused by the antisymmetric surface plasmon mode.

---

* We will henceforth generally use the simpler notation ω_p to designate the actual plasma frequency of the metal, and use ω_{po} only when the core polarizability needs to be emphasized.

These narrow resonances correspond to the excitation of true longitudinal plasma resonances of wavelength $\lambda_L = 2t/n$, where n = 1,3,5 ....., and should be spaced by $\delta E \sim (3\hbar/5\omega_p)(2\pi v_F^2/t)^2$, under the assumption that $\omega^2 \simeq \omega_p^2 + 3/5\ v_F^2\ K^2$ describes the longitudinal dispersion relation[76] for a free-electron gas. These optically excited longitudinal plasmons have recently been observed in Ag[62] and K.[77]

C.2.a. Antisymmetric (normal) coupled surface plasmon modes:

Surface plasmon modes correspond to collective oscillatory motion of electrons along the surface of a metal, and can easily be shown to have an eigenfrequency $\omega_s = \omega_p/\sqrt{2}$ in the absence of another surface in the immediate vicinity. However when two surfaces of the metal are brought close together, as in a thin film of thickness less than the E-field penetration depth from the surfaces (typically ~ 10^3 Å), the two surface modes interact, yielding two coupled modes (as seen in Figure 15):

(a) A symmetric mode in which the two surface waves are in phase. This corresponds to a symmetric arrangement of charge deficiency or excess at opposing points on the two faces and a polarization current pattern which is primarily parallel to the surface. This is called the tangential surface plasmon mode.

(b) An antisymmetric mode in which the two surface waves are displaced by 180°, i.e., are out of phase. In this mode, an excess of charge density at a point on one surface is accompanied by a deficiency at a point directly across the film. Thus the polarization currents are predominantly normal to the film, even though the travelling waves

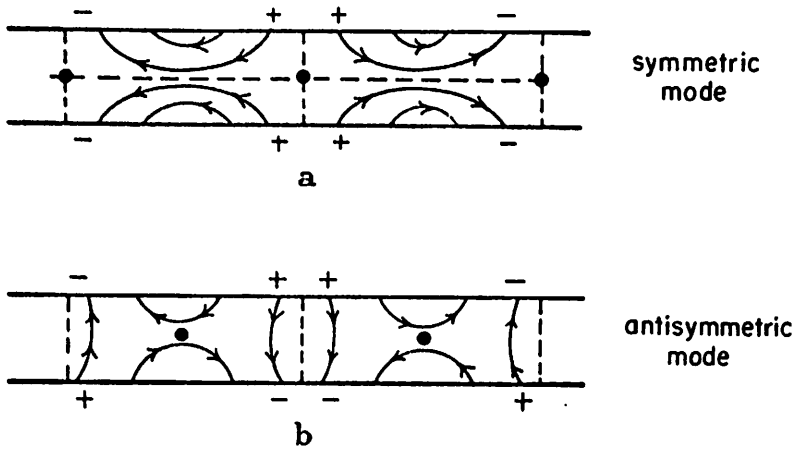

Fig. II-15 : Electric field for modes in a thin film due to coupled surface plasma oscillations: (a) Symmetric or ω^- mode (non-radiative), (b) anti-symmetric or ω^+ mode (radiative). (Reprinted from Ref. 86).

propagate along the surface. This gives the mode a transverse character. Ferrell[72] has shown that this normal surface mode is primarily responsible for the emission of light at ω_p when fast electrons traverse thin metallic foils.[48] This radiation is best understood by examining the dispersion curves for the two modes. These have been obtained by solving Maxwell's equations including retardation,[79,80] with the proper boundary conditions, and have been studied in detail by several authors.[78,80]

Figure 16 (essentially due to Ritchie[78]) gives the dispersion curves and radiative coupling characteristics for the special case of a lossless free electron gas in a film of thickness $t = c/2\omega_p = \lambda_p/4\pi$. The dispersion curves below the line $\omega = cK$ correspond to non-radiative character in both the normal and the tangential coupled surface plasmon modes, and the dotted line indicates the uncoupled or "thick film" surface plasmon dispersion. However the normal or antisymmetric mode also has a dispersion branch in the region $\omega > cK$; since this corresponds to a phase velocity greater than c, this mode is radiative.[81] For the plotted (solid line) curve, ω and K denote the real part of these quantities in the actual dispersion relation. The imaginary part of these quantities, which further illustrate details of the radiative character of this mode is depicted by the contour plots (dashed lines) which show, in arbitrary units, the ratio of the probability density for finding the plasmon inside the slab to the probability density for finding it outside. A peak in this ratio function (as is the case of $K << \omega_p/c$) corresponds to peaked character in the radiative resonance.

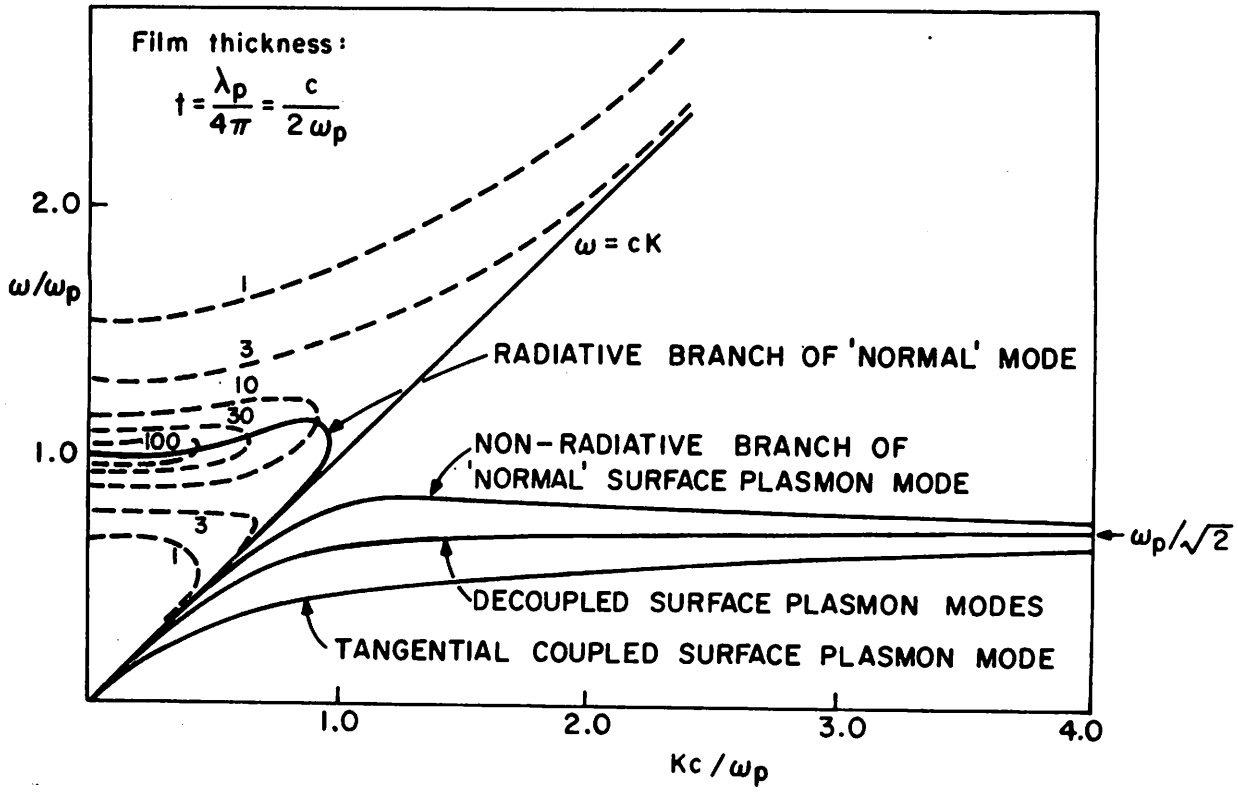

Fig. II-16: Dispersion curves (essentially due to Ritchie, Ref. 78) and radiative coupling characteristics for the surface modes in a thin film of a free electron gas. The region lying below the line $\omega = cK$ shows dispersion curves for the "real" surface modes. Both the tangential SP and the branch of the normal SP lying in this region are essentially non-radiative for ideally smooth boundaries. The region above the line $\omega = cK$ shows a contour plot of the ratio (in arbitrary units) of the probability density for finding the plasmon inside the film to the probability density for finding it in the vacuum. For $K << \omega_p/c$ this ratio is strongly peaked about the frequency ω_p. As K increases the resonance becomes broader and shifts upward in frequency slightly. The peak disappears for large K.

From these curves it is clear that the radiative (normal SP) dispersion mode is essentially a long-wavelength mode ($K << \omega_p/c$) with sharply peaked character at $Re(\omega) \simeq \omega_p$ [The dispersion relation for this mode yields a complex solution for ω, which for $K \to 0$ is $\omega \simeq \omega_p + i\gamma_r$, where γ_r corresponds to the radiation damping of this "virtual mode"[80]]. Let λ_T denote this wavelength.

The above dispersion curve analysis thus reveals the existence of a long-wavelength ($\lambda_T > t$) coupled surface plasmon mode at $\omega \simeq \omega_p$ which (when excited, say by fast electrons) may decay radiatively. Furthermore since the electric polarization of this antisymmetric mode has no component perpendicular to the plane defined by the normal and the K-vector (which by definition is parallel to the surface), the radiation must be polarized in the plane of emission (p-polarized). The angular dependence[72] of the radiation was also determined by Kliewer and Fuchs,[80] and is determined primarily by

$$\gamma_r \simeq \left(\omega_p^2\, t/4c\right) \sin\theta \tan\theta \qquad (18)$$

which vanishes for $\theta = 0$, i.e. in a direction perpendicular to the film. In the absence of non-radiative damping, the radiation shows a $\sin^2\theta$ dependence, as would be expected from the vibrating dipole character of the normal mode oscillation.[72]

Because the radiative character of the mode is indicative of strong photon $\leftrightarrow$ plasmon coupling, it may be expected that such a long wavelength surface plasmon mode may be easily excited in thin films by p-polarized radiation at ω_p, with a coupling efficiency

that shows the same angular dependence as the emitted radiation (i.e. γ_r). Such an excitation should result in a peak in the absorptance $A_p(\omega)$ and a dip in the transmittance $T_p(\omega)$ of p-polarized radiation at ω_p, and also a peak in the reflectance $R_p(\omega)$ because of re-radiation. McAlister and Stern[53] have calculated expressions for $R_p(\omega)$ and $T_p(\omega)$ in the framework of classical optics, i.e., using the usual Fresnel equations for a metallic film of thickness t and of dielectric function $\varepsilon(\omega) = 1 - \omega_p^2/\omega^2$, while ignoring the possibility of exciting bulk longitudinal plasma waves in the metal. For the case of very thin films ($t < \lambda_p/\pi$), in the neighborhood of ω_p (i.e. $|\varepsilon| << \sin\theta$ if the angle of incidence θ is not too small), we have

$$R_p = \frac{\gamma_r^2}{\gamma_t^2 + 4(\omega-\omega_p)^2} \tag{19a}$$

$$T_p = \frac{\gamma_d^2 + (\omega-\omega_p)^2}{\gamma_t^2 + 4(\omega-\omega_p)^2} \tag{19b}$$

$$\text{and} \quad A_p = 1 - R_p - T_p = \frac{2\gamma_r \gamma_d}{\gamma_t^2 + 4(\omega-\omega_p)^2} \tag{19c}$$

which show the expected peak in reflection and absorption, and the expected dip in transmission. In the above expressions,

$\gamma_d = \frac{2\varepsilon_2}{(d\varepsilon_1/d\omega)} \approx \Delta\omega_p$ is the linewidth of the plasma resonance, or the rate of intrinsic damping.

$\gamma_r = \left(\frac{\omega_p^2 \, t}{2c}\right) \sin\theta \tan\theta$ is the rate of radiation damping.

and $\gamma_t = \gamma_d + \gamma_r$ is the total damping rate.

The optical excitation of this long-wavelength plasma mode has been verified by several workers.[44,51-53, 59, 82] Some of the data for Ag (Ref. 51) and K (Ref. 82) is shown in Figs. 17 and 18 respectively. It is seen that the interpretation of the results for Ag is partly complicated by the onset of the 4eV interband absorption, but that the transmission spectra for K are in excellent agreement with theoretical expectations.

C.2.b. Longitudinal bulk plasmon modes:

Sauter[83] first pointed out the importance of including the excitation of a bulk longitudinal wave into the boundary conditions for the reflection and transmission of p-polarized light at $\omega \simeq \omega_p$. Inspired partly by Ferrell's physical picture[72] and by the inadequacy of the classical calculations,[53,73] Melnyk and Harrison[74] included the possibility of exciting longitudinal electric polarization waves ($\bar{k}_L \times \bar{E}_L = 0$) besides the usual transverse wave ($\bar{k}_T \cdot \bar{E}_T = 0$) in their thin film calculations. They derived expressions analogous to the ones derived by McAlister and Stern,[53] except for the inclusion of additional terms corresponding to the longitudinal wave. These terms were found to yield relatively narrow longitudinal resonances[84] of short-wavelength ($\lambda_L << \lambda_T$), superimposed over the coupled SP mode transverse character resonances discussed above. Figure 19 (due to Melnyk and Harrison) illustrates the inclusion of these longitudinal resonances in the calculated spectral dependence of the

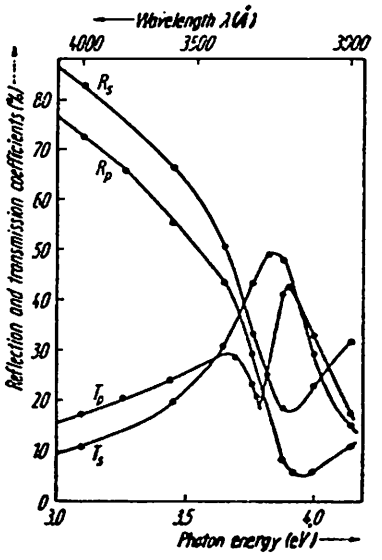

Fig. II-17:

Transmission and reflection spectra of a 424 Å Ag film irradiated by p- and s- polarized light at $\theta = 45^{\circ}$ (after Yamaguchi, Reprinted from Ref. 44).

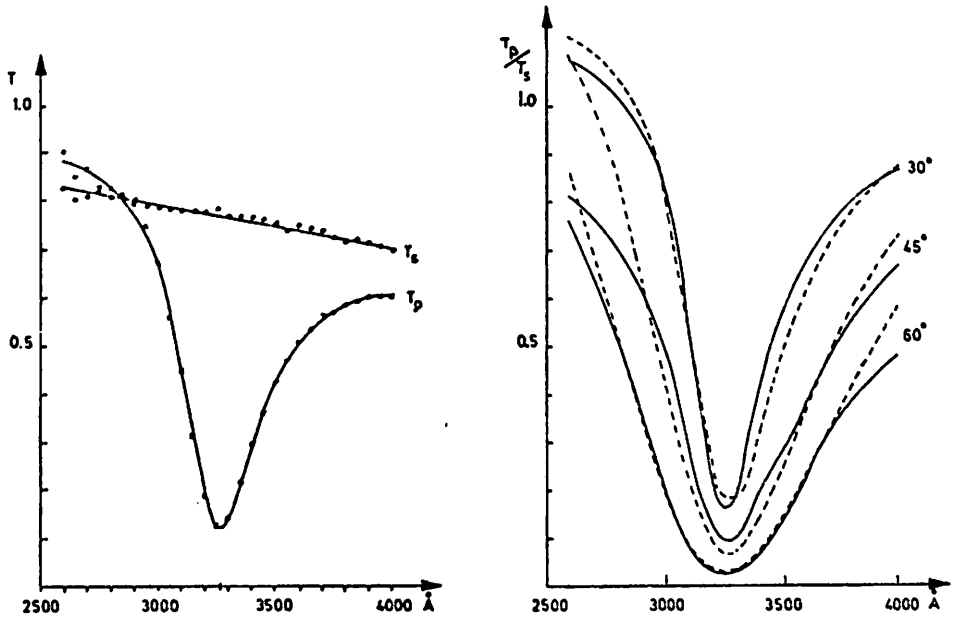

(a) (b)

Fig. II-18: (a) Transmission spectra of a 300 Å K film on sapphire for p- and s-polarized light incident at $\theta = 30^{\circ}$ (after Brambring, Ref. 82).

(b) Experimental (solid) and calculated (dashed) curves for the spectra of T_p/T_s of a 300 Å K film on sapphire for three angles of incidence (after Brambring, Ref. 82).

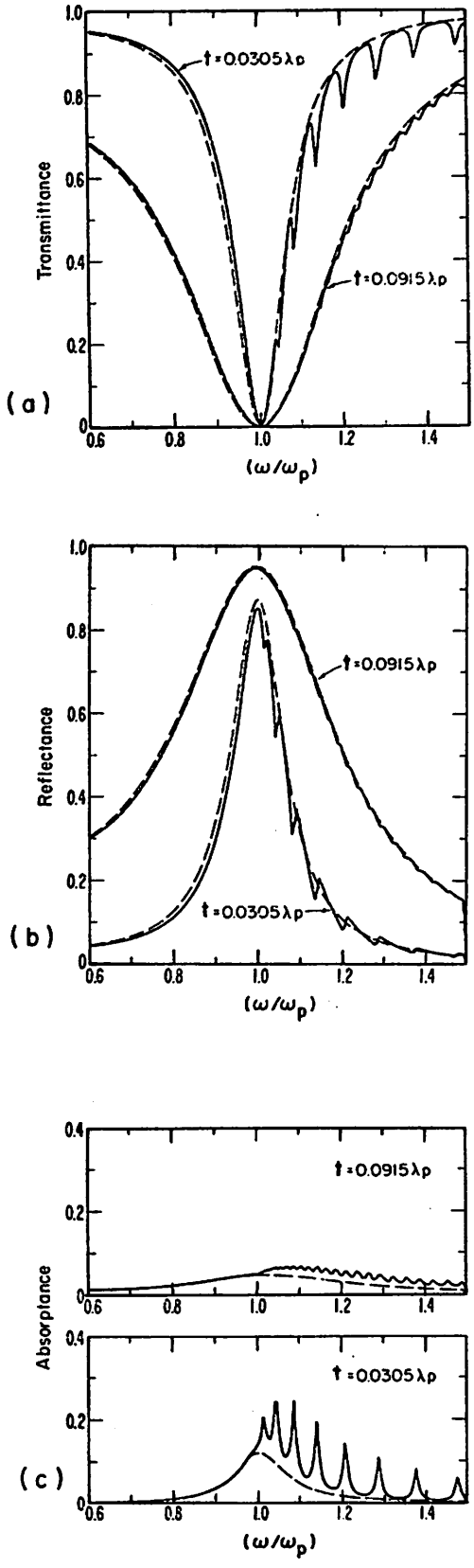

Fig. II-19:

Spectral plots of the theoretical (a) transmittance, (b) reflectance and (c) absorptance near $\omega = \omega_p$, for two film thicknesses (according to Melnyk and Harrison, Ref. 74). The dashed curves correspond to the usual transverse plasma resonances and the solid lines show the effect of including the longitudinal resonances. These results are calculated for p-polarized radiation incident at an angle of 60^o on a film of thickness t, with a Fermi velocity $v_F = 1.4 \times 10^8$ cm/sec and a collision time τ corresponding to $\omega_p \tau = 100$; thus, these plots correspond closely to 100 Å and 300 Å films of Ag.

reflectance, transmittance and absorptance near ω_p. It should be noted that these calculations correspond to the case of 100 Å and 300 Å films of Ag; the hybrid character of the Ag plasma resonance has been ignored and so has the effect of the interband absorption just above ω_p. Also the assumed value of $\omega_p\tau = 100$ is somewhat higher than those usually obtained in practice, and so experimentally observed longitudinal resonances will generally not be as sharp. These resonances are better resolved in thinner films due to the reduced effect of scattering on the longitudinal waves and due to the inverse dependence of the spacing of adjacent longitudinal resonances on film thickness, i.e.,

$$\delta E \sim \left(\frac{3\hbar}{5\omega_p}\right)\left(2\pi\ v_F^{\,2}/t\right)^2$$

Finally, since surface scattering can be very detrimental to these resonances, extremely smooth ($\delta t \ll t$) surfaces will generally be required to observe these resonances, which might be hard to attain when the films are also extremely thin ($t \lesssim 100$ Å).

The resonant excitation of such longitudinal resonances has been observed in Ag films of ~ 120 Å thickness by Lindau and Nilsson.[62] The authors emphasized the importance of the above stringent conditions on surface preparation and also noted that exposure to the air for more than a day affected these surfaces enough to inhibit the excitation of the longitudinal resonances. It also seems that for Ag the effect of single-particle excitations (interband absorptions) on at least the first two resonances[85] is negligible. This is of particular interest in the present work where the enhancement

of the tunneling current due to plasma excitation in Ag is investigated.

It should also be mentioned that more general approaches[75] including nonlocal dielectric functions have been taken, and the results for frequencies ω in the vicinity of ω_p are essentially the same as those due to Melnyk and Harrison.[74] However, Fuchs and Kliewer[75] have pointed out that single-particle excitations may influence the longitudinal plasma resonances for $\omega \gtrsim 1{\cdot}1\ \omega_p$, as seen by the introduction of self-consistent-field nonlocal dielectric functions. This perhaps explains the absence of the higher longitudinal resonances in Lindau and Nilsson's data.[62]

II. References

1. For instance see:
   a) M. Born and E. Wolf, Principles of Optics, (Pergamon Press, New York, 4th ed., 1970), Chap. 10.
   b) J. M. Ziman, Theory of Solids, (Cambridge Univ. Press, London, 2nd ed., 1972), Chap. 8.
   c) M. Parker Givens, in Solid State Physics, edited by F. Seitz and D. Turnbull, (Academic, New York, 1966), vol. 6, p. 313.
   d) A. H. Wilson, Theory of Metals, (Cambridge Univ. Press, 2nd ed., 1953).
   e) Several other references below (e.g. Ref. 11, 13).
2. It may also be noted that if any one of these properties (e.g. the reflection or absorption coefficient is known over an extended energy range, it is possible to deduce the other constants from it. For instance see:
   a) F. C. Jahoda, Phys. Rev. 107, 1261 (1957).
   b) H. R. Philipp and E. A. Taft, Phys. Rev. 113, 1002 (1959).
   c) H. R. Philipp and H. Ehrenreich, J. Appl. Phys. 35, 1416 (1964).
3. See Ref. 1 above. We shall use c.g.s. units throughout this Chapter.
4. A constant that is often used instead of $\mathcal{N}$ is the complex propagation vector $\kappa = \kappa_1 + i\kappa_2$ related to $\mathcal{N}$ by $\kappa = \mathcal{N}\frac{\omega}{c}$.
5. For more complex crystals ε_L and ε_T have to be specified for each direction.

II. References

6. The long-wavelength limit considerations are good for photon energies at which the wavelength is much greater than the interatomic distance ($\lesssim 10$ Å), which is obviously true for the optical range defined by $\hbar\omega < 10$eV.

7. Assuming the magnetic permeability $\mu = 1$, which is closely true for all the metals discussed herein, throughout the optical range of interest.

8. These can easily be inverted to:

$$n^2 = 1/2[\varepsilon_1 + (\varepsilon_1^2 + \varepsilon_2^2)^{1/2}]$$

and

$$k^2 = 1/2[-\varepsilon_1 + (\varepsilon_1^2 + \varepsilon_2^2)^{1/2}]$$

9. P. Drude, Theory of Optics (Longmans Green, New York, 1902), p. 382.

10. H. A. Lorentz, The Theory of Electrons (Teubner, Leipzig, 1909), Chap. 4.

11. F. Seitz, The Modern Theory of Solids (McGraw-Hill, New York, 1940). Chap. 17, Section 148.

12. L. P. Kadanoff and P. C. Martin, Phys. Rev. 124, 670 (1961).

13. H. Ehrenreich, in The Optical Properties of Solids, edited by J. Tauc (Academic Press, New York, 1966), p. 106.

14. M. H. Cohen, ibid (OPS - ed. J. Tauc).

15. V. L. Bonch-Bruevich, ibid (OPS - ed. J. Tauc), p. 331.

16. D. Pines, Elementary Excitations in Solids, (Benjamin, New York, 1964), Chap. 4.

II. References

17. C. Kittel, Introduction to Solid State Physics, (Wiley, New York, 4th ed., 1971), Chap. 13.

18. It should be noted that the Drude result [Eq. (6)] is a special case of the Lorentz result [Eq. (7)] for $\omega_\ell = 0$.

19. H. Ehrenreich and H. R. Philipp, Phys. Rev. 128, 1622 (1962).

20. M. H. Cohen, Phil. Mag. 3, 762 (1958).

21. H. Ehrenreich and M. H. Cohen, Phys. Rev. 115, 786 (1959).

22. P. O. Nillson, in Optical Properties of Solids, ed. by E. D. Haidemenakis, (Gordon and Breach Publ., New York, 1969), Chap. 7.

23. F. Abelès, in Optical Properties of Metals, ed. by F. Abelès, (North-Holland Publ., Amsterdam, 1972), Chap. 3.

24. From Eq. (14), one also has the static conductivity, $\sigma_o = \frac{\omega_p^2}{4\pi\gamma}$ which is often used to determine the approximate relaxation time.

25. E. Hagen and H. Rubens, Ann. Physik 11, 873 (1903).

26. M. L. Théye, Phys. Rev. B2, 3060 (1970).

27. E. A. Taft and H. R. Philipp, Phys. Rev. 121, 1100 (1961).

28. (a) L. G. Schulz, Phys. Rev. 93, 922 (A), (1953);
(b) L. G. Schulz, Journ. Opt. Soc. Am. 44, 540 (1954).
(c) L. G. Schulz, J. Opt. Soc. Am. 44, 357 (1954);

29. P. B. Johnson and R. W. Christy, Phys. Rev. B6, 4370 (1972).

30. (a) H. E. Bennett, M. Silver and E. J. Ashley, J. Opt. Soc. Am. 53, 1089 (1963);
(b) R. P. Madden, L. R. Canfield and G. Hass, J. Opt. Soc. Am. 53, 620 (1963).

II. References

31. (a) J. Valasek, International Critical Tables, Vol. V, (McGraw-Hill, New York, 1929), p. 248.

(b) L. F. Drummeter and G. Hass, Physics of Thin Films, ed. by G. Hass and R. E. Thun (Academic Press, New York, 1964), p. 305.

(c) T. J. Love, Radiative Heat Transfer, (Charles E. Merrill Publ. Co., Columbus, Ohio, 1968), p. 217.

32. At room temperature ($300^{o}K$), in a typical metal the mean free path for electron-phonon collisions dominates, since it is shorter than that due to electron-electron collisions by at least a factor of 10 (Ref. 17, p. 283). For good conductors, this value of L is typically a few hundred Angstroms at $300^{o}K$ (e.g., for Cu, $\tau_{300} \simeq 2\times10^{-14}$ sec, $\therefore L_{300} = v_F \tau_{300} \simeq 300$ Å), but as the temperature is lowered to $4^{o}K$, the value of L rises typically by a factor of 10^2 (low purity) to 10^6 (extremely pure), depending on the purity of the sample (Ref. 17, p. 259).

33. (a) G.E.H. Reuter and E. H. Sondheimer, Proc. Roy. Soc. (London) A195, 336 (1948);

(b) R. B. Dingle, Physica 19, 729 (1953);

(c) See Ref. 1c, p. 335.

34. (a) H.B.G. Casimir and J. Ubbink, Philips Tech. Rev. 28, 300 (1967);

(b) F. Wooten, Optical Properties of Solids, (Academic Press, New York, 1972), p. 92.

II. References

35. Band structure of Cu:

(a) B. Segall, Phys. Rev. 125, 109 (1962);

(b) C. N. Berglund and W. E. Spicer, Phys. Rev. 4A, A1044 (1964);

(c) N. V. Smith, Phys. Rev. B3, 1862 (1971).

36. Band structure of Ag:

(a) B. Segall (unpublished, but cited in Ref. 35(b));

(b) E. C. Snow, Phys. Rev. 172, 708 (1968);

(c) N. E. Christensen, Phys. Stat. Sol. (b)54, 551 (1972);

(d) Detailed structure near 4.0 eV: R. Rosei, C. H. Culp and J. H. Weaver, Phys. Rev. B, 484 (1974).

37. Band structure of Au (relativistic calculation):

(a) N.E. Christensen and B. O. Seraphin, Phys. Rev. B4, 3321 (1971), and other references therein.

38. For instance, see: L. D. Landau and E. M. Lifshitz, Electrodynamics of Continuous Media, (Pergamon Press, New York, 1969), paragraph 62.

39. H. Bode, Network Analysis and Feedback Amplifier Design, (D. Van Nostrand and Co., Princeton, N. J., 1945).

40. Taken from: H. R. Philipp and H. Ehrenreich, J. Appl. Phys. 35, 1416 (1964). [Ref. 2(c) above].

41. Cited in ref. 23, Absorptance data due to: L. W. Bos and D. W. Lynch, Phys. Rev. 25, 156 (1970).

42. H. Fröhlich and H. Pelzer, Proc. Phys. Soc. (London) A 68, 525 (1955).

43. D. Pines, Elementary Excitations in Solids, (Benjamin, New York, 1964) [Ref. 16 above].

II. References

44. W. Steinmann, Phys. Stat. Sol. 28, 437 (1968).

45. These themselves have been determined from the reflectance data, as outlined earlier.

46. For instance see Ref. 17, p. 277. This point is also discussed in Ref. 23 and 34(b).

47. J. Daniels, Z. Phys. 203, 235 (1967); Z. Phys. 200, 186 (1967).

48. (a) W. Steinmann, Phys. Rev. Lett. 5, 470 (1960).

(b) W. R. Brown, P. Wessel and E. P. Trounson, Phys. Rev. Lett. 5, 472 (1960).

49. (a) A. L. Frank, E. T. Arakawa and R. D. Birkhoff, Phys. Rev. 126, 1947 (1962).

(b) E. T. Arakawa, N. O. Davis and R. D. Birkhoff, Phys. Rev. 135, A224 (1964).

50. U. Bürker and W. Steinmann, Phys. Stat. Sol. 12, 853 (1965).

51. S. Yamaguchi, J. Phys. Soc. Japan 18, 266 (1963).

52. (a) N. Matsudaira, J. Phys. Soc. Japan 18, 380 (1963).

(b) M. Hattori, K. Yamada and H. Suzuki, J. Phys. Soc. Japan 18, 203 (1963).

53. A. J. McAlister and E. A. Stern, Phys. Rev. 132, 1599 (1963).

54. J. Brambring and H. Raether, Phys. Rev. Lett. 15, 882 (1965).

55. W. Steinmann, J. Hoffmann and K. Stettmaier, Phys. Letters (Netherlands) 23, 234 (1966).

56. J. Brambring and H. Raether, Z. Phys. 199, 118 (1967).

57. J. Bosenberg and H. Raether, Phys. Rev. Lett. 18, 397 (1967).

58. P. Schreiber, Z. Phys. 211, 257 (1968).

59. D. Schulz and M. Zurheide, Z. Phys. 211, 165 (1968).

II. References

60. A. Otto, Phys. Stat. Sol. 26, K99 (1968).

61. P. O. Nilsson, I. Lindau and S.B.M. Hagström, Phys. Rev. B1, 498 (1970).

62. (a) I. Lindau and P.O. Nilsson, Phys. Scripta 3, 87 (1971);
(b) I. Lindau and P.O. Nilsson, Phys. Lett. 31A, 352 (1970).

63. J. Brambring, Z. Phys. 200, 186 (1967).

64. C. Kunz, Phys. Lett. 15, 312 (1965).

65. J. B. Swan, Phys. Rev. 135, A1467 (1964).

66. See Ref. 17 (Kittel) above, p. 273.

67. J. Geiger and K. Wittmaack, Z. Phys. 195, 44 (1966).

68. E. T. Arakawa, R. J. Herickhoff and R. D. Birkhoff, Phys. Rev. Lett. 12, 319 (1964).

69. B. Feuerbacher and B. Fitton, Phys. Rev. Lett. 24, 499 (1970).

70. Handbook of Physics and Chemistry, The Chemical Rubber Company, 51st Edition (1970-1971).

71. F. Forstmann, Z. Phys. 203, 495 (1967).

72. R. A. Ferrell, Phys. Rev. 111, 1214 (1958).

73. R. A. Ferrell and E. A. Stern, Am. J. Phys. 31, 810 (1962).

74. (a) A. R. Melnyk and M. J. Harrison, Phys. Rev. Lett. 21, 85 (1968).
(b) A. R. Melnyk and M. J. Harrison, Phys. Rev. B2, 835 (1970).

75. (a) W. E. Jones, K. L. Kliewer, and R. Fuchs, Phys. Rev. 178, 1201 (1969).
(b) R. Fuchs and K. L. Kliewer, Phys. Rev. 185, 905 (1969).

76. For instance, see
(a) D. Pines, Rev. Mod. Phys. 28, 184 (1956).
(b) Ref. 16 and 1(b).

II. References

77. M. Anderegg, B. Feuerbacher and B. Fitton, Phys. Rev. Lett., 27, 1565 (1971).

78. R. H. Ritchie, Phys. Rev. 106, 874 (1957).

79. R. H. Ritchie and H. B. Eldridge, Phys. Rev. 126, 1935 (1962).

80. K. L. Kliewer and R. Fuchs, Phys. Rev. 153, 498 (1967).

81. Actually there are several "virtual modes" with radiative character similar to this one (see Ref. 80); however this is the only mode of interest in the present discussion due to its distinct peaked behavior at ω_p.

82. J. Brambring, Z. Phys. 200, 186 (1967).

83. F. Sauter, Z. Phys. 203, 488 (1967).

84. These longitudinal resonances in metal films are exactly analogous to the bulk plasma waves in gaseous plasmas, which are seen as a spectrum of discrete lines known as the Tonks-Dattner resonances:

(a) L. Tonks, Phys. Rev. 37, 1458 (1931).

(b) A. Dattner, Ericsson Technics 8, 1 (1963).

85. For a film thickness of 120 Å, these occur at $\omega \simeq 1.014\ \omega_p$ and $1.031\ \omega_p$, corresponding to n = 3 and n = 5 respectively. The corresponding free space wavelengths for the exciting radiation are 3235 Å and 3180 Å, assuming that λ_p = 3280 Å.

86. H. Raether, in Springer Tracts in Modern Physics, vol. 38, (Springer-Verlag, New York, 1965).

III. OPTICAL EXCITATION OF ELECTRON TUNNELING CURRENTS IN METAL-BARRIER-METAL JUNCTIONS

A. INTRODUCTION

The preceding review of the optical properties of metals clearly indicates that at long wavelengths (e.g., $\lambda \gtrsim 6000$ Å for Au), incident radiation causes only intraband absorption under most conditions.[1] Intraband absorption corresponds to "free electron" behavior (for bands that are nearly parabolic) in most metals, and the metallic response is typified by high reflectivity, indicative of re-radiation by easily induced oscillating electron currents.

Thus, when one considers the problem of the optical excitation of tunneling currents in a metal-barrier-metal (MBM) junction, it is seen that at frequencies below ω_i (the onset of interband absorption), efficient coupling into the junction may be achieved by coherent "forced" excitation of optical frequency electron currents in a suitable antenna geometry.[2] The induction of such optical frequency currents may also be considered to result in an effective modulation of localized electron densities at any point on the metal surface and in particular at the barrier. This explains the plausibility of the "Fermi-level modulation" type of analysis used by several authors[3,4] to explain the detection characteristics of point-contact MBM junctions for wavelengths as short[3] as 6328 Å.

However at higher frequencies, with the onset of interband absorption (typically in the near infrared, visible or near-ultraviolet region of the spectrum as seen in Section II), the metallic reflectivity drops drastically and antenna coupling is expected to be poor,

corresponding to the damping of the free electron oscillations by interband absorption. At such photon energies however, direct excitation of electrons to higher energies (due to interband absorption), and other coupling mechanisms could lead to a large contribution in the tunneling current. In particular, with an appropriate choice of MBM geometry and conditions favoring plasma resonance absorption in one of the metals, a large enhancement of tunneling current might occur via the photon → plasmon → single electron excitation process, and also due to the direct modulation of electron densities at the nonlinear tunneling barrier by the collective electron oscillations.

In the present section, the contribution of interband absorption and plasma resonance absorption to the tunneling current are considered. Photon-assisted tunneling is modelled by a three-step process similar to photoemission:[5] the electrons are first excited by light to states of higher energy; they then move to the potential barrier (with or without scattering) and finally tunnel through it with a probability that is a strongly increasing function of the energy of this excited state. This tunneling electron current will also manifest itself externally as an "optically-induced" voltage which should be easily measurable for high impedance tunneling junctions.

B. NOTATION AND CONVENTIONS

The geometry of the structure under investigation and the corresponding energy level diagram are shown in Fig. 1(a) and Fig. 1(b) respectively. Metal 1 (e.g., Al) is in the form of a thick layer (~ 5000 Å) or a highly-polished pure metal substrate. On this an extremely thin barrier (s < 50 Å) of an insulating material with a

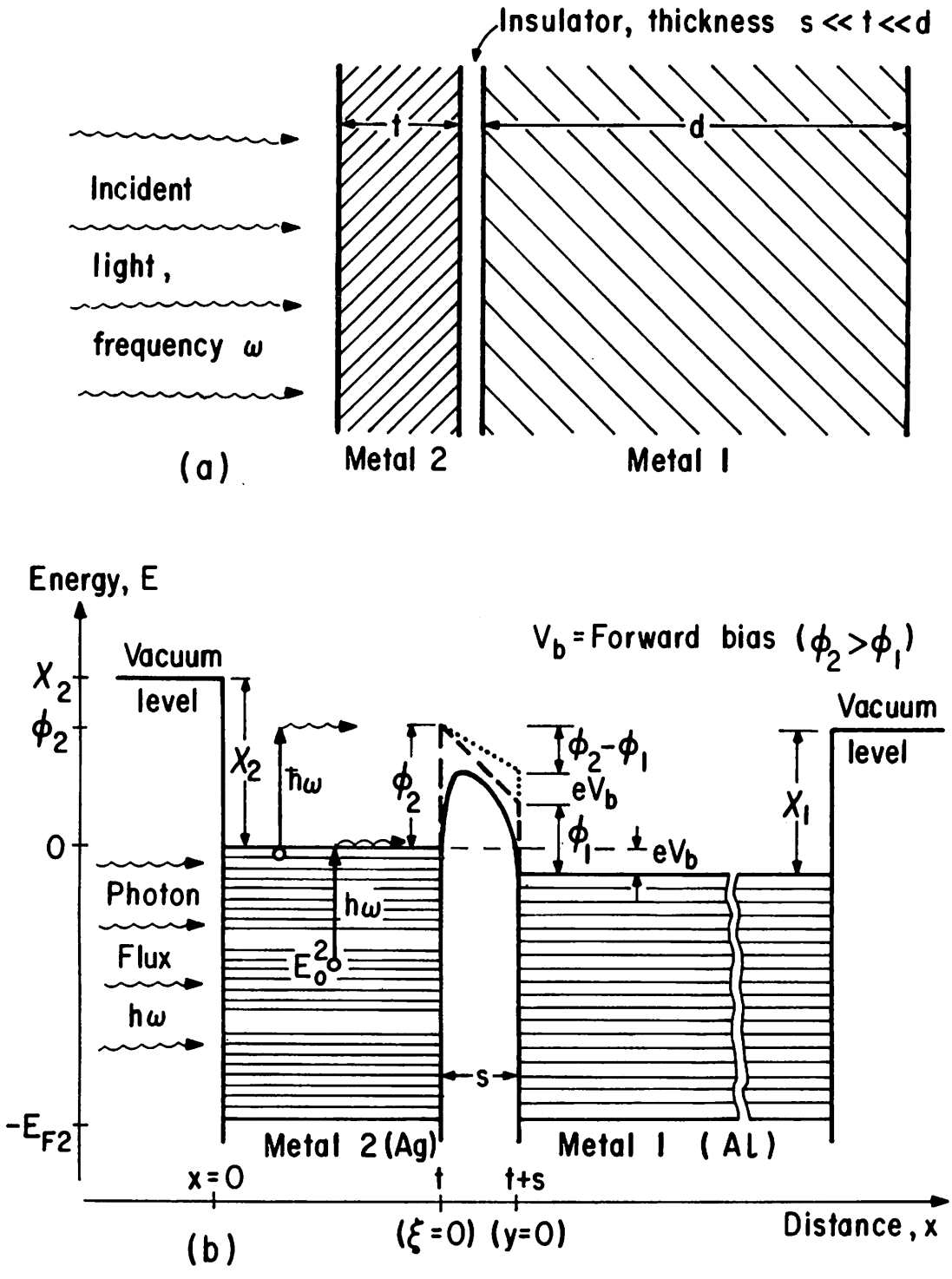

Fig. III-1: (a) Schematic of Metal-Barrier-Metal Geometry

(b) Energy-coordinate diagram of given MBM structure with appropriate energy and distance parameters.

large band gap (e.g., Al_2O_3) and a thin layer (t ~ 300 Å) of metal 2 (e.g., Ag) are successively deposited to yield the M-B-M junction whose energy parameters are displayed in Fig. 1(b).

B.1. Symbols:

The symbols $\hbar$, h, ω, ν, e and c have their usual meanings (as used above), m is used for the effective mass of the electron and i as subscript denotes quantities within each metal (i = 1,2); and i as superscript refers to energy states in metal i (as in the superscript notation of Section I), but with reference to a common zero of energy which is arbitrarily defined to be at the Fermi level of metal 2. The rest of the commonly used symbols are defined briefly as follows:

n_{inc} = Photon flux of incoming radiation, assumed incident on metal 2.

θ = Angle of incidence of incoming radiation.

n_{pi} = Photon flux just inside the surface of each metal i, in the direction of incidence.

t = Thickness of metal 2 (typically 200-400 Å).

$R(\theta,\omega)$ = Reflectivity of metal 2 at frequency ω, for an angle of incidence θ.

s = Thickness of the insulating film (typically 15-30 Å).

x = Distance co-ordinate (left to right) with the origin at the surface of incidence of light on metal 2.

ξ = Distance co-ordinate (left to right) in the barrier with origin at the interface of metal 2 and the insulator. Thus, $\xi = x - t$.

y = Distance co-ordinate (left to right) in metal 1 with origin at the interface of metal 1 and the insulator. Thus, $y = \xi - s = x - (t + s)$.

E_o ≡ Initial energy* of electron, before a transition.

E ≡ Energy* of tunneling electron referred to the arbitrarily defined zero at the Fermi level of metal 2. Clearly $E = E_o + \hbar\omega$.

ϕ_i = Barrier height at interface of metal i (in the "abrupt barrier" model).

ψ_i = Work function of metal i .

$\Delta\phi$ = $\phi_2 - \phi_1 = \psi_2 - \psi_1$ [Assumed: $\phi_2 > \phi_1$]

J_{ij} = Tunneling current density <u>from</u> metal i to metal j.

$R_i(E)dE$ = Rate of tunneling (no. of electrons/sec/area) at an energy E from metal i.

$G_i(E)dE$ = Total rate/unit area at which electrons are excited to energies between E and E + dE.

$D(E)$ = Probability of transmission through the barrier for an electron with energy E.

$\phi(\xi)$ = Potential barrier with necessary image force contributions.

---

* Subscripts or superscripts <u>i</u> will be used whenever precise distinctions between the metals or explicit comparison with the zero reference needs to be made. However, in most instances these will be dropped for simplicity.

$\xi_i(E)$ = Classical turning points (near metal i) in the potential barrier $\phi(\xi)$, for electrons at level E.

$\Delta\xi(E) = \xi_2(E) - \xi_1(E)$.

$\alpha_i(\omega)$ = Total absorption coefficient of metal i at frequency ω (typically ~ 10^6 cm^{-1}).

$\alpha_{\omega i}(E)dE$ = Portion of the absorption coefficient $\alpha_i(\omega)$ at frequency ω that is due to transition from initial states around $E_o = E - \hbar\omega$ to final states around E. Thus $\alpha_i(\omega) \triangleq \int_o^\infty \alpha_{\omega i}(E)\, dE$.

$W_i(E,\omega)$ = Quantum mechanical transition rate from states at E_o to states at $E = E_o + \hbar\omega$. Thus[6]

$$\alpha_\omega(E) = \frac{\varepsilon(\omega)\ W\ (E,\omega)}{n(\omega)c}$$

$\delta_i(\omega) = (\alpha_i(\omega))^{-1}$, is the penetration depth of light (at ω).

$\ell_{ei}(E)$ = Mean free path (MFP) of electrons (with energy E) in metal i due to electron-electron interactions, (typically several thousand Ångstroms). These "collisions" are generally very inelastic.

$\ell_{pi}(E)$ = MFP due to electron-phonon interactions (typically $\gtrsim$ 500 Å at E_F). These collisions are nearly perfectly elastic.

$L_i(E)$ = Total MFP due to both electron-electron and electron-phonon interactions. This is the "effective" MFP (typically $\lesssim 500$ Å), and is used for transport considerations in the present calculations.

$\mathcal{N}_i$ = Total conduction electron density in metal i.

$\mathcal{N}_i(E)$ = Effective density of electrons at energy E.

$v(E)$ = Effective velocity component of an electron in the direction of the barrier (x-direction).

Besides the above symbols, a few more will be introduced in the following discussion when necessary. Also, several trivial relations follow directly from the definition of the above quantities. Some of these are:

$$n_{p2} = n_{inc} R(\theta,\omega)$$

$$E^i = E_o{}^i + \hbar\omega$$

$$R_i(E) = G_i(E)\, D(E) \tag{1}$$

$$\alpha_i(\omega) = \int_o^\infty \alpha_{\omega i}(E)\, dE = \frac{4\pi\sigma_i(\omega)}{n(\omega)c}$$

$$J_{ij} = e\int R_i(E)\, dE = e\int G_i(E)D(E)\, dE \tag{2}$$

B.2 "Forward direction" Convention

As in Simmons,[7] the forward characteristic is defined when the metal with the lower work function (χ) is positively biased.* Thus, the applied bias (Aℓ positive) shown in the Ag-$A\ell_2O_3$ - Aℓ structure of Fig. 1(b) corresponds to forward bias, since the work function of Aℓ ($\chi_{A\ell}$ ~ 4.20 eV) is lower than that of Ag (χ_{Ag} ~ 4.73 eV), as may be seen from the work function data in Sec. II, Table 2. Also, since most of the light absorption (and consequently photo-excitation) in the present geometry occurs in the thin "top" layer of Ag, subsequent tunneling of these photo-excited electrons into the Aℓ "electrode"will be enhanced when Aℓ is biased positive. Thus, the direction of forward bias will yield much larger tunneling currents and is of greater practical interest in the present discussion.

It should also be noted that in Fig. 1 the metal (Aℓ) with the lower work function has been designated as metal 1 in agreement with Simmons' notation; however, in contrast to that reference, metal 1 in this discussion is on the right. This results in a slightly different form for the potential barrier, as seen in Eqs. (11) and (12) below.

---

* According to this convention, the forward bias increases the field in the insulator whereas the reverse bias opposes the built-in potential (ϕ_2-ϕ_1). This is apparent in Fig. 1 from the shape of the unbiased trapezoidal (abrupt barrier model, ignoring image potential) barrier, and its modification by the forward bias V_b.

C. TUNNELING MODEL - PRINCIPAL ASSUMPTIONS:

The light-induced tunneling current is assumed to be essentially due to a semi-classical three-step process: (1) the absorption of light in the volume of metal 2, resulting in the eventual excitation of electrons (at each point x) from states below the Fermi level to states above it ; (2) the transport of these photo-excited electrons to the barrier; and finally, (3) the transmission of these electrons through the barrier with a much higher probability than in the absence of the photo-excitation. This assumption essentially attempts to reduce the exact quantum mechanical problem to three distinct and decoupled semi-classical processes. A similar model[8] has been used in the study of photo-emission, and results in a good theoretical approximation to the experimental energy distribution curves of electrons photo-emitted by the noble metals.[9] Some important aspects of such a three-step model applied to photo-assisted tunneling are discussed below.

C.1. Electron excitation due to absorption of light:

In contrast to the earlier tunneling analyses[3,4] that attribute detected tunneling signals to a modulation of the Fermi levels, the present work assumes that the optical excitation occurs due to electron excitations from states of energy E_o to states $E_o + \hbar\omega$. These single electron transitions are either induced (i) directly by incoming photons, or (ii) via plasma excitations. Since essentially only single electron excitations occur at optical frequencies far from ω_p, whereas near ω_p plasma

excitations can predominate, the two cases may be analyzed separately as will be done in the next section. One essential difference in these two methods of optical excitation is that for the single electron excitation (e.g. interband absorption), the excitation decays exponentially along the direction of incidence, whereas the plasma resonance absorption results in excitations that are essentially distributed uniformly over the thickness of the film. In deriving expressions for the absorption, additional assumptions are made for both of the above cases.

C.1.a. Single electron excitations

At frequencies ω far away from ω_p, the absorption $\alpha(\omega)$ is essentially due to a continuum of interband or intraband transitions from initial energy levels E_o to final levels at $E = E_o + \hbar\omega$. Thus the total absorption coefficient $\alpha(\omega)$ is due to a continuum of 'partial absorption' coefficients $\alpha_\omega(E)$, between all the various states in the bands, such that $\alpha(\omega) = \int_o^\infty \alpha_\omega(E)\, dE$. However since the tunneling probability (and in cases of large $\hbar\omega$, the electron mean free path for considerations of electron transport to the barrier) is strongly dependent on the final energy of the excited electrons, an estimate for the partial absorption coefficients $\alpha_\omega(E)$ is quite important. This can be expressed as

$$\alpha_\omega(E) = \frac{W(E,\omega)\ \epsilon_1(\omega)}{n(\omega)\ c} \qquad (3)$$

by direct analogy with the absorption coefficient α_{ij} for the two-level case,[6] viz.

$$\alpha_{ij} = \frac{W_{ij}\epsilon_1}{nc} . \tag{4}$$

In the above expressions, W_{ij} is the quantum-mechanical transition rate from state Q_i to state Q_j (i.e. from level i to level j) under the presence of the usual dipole perturbation $H' = \frac{1}{m}(\bar{A}.\bar{p})(e^{i\omega t} + e^{-i\omega t})$ and is given by[10]

$$W_{ij} = \frac{2\pi}{\hbar} |V_{ij}|^2 \delta(E_{ji}-\hbar\omega) \tag{5}$$

where $V_{ij} = \langle\phi_i|H'|\phi_j\rangle$.

Equation (5) is just a special case of Fermi's Golden rule which is generally expressed as[11]

$$W_{ij}(E_j) = \frac{2\pi}{\hbar} |V_{ij}|^2 \rho(E_j) \tag{6}$$

for the transition rate from a discrete level i to a continuum of levels j. In the above expression it has been assumed that the matrix elements $|V_{ij}|^2$ are sufficiently independent of E_{ij} . Once again one can extend the above expressions (5) and (6) to the case where <u>both</u> the initial and final states lie within bands (i.e. in continuum of states). For such a case the <u>partial</u> transition rates are given by

$$W(E,\omega) = \frac{2\pi}{\hbar} |V_{ij}|^2 \rho(E_i) \rho(E_j) \tag{7}$$

If one assumes that the matrix elements V_{ij} do not vary much

throughout the bands i and j , then one can define an effective mean quantum mechanical transition rate for any photon energy $\hbar\omega$:

$$\bar{W}(\omega) \triangleq \int_{E_1}^{E_1+\hbar\omega} W(E,\omega)\, dE = \frac{2\pi}{\hbar} |V_{ij}|^2 \int_{E_1}^{E_1+\hbar\omega} \rho(E-\hbar\omega)\, \rho(E)\, dE \qquad (8)$$

Note that the limits E_1 and $E_1+\hbar\omega$ suffice for consideration of interband transitions between two distinct bands. These limits could be extended to zero and infinity for generality; however in such a case $|V_{ij}|^2$ would depend considerably on energy and cannot be pulled out of the integral. With the above approximation, known as the constant matrix elements approximation in band structure discussions and photoemission literature,[9] one can write the interband absorption coefficient as

$$\alpha(\omega) = \frac{\bar{W}(\omega)\, \varepsilon_1(\omega)}{n(\omega)c} = \frac{2\pi\, \varepsilon_1(\omega)\, |V_{ij}|^2}{\hbar c n(\omega)}\, J(E_1,\omega) \qquad (9)$$

$$\text{where } J(E_1,\omega) = \int_{E_1}^{E_1+\hbar\omega} \rho(E-\hbar\omega)\rho(E)\, dE \qquad (10)$$

is called the "joint-density-of-states" function.

It should be noted that in Eqs. (7) to (10), momentum or $\bar{k}$-conservation has been ignored. If the wave-functions for the initial and final states are well extended (e.g. if they are well described by Bloch functions), over the volume of the crystal, then $\bar{k}$-conservation is very important, and the matrix elements W_{ij} vanish if $\bar{k}_i \neq \bar{k}_j$.

This is the well-known case of direct transitions in semiconductors. However in the noble metals (Cu, Ag, etc.), the valence states (subscript i) are highly localized d-band states, and consequently the selection rule on $\bar{k}$ for these transitions can be relaxed, leading to the non-direct model.[12] Eqs. (7) to (10) apply very well for the non-direct model, which has been shown to describe photoemission results for Ag and the other noble metals quite adequately.[9]

C.1.b. Collective electron excitations

At frequencies near the plasma frequency of the top metal, the absorption of radiation due to plasma excitations might predominate, as will be the case when the incident radiation couples efficiently to either the antisymmetric surface plasma modes of the thin metallic film, or when the dispersion relation and boundary conditions of the metallic film favor establishment of a resonance bulk plasma mode. This has been adequately discussed in Sec. II.C. for the case of a thin unsupported film of a metal, i.e. with vacuum (air) on either side of the "metallic slab." In the present case, the above ideal conditions are perturbed by the presence of the extremely thin insulator ($A\ell_2O_3$) and the base or "probe" metal (Aℓ) on one side of the resonantly excited Ag film. However since the optical constants of such a substrate (the combination of $A\ell_2O_3$ and Aℓ) do not vary significantly over the linewidth of the usual optical plasma absorption of the Ag film, the effect of this substrate is negligible, and will be ignored in the present work. This assumption is further justified by the work of Lindau and Nilsson,[13] whose computer calculations

indicate that the effect of a lossy substrate is to just broaden the resonance peaks slightly (i.e. increase the damping).

C.2. Geometry and transport considerations

The second step in our three-step model of photon-assisted tunneling is that in which the photo-excited electron moves to the tunneling barrier. After photo-excitation the electron will generally have a random velocity, but subsequent scattering events might cause it to have a net motion towards the barrier. We will attempt to ignore all the scattering detail and parametrize this complex transport process by simple "collisional lengths" or "mean free paths" between collisions, for a discussion of the net motion in the desired (x) direction.

The two most important scattering processes are (a) electron-electron scattering and (b) electron-phonon scattering. Electron-electron scattering is a highly inelastic process, causing an electron to suffer a significant loss of energy. However, this process is important only when the energy of the "primary" electron is large, i.e. well above the Fermi level. Typical mean free paths ℓ_e for Ag (and similarly for Au and Cu) are well above 10,000 Å for electron energies at the Fermi level,[14-16] whereas they are of the order of 100 Å for electrons 4eV above the Fermi level.[16]

For Ag, the photon energy at which photo-excitation becomes significant is approximately 4eV, corresponding to the onset of interband absorption in both the $L_3 \rightarrow L_2'$ and the L_2' to L_1 transitions,[17,18] which yield respectively, final states at the Fermi level (L_2') and approximately 4eV above it (the L_1 states). However since the $L_3 \rightarrow L_2'$ transition is known to be much stronger than the L_2' to L_1 transition,[19] most of the photo-excited electrons will be in final states just above the Fermi level of Ag. Clearly for these electrons (especially for film thicknesses less than 1000 Å), the inelastic electron-electron scattering is negligible and may generally be ignored. However it is precisely in such a circumstance that the second type of scattering viz. electron-phonon scattering becomes important.

Optical phonon scattering is essentially an elastic scattering process since the phonon energy E_p is negligible compared to even the "low energy" Fermi-level electrons. The mean free path ℓ_p for electron-phonon collisions is typically of the order of 500 Å for Fermi level electrons in the noble metals,[14,20] and decreases with increasing electron energy. Electron-phonon collisions essentially result in randomizing the motion of the electrons without any significant loss of energy. In the present context (see Fig. 1) if $t << \ell_e$ and if the scattering of the electrons at the film surfaces is assumed elastic, then an important consequence of electron-phonon scattering is that effectively all the photo-excited electrons approach the barrier perpendicularly at some time or the other during their multi-collisional motion. However, since the net distance travelled by the electron increases, the

probability of an electron-electron collision also increases, and for net motion in any particular direction, one must consider a total mean free path L, determined both by ℓ_p and ℓ_e. This total mean free path effectively determines the attenuation length of an electron's energy due to scattering, and is best calculated by Monte Carlo methods.[20,21] Figure 2 (due to ref. 20) shows a plot of ℓ_e, ℓ_p and L versus electron energy E for Ag; this indicates a mean free path L of approximately 600 Å for Ag at $E = E_F$.

Obviously, the geometry of the photoexcited volume and its distance from the barrier are matters of prime concern in a discussion of electron transport. We will assume the geometry of Fig. 1, with $1/\alpha \lesssim t \lesssim L$, i.e., the film thickness t is larger than the absorption depth $1/\alpha$ of the medium, but smaller than the total mean free path L. Note that for free electron or intraband absorption, the condition $1/\alpha < L$ implies either the anomalous or extreme anomalous skin effect.[22] However, for the present case of interband transitions, the absorption still corresponds to the usual $1/\alpha$ penetration depth, and will therefore be treated as 'normal' in our three-step model. Also since t is larger than $1/\alpha$, for such frequencies one can assume that the reflection coefficient of the Ag film is essentially that of the bulk metal. For the small amount of residual light that reaches the barrier (and the other metal, Aℓ), reflections at the barrier are ignored and photo-excitation in Aℓ is computed with the appropriate absorption coefficient integrated from $x = t+s$ to $x = d$ or $x = \infty$. With the given geometry, the tunneling current from metal 1 (Aℓ) to metal 2 (Ag) will be negligible, not only because of the much

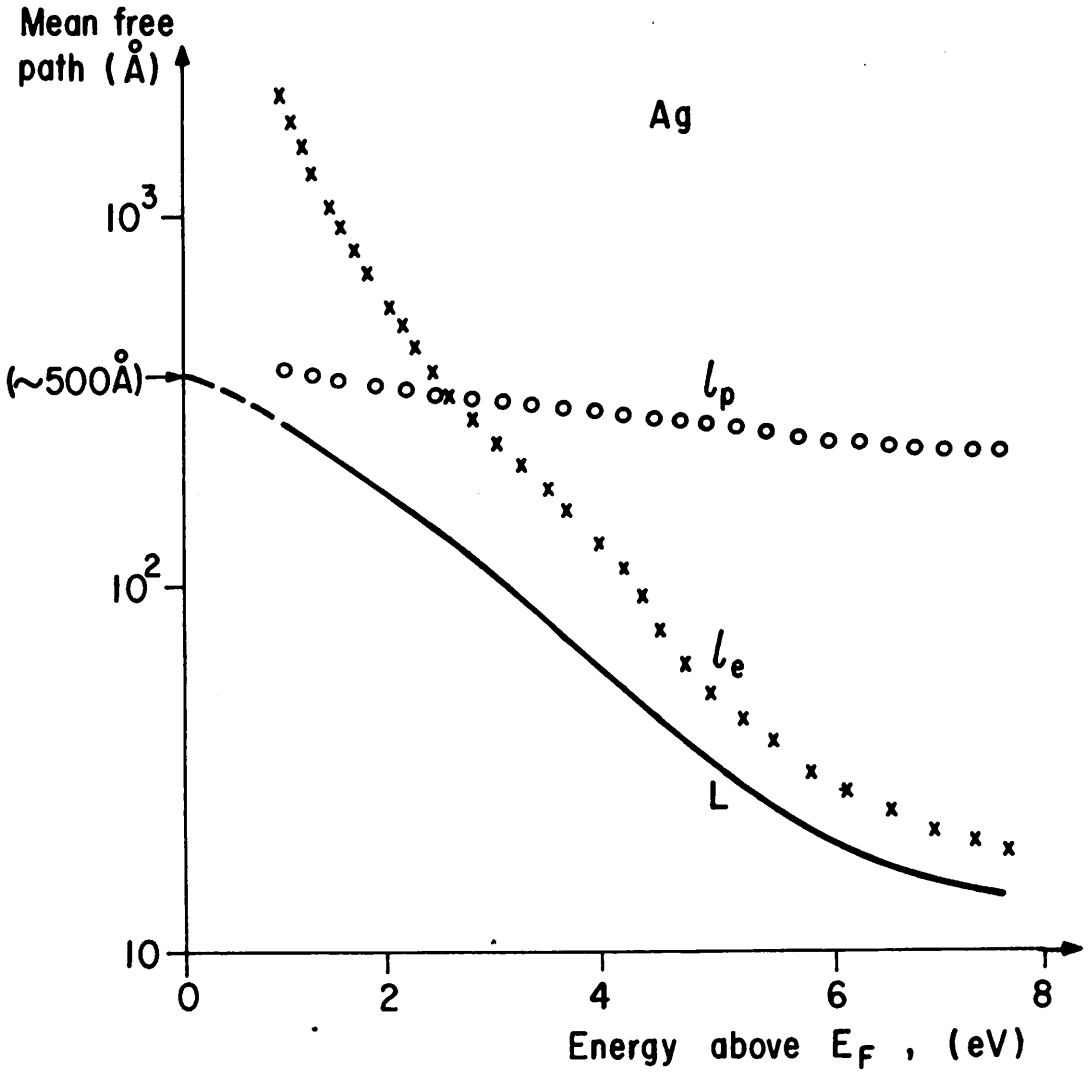

Fig. III-2: Mean free path data for Ag, essentially due to Kanter (Ref. 20).

smaller photo-excitation and lower tunneling probabilities (reduced by the forward bias), but also because of transport considerations. Only a negligible fraction of the electrons excited in metal 1 will have a significant component of velocity perpendicular to the barrier, and most will decay energetically due to electron-electron collisions before being scattered in the right direction, in contrast to the case for the thin film of metal 2, where $t << \ell_e$. This fact can be incorporated in the expressions for the electron excitation rate at the barrier by inclusion of an additional scattering parameter Λ , which may be assumed to have the values of 1/2 and 1 in metals 1 and 2 respectively.

C.3 Potential barrier and transmission probability

The two steps discussed above lead to a photo-excited electron having reached the barrier. The final step in the three-step model involves the tunneling of this electron through the barrier, and this involves assumptions in (a) the potential barrier, and in (b) the transmission probability.

(a) The potential barrier $\phi(\xi)$ may be assumed to be described essentially by the image-force corrections on a constant dielectric medium (the insulator), as proposed by Simmons.[7] In this approximation, the presence of impurity levels and the possibility of photo-excitations within the barrier will be ignored. Thus, the conduction band of the insulator is assumed to do nothing more than lower the effective work function (and therefore the barrier height). Also as in Simmons' work,[7] the transit of the electron within the barrier

is assumed to be well-described by the effective mass approximation. Thus, specific band structure effects,[23] and the variation of the energy-momentum relationship in the insulator[23,24] are ignored. This is justified if the bias voltages are small compared to the insulator band gap,[25] and if the energies of the tunneling electrons do not vary much compared to the width of the gap. This last condition is adequately satisfied when the final energies of the photo-excited electrons are in the vicinity of the Fermi level of the metal, as is true for Ag.

Thus we essentially have an independent electron model of tunneling, where the potential barrier is essentially described by Simmons' expressions[26] as

$$\phi_F(\xi) \approx \phi_2 - (\Delta\phi + |eV_b|)(\xi/s) - 2.86s/K\xi(s-\xi) \qquad (11)$$

and

$$\phi_R(\xi) \approx \phi_2 - (\Delta\phi - |eV_b|)(\xi/s) - 2.86s/K\xi(s-\xi) \qquad (12)$$

for the forward and the reverse biases respectively. Here the units of energy are in electron-volts, the units of distance are in Angstroms, V_b is the applied bias voltage, K is the effective dielectric constant of the insulator, and all the other symbols are as defined earlier.

(b) The transmission probability for an electron at energy E is assumed to be given by an extension of the usual semi-classical WKB approximation.[27] According to this generalized formula, due to Miller and Good,[28] the transmission coefficient D(E) for an electron

at energy E is given by:

$$D(E) = \left\{1 + \exp\,[2Q(E)]\right\}^{-1} \tag{13a}$$

$$\text{where} \quad Q(E) = \int_{\xi_1(E)}^{\xi_2(E)} \kappa(\xi, E)\, d\xi \tag{13b}$$

$$\text{and} \quad \kappa(\xi,E) = \left[2m(\phi(\xi)-E)/\hbar^2\right]^{1/2} \tag{13c}$$

ξ_1 and ξ_2 are the classical turning points. The advantage of the Miller-Good approximation (Eq. 13) for the transmission coefficient over the usual WKB approximation, is that it is valid even for the case when the energy of the electron is greater than the height of the barrier, which may be the case for the small fraction of electrons excited into the L_1 band in our present tunneling problem. Note that it is assumed that the energy E of the electron corresponds essentially to the kinetic energy of a free electron travelling perpendicular to the barrier, and that effects of non-perpendicularity have been accounted for by a modified mean free path L in the transport considerations.

C.4 Miscellaneous details

One more point may be noted. For frequencies close to the plasma resonance, it is very likely that the collective electron oscillations will contribute to the tunneling current by means of an oscillatory perturbation similar to the one described by a Fermi-level modulation.[3] Note that this is not a new source of energy contributing to the tunneling current, but is an interaction that might result in tunneling characteristics quite different

from those caused by the excitation mechanism discussed earlier. The magnitude of this modulation is determined by the field strength $\overline{E} = 4\pi Ne(\delta x)$, where δx is the amplitude of the plasma oscillations and N represents the electronic density.

D. EXPRESSIONS FOR THE TUNNELING CURRENT

D.1. Single electron excitations, normal incidence

In accordance with the notation and conventions* of Section III.B and the assumptions of Section III.c, $G_2(E,\omega)dE$, the total rate/area at which electrons in metal 2 are excited and transported to the barrier with energies between E and E+dE by radiation at frequency ω, is given by:

$$G_2(E,\omega) = n_{p2} \int_0^t \left\{ \alpha_{\omega 2}(E)\, e^{-\alpha_2(\omega)x} \right\} \left\{ \Lambda_2\, e^{-(t-x)/L_2} \right\} dx \qquad (14)$$

As indicated in Section III.B, n_{p2} is the photon flux (no. of photons/sec-area) just inside the surface of metal 2, and is given by $n_{p2} = n_{inc}\,[1-R(\omega)]$ where n_{inc} is the incident photon flux; the first factor $\{\ldots\}$ in the integrand represents the partial absorption of the light to yield final states at energy E, whereas the second factor $\{\ldots\}$ corresponds to the transport of these excited electrons to the barrier. Λ_2 is the scattering factor that accounts for the loss of excited electrons due to solid angle considerations; and since for the thin film ($t < L_2$),

*Note the addition of subscripts for each metal in this section to the more general expressions of Section III.c.

essentially all the excited electrons reach the barrier due to random multiple scattering, $\Lambda_2 \approx 1$. Using this approximation and performing the above integration, we have:

$$G_2(E,\omega) = n_{p2}\ \alpha_{\omega 2}(E)\ \frac{[e^{-\alpha_2(\omega)t} - e^{-t/L_2}]}{[1/L_2 - \alpha_2(\omega)]} \tag{15}$$

which can be inserted into the expression for the tunneling current density. $J_2(\omega)$ from metal 2 to metal 1. Thus

$$\begin{aligned} J_2(\omega) &= e\int R_2(E,\omega)\ dE \\ &= e\int D(E)\ G_2(E,\omega)\ dE \end{aligned} \tag{16}$$

The tunneling current can now be evaluated by combining Eqs. (3), (7), (13), (15) and (16); however before proceeding to do that, let us examine the expression for the excitation rate $G_2(E,\omega)$ more closely. Neglecting the metal-referencing subscripts, Eq. (15) can be written as:

$$G(E,\omega) = \left[\frac{\alpha_\omega(E)}{\alpha(\omega)}\right] n_p\ f_2(\alpha,L,t) \tag{17}$$

Here, $\alpha_\omega(E)/\alpha(\omega)$ gives the energy distribution of the excited electrons, and the dimensionless quantity

$$f_2(\alpha,L,t) = \alpha L\left(\frac{e^{-\alpha t} - e^{-t/L}}{1 - \alpha L}\right) \tag{18}$$

can be defined as the effective "excitaton parameter". This parameter incorporates both the absorption and transport processes, as can be seen more explicitly by writing $f_2 = f_{abs}\ f_{trans}$

where $f_{abs} = (1 - e^{-\alpha t})$ is the absorption factor and

$f_{trans} = \left(\frac{\alpha L}{1-\alpha L}\right) \cdot \left(\frac{e^{-\alpha t} - e^{-t/L}}{1 - e^{-\alpha t}}\right)$ represents the transport factor. One advantage of defining the excitation parameter is that it permits us to study the relative efficiency of the excitation at the barrier in terms of the relative sizes of $1/\alpha$, L and t. In particular, given values of the absorption coefficient $\alpha(\omega)$ and the mean free path L, the photo-excitations reaching the tunneling junction may be maximized by picking a film thickness t that will maximize $f_2(\alpha,L,t)$.

Let us consider the excitation parameter for the particular case of a Ag film. Depending on sample purity, the total mean free path L is typically between 400 Å and 600 Å. Also, as seen from Fig. 5 of Section II, the absorption coefficient of Ag in the near ultra-violet varies from 10^5 cm^{-1} to 10^6 cm^{-1}, i.e. $1/\alpha$ ~ 100 Å to 1000 Å . Assuming fixed values of t and L, the dependence of the excitation versus frequency will be largely determined by the dependence of f on this frequency-dependent absorption coefficient. Figure 3 shows such a plot of f_2 vs $1/\alpha L$, for the case t = 0.75L.

A specific choice of L = 400 Å makes the curve applicable to the special case of a 300 Å Ag film, with $1/\alpha$ varying from 100 Å (at the maximum of f_2) to 1000 Å. Thus, except for extremely small values of $1/\alpha$ (i.e. $1/\alpha < L-t$), there is a general decrease in the effective excitation with a decrease in the absorption coefficient, as expected.

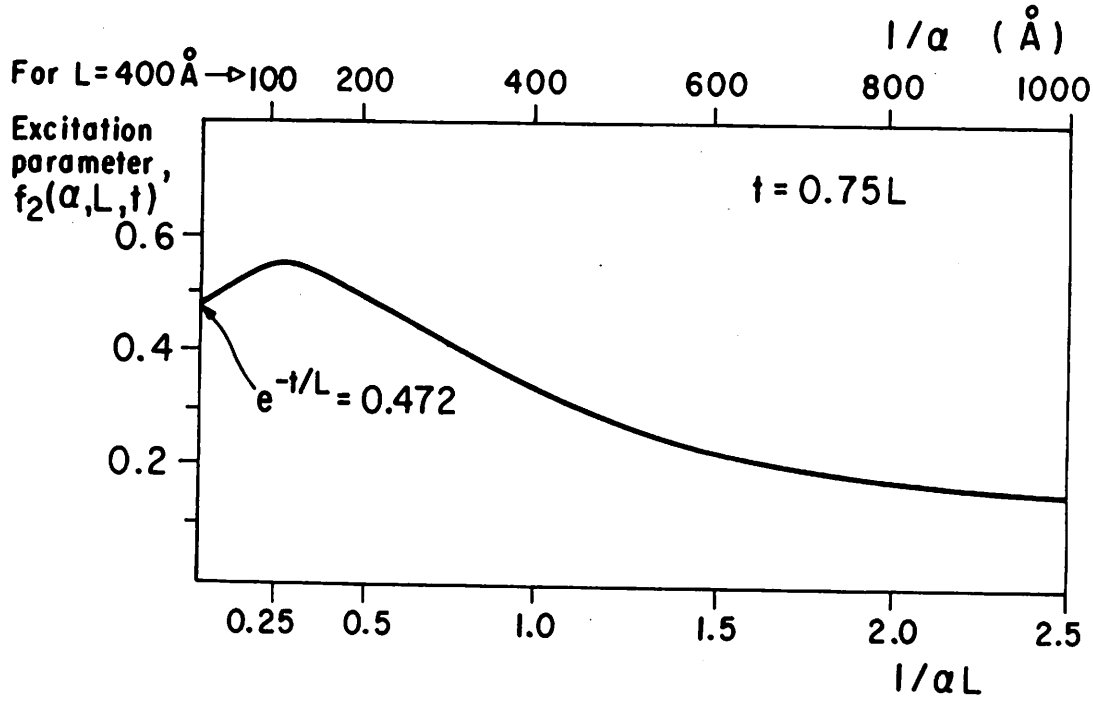

Fig. III-3: Plot of $f_2(\alpha,L,t)$, the excitation parameter in metal 2 versus $1/\alpha L$. It is assumed that the film thickness t is such that t = 0.75L. Also as seen above for a choice of L = 400 Å , the penetration depth $1/\alpha$ covers the entire range of experimental values for Ag in the visible and near ultraviolet.

Another case of interest is the maximization of the excitation for a specific frequency (i.e. for a given value of α, assuming L is fixed) by a suitable choice of film thickness. Setting df_2/dt to zero gives the optimum value of film thickness as $t_{opt} = L\ \ell n\ (\alpha L)/(\alpha L-1)$. Thus, for $L \approx 500$ Å and $\alpha \approx 4\times10^5\ cm^{-1}$ (i.e. $1/\alpha \approx 250$ Å), the optimum film thickness would be $t_{opt} \simeq 350$ Å. For such a case, $f_2 \simeq 0.5$, which may in turn be decomposed to an absorption factor (f_{abs}) of ~ 0.75 and a transport factor (f_{trans}) of ~ 0.66. It can also be noted that for all the values of α, L and t of interest, the excitation parameter is of the order of unity (order of magnitude).

Assuming that the excitation factor has been appropriately optimized, let us return to the problem of evaluating the tunneling current. Combining Eqs. (16) and (17), we have

$$J_2(\omega) = \frac{en_{p2}f_2(\alpha,L,t)}{\alpha_2(\omega)} \int_0^\infty D(E)\ \alpha_{\omega 2}(E)\ dE \qquad (19)$$

Considering the Fermi occupancies, the partial absorption coefficient of Eq. (3) gets modified to:

$$\alpha_{\omega 2}(E) = \frac{W_2(E,\omega)\ p_2(\omega)}{c}\ F(E_o)\ [1 - F(E)] \qquad (20)$$

where $E_o = E - \hbar\omega$, F(E) is the Fermi function and the dimensionless quantity $p(\omega)$ is <u>defined</u>* as $p(\omega) \equiv \varepsilon_1(\omega)/n(\omega)$.

---

* This definition is introduced primarily to avoid a possible source of confusion when the metal-referencing subscripts 1 and 2 are added to $\varepsilon_1(\omega)$, the real part of the dielectric constant.

Combining Eqs. (19) and (20), the expression for the tunneling current at $0^{o}K$ is given by:

$$J_2(\omega) = \frac{en_{p2}f_2(\alpha_2,L_2,t)p_2(\omega)}{\alpha_2(\omega)c} \int_{E_1}^{E_2} D(E)W_2(E,\omega)dE \qquad (21)$$

The limits of integration E_1 and E_2 in the above expression are generally determined by the Fermi function in <u>both</u> the metals. In other words, one must take into account the fact that neither an optical transition nor a tunneling transition can occur into a state that is already occupied. Thus, the lowest level in metal 2 to which an optical transition can occur is just above its Fermi level. And for the forward bias condition, the Fermi level of metal 1 is depressed with respect to metal 2; so the tunneling transition does not impose any additional restrictions. Consequently, for the forward bias the lower limit of integration E_1 corresponds to the Fermi level of metal 2, which has also been arbitrarily designated as zero in the present context. Similarly the highest state to which a transition is possible will just be $\hbar\omega$ above the highest occupied state. Thus $E_2 \equiv \hbar\omega$. So J_{2F}, the tunneling current density from metal 2 to metal 1, in the presence of a small forward bias is given by:

$$J_{2F}(\omega) = A_2(\omega) \int_{o}^{\hbar\omega} D_F(E)\ W_2(E,\omega)\ dE \qquad (22)$$

$$\text{where } A_2(\omega) \equiv \frac{en_{p2}f_2(\alpha_2,L_2,t)\ p_2(\omega)}{\alpha_2(\omega)\ c} \qquad (23)$$

and $D_F(E)$ is obtained from Eq. (13) by replacing $\phi(\xi)$ with the forward bias potential $\phi_F(\xi)$ (See Eq. (11)).

Similar expressions can be obtained for the other tunneling current densities viz. J_{2R}, J_{1F} and J_{1R}, where the subscripts 1 and 2 refer to the metal from which the current flows, and the subscripts F and R denote the forward and reverse bias conditions. However, great care must be taken with consistency in the zero reference of energy wherever energy occurs as an independent variable, and in determining the limits of integration in light of the above Fermi-occupancy restrictions. Thus we have:

$$J_{2R}(\omega) = A_2(\omega) \int_{|eV_b|}^{\hbar\omega} D_R(E)\, W_2(E,\omega)\, dE \tag{24}$$

and similarly the currents corresponding to photo-excitations in metal 1 are given by *

$$J_{1F}(\omega) = A_1(\omega) \int_{0}^{\hbar\omega - |eV_b|} D_F(E)\, W_1'(E,\omega)\, dE \tag{25a}$$

and

$$J_{1R}(\omega) = A_1(\omega) \int_{|eV_b|}^{\hbar\omega + |eV_b|} D_R(E)\, W_1'(E,\omega)\, dE \tag{26a}$$

---

* Assuming that $|eV_b| < \hbar\omega$. Ideally, we should have $|eV_b| \ll \hbar\omega$ for consistency with the assumptions on the electron-transition in the insulator.

where $$A_1(\omega) \equiv \frac{e\, n_{p1}\, f_1(\alpha_1, L_1, d)\, p_1(\omega)}{\alpha_1(\omega)\, c} \tag{27}$$

Note that $f_1(\alpha_1, L_1, d)$, the excitation factor in metal 1 will have a form that is quite different from the one in metal 2, and should also include a scattering factor Λ of 1/2; nevertheless, the method of deriving $f_1(\alpha,L,d)$ is essentially illustrated in the discussion of $f_2(\alpha,L,t)$. Also the transition probability $W_1'(E,\omega)$ is essentially expressed with respect to a zero at the Fermi level of metal 1. Let E' represent the range of energies corresponding to a zero defined at the Fermi level of metal 1. Then, the usual transition probability in metal 1 is given by Eq. (7) as

$$W_1(E',\omega) = \frac{2\pi}{\hbar}\left\{|V_{ij}|^2\right\}_1 \rho_1(E'-\hbar\omega)\, \rho_1(E')$$

where the density of states $\rho_1(E')$ are also expressed in terms of the same zero reference of energy. Thus in Eq. (25a), $W_1'(E,\omega) \equiv W_1(E',\omega)$. Also, as seen from Fig. 4, E and E' are related by $E' = E + eV_b$, where V_b will be positive for forward bias and negative for reverse bias. If the variable of integration in Eqs. (25a) and (26a) are replaced by $E' = E + eV_b$, i.e., the quantities in the integrand are expressed in terms of a zero at the Fermi level of metal 1, we have

$$J_{1F}(\omega) = A_1(\omega) \int_{|eV_b|}^{\hbar\omega} D_F(E' - |eV_b|)\, W_1(E', \omega)\, dE' \tag{25b}$$

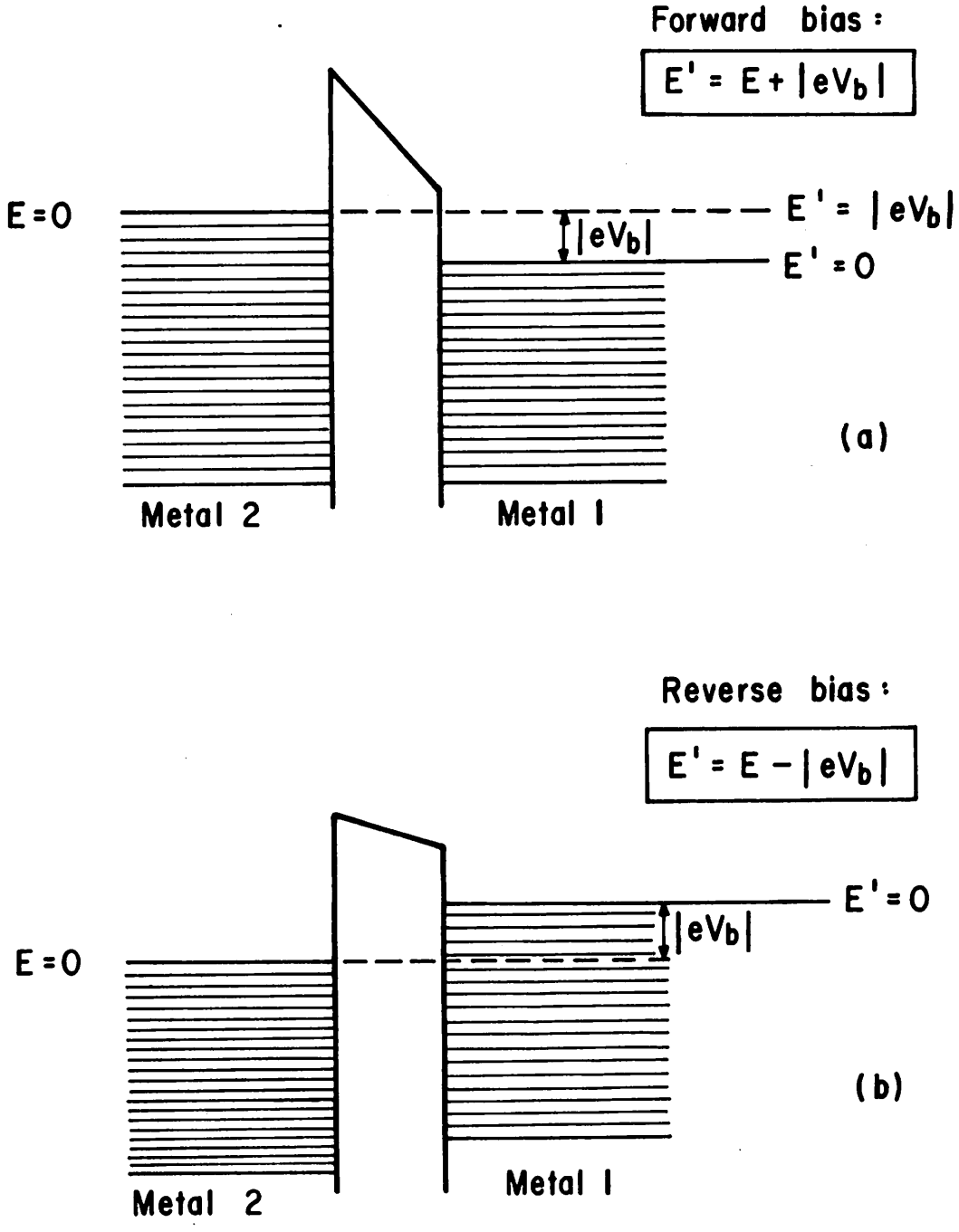

Fig. III-4: Illustration of the basic relation between E' and E, the energy variables with origin at the Fermi levels of metal 1 and 2 respectively: (a) Forward bias; (b) Reverse bias. Thus, for either bias $E' = E + eV_b$.

and

$$J_{1R}(\omega) = A_1(\omega) \int_0^{\hbar\omega} D_R(E' + |eV_b|)\, W_1(E',\omega)\, dE' \qquad (26b)$$

In the present form, Eqs. (25) and (26) show a strong similarity with Eqs. (24) and (22) as expected, the only difference being in the forms of the transmission coefficients. This is obviously due to the fact that they are still expressed in Eqs. (25) and (26) in terms of "the energy zero of metal 2" although the other quantities in these equations are expressed with respect to "the energy zero of metal 1". In the above expressions it has been assumed throughout that $|eV_b| < \hbar\omega$.

Thus the <u>net</u> tunneling current densities for currents from metal 2 to 1 are given by

$$\left\{J_{21}(\omega)\right\}_F = J_{2F}(\omega) - J_{1F}(\omega)$$

and

$$\left\{J_{21}(\omega)\right\}_R = J_{2R}(\omega) - J_{1R}(\omega) \quad ,$$

where each of the currents J_{2F}, J_{1F}, J_{2R} and J_{1R} are as expressed in Eq. (22) through (26). Since the treatment for each of these quantities is essentially the same, we will focus our attention on $J_{2F}(\omega)$ for the rest of this discussion. This is also the dominant term in the forward bias case and is much larger than the reverse current densities for comparable magnitudes of forward and reverse bias. Thus, assuming forward bias and using Eq. (7) for $W_2(E,\omega)$, Eq. (22) can be written as:

$$J_{2F}(\omega) = \frac{en_{p2}\, f_2(\alpha_2, L_2 t)\, B_2(\omega)\, |V_{ij}|^2}{\alpha_2(\omega)} \int_0^{\hbar\omega} D_F(E)\rho_2(E)\rho_2(E-\hbar\omega)dE \qquad (27)$$

where $B_2(\omega) \equiv \frac{2\pi}{\hbar}\frac{p_2(\omega)}{c}$ (28)

However, by Eqs.(9) and (10), $\alpha_2(\omega)$ can be written as

$$\alpha_2(\omega) = B_2(\omega)\, |V_{ij}|^2 \int_0^{\hbar\omega} \rho_2(E)\,\rho_2(E-\hbar\omega)\, dE \qquad (29)$$

Thus, the forward current density is given approximately by:

$$J_{2F}(\omega) = en_{p2} f_2(\alpha_2, L_2, t) \frac{\int_0^{\hbar\omega} D_F(E)\,\rho_2(E)\,\rho_2(E-\hbar\omega)\, dE}{\int_0^{\hbar\omega} \rho_2(E)\,\rho_2(E-\hbar\omega)\, dE} \qquad (30)$$

If we define the quantity

$$\overline{D(\omega)} = \frac{\int D(E)\,\rho(E)\,\rho(E-\hbar\omega)\, dE}{\int \rho(E)\,\rho(E-\hbar\omega)\, dE} \qquad (31)$$

as the "average transmission coefficient", then Eq. (30) becomes simply:

$$J_{2F}(\omega) = en_{p2} f_2(\alpha_2, L_2, t)\, \overline{D_{2F}(\omega)} \qquad (32)$$

and similar equations can easily be derived for the other current densities.

The density of states for several metals (including Ag) have been calculated[29] to a high degree of accuracy in recent years from

the theoretical (confirmed indirectly experimentally) band structures of these metals. Figure 5 shows a plot of the density of states versus energy for Ag, as calculated recently by Christensen.[30] Thus by using numerical integration techniques first to determine $D_F(E)$ from Eqs. (11) and (13) and then to determine $\overline{D(\omega)}$, a relatively accurate plot of the current density versus photon energy can easily be obtained. However in the present context we will just attempt an order-of-magnitude estimate of the expected current density and the consequent photo-induced voltage for a specific tunneling condition.

Consider for instance, the planar Ag-$A\ell_2O_3$-$A\ell$ structure of Fig. 1 with $t \approx 300$ Å, $s \approx 20$ Å and junction area $\approx 10^{-2}$ cm^2. This could be fabricated easily in a cross-stripe geometry: a 1 mm wide stripe of a relatively thick layer of $A\ell$ can be evaporated, plasma oxidized and covered with a 300 Å thick stripe (of the same width running in a perpendicular direction. Let us assume that this is uniformly irradiated with an incident intensity of 1 $Watt/cm^2$ of ultraviolet light at $\hbar\omega \approx 4$eV. Assuming that the specific photon energy corresponds to a reflectivity of 99%, we have $n_p \approx 0.01\, n_{inc} \approx 1.6\times10^{16}$ photons/sec-cm^2. Next let us make some simplifying assumptions on the exact form of the density of states $\rho(E)$ and the transmission coefficient $D(E)$. The density of states may be replaced by a piece-wise linear or step approximation, as shown in Fig. 6(a). In this approximation, it is clear that the most significant contribution per unit energy interval to both integrals in Eq. (32) occurs in the energy range $0 < E < 0.2$eV corresponding to the critical point for the $L_3 \rightarrow L_2'$ transition.

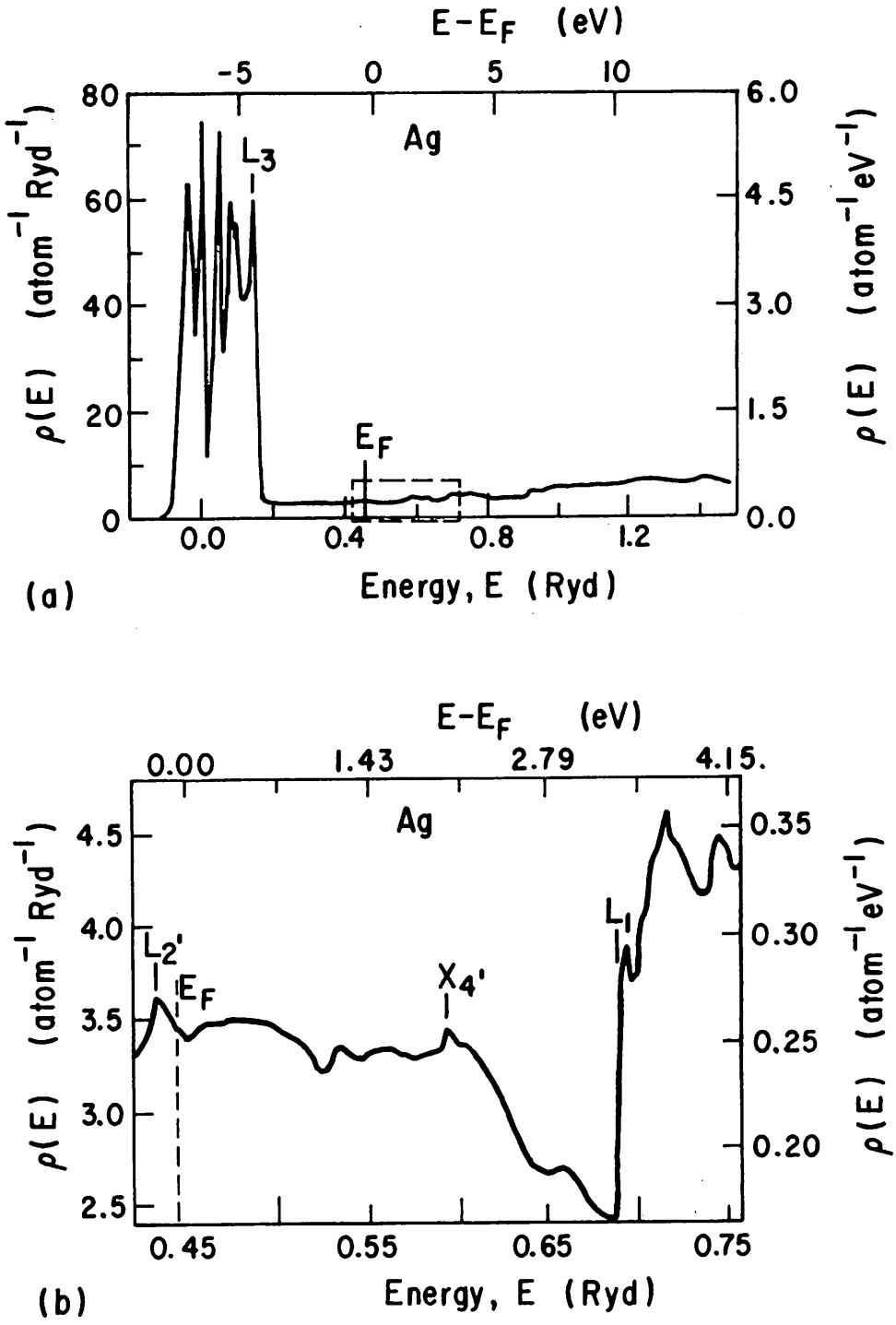

Fig. III-5: (a) Density of states $\rho(E)$ versus energy for silver as calculated numerically from the theoretical band structure by Christensen (Ref. 30). (b) Same for $E \gtrsim E_F$ (the region inside the broken rectangle of Fig. 5(a)) on an expanded scale, showing the correspondence of structural detail with critical points in the bands.

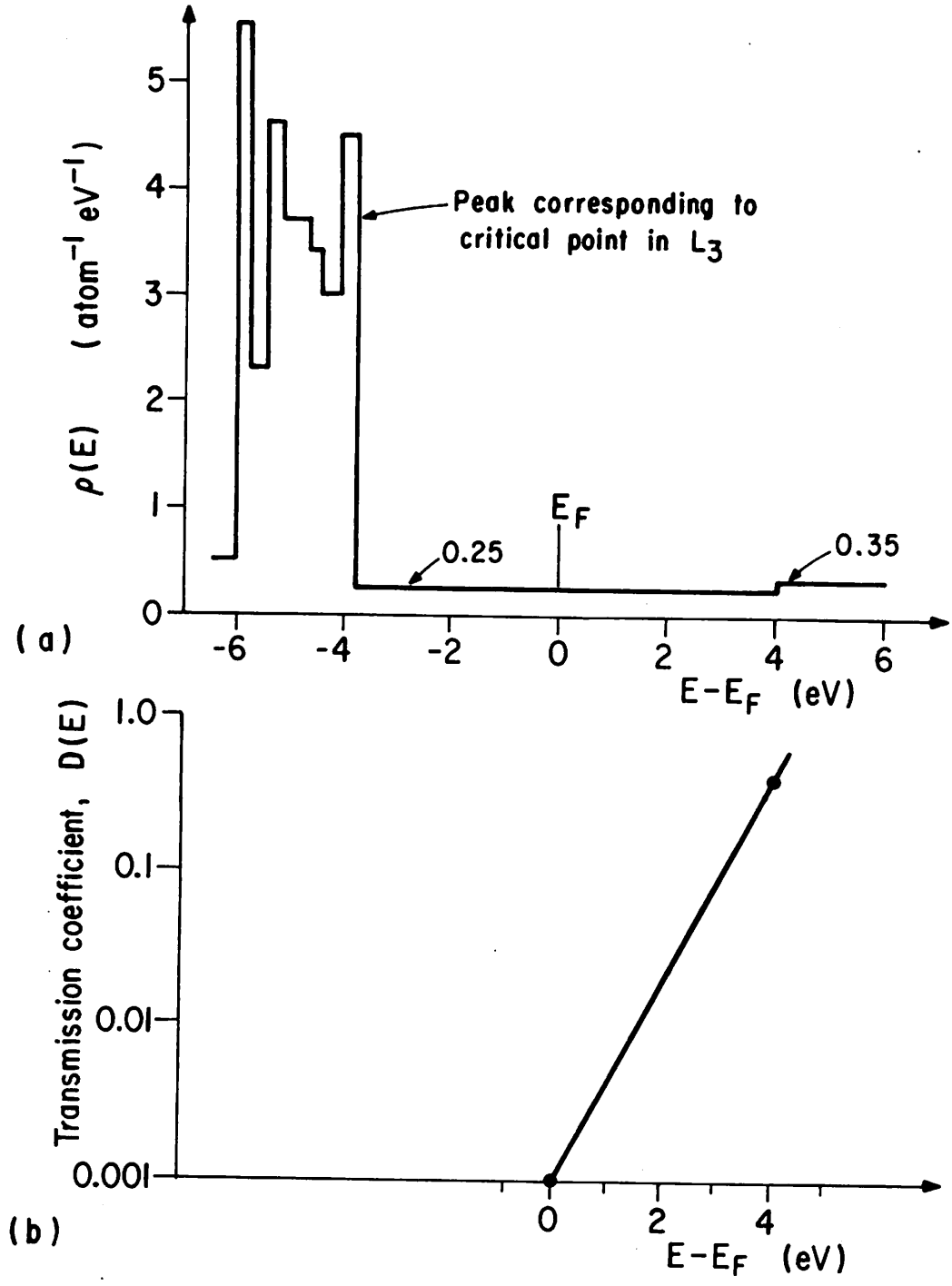

Fig. III-6: (a) Step-approximation for the density of states $\rho(E)$ data (for Ag) given in Fig. III-5.

(b) Transmission coefficient D(E) in the exponential approximation (See text).

Although at higher energies the density of states is low with a diffuse character corresponding to several weak interband transitions (including the $X_5 \rightarrow X_4$, and $L_{2'} \rightarrow L_1$ transitions), their net contribution is by no means significant. As a matter of fact, these relatively weak and diffuse interband transitions provide the dominant contribution for the integral in the numerator, since the transmission coefficient itself is a very rapidly increasing function of electron energy.

Several points may be noted before determining an approximate dependence of the transmission coefficient on energy. A rough calculation[31] for D(E) using Eqs. (11) and (13) with $\phi_1 = 4.2$ eV and $\phi_2 = 4.75$ eV in the presence of an infinitesimal forward bias[32] yields $D(0) \simeq 10^{-3}$ and $D(4\text{eV}) \simeq 0.4$. Also, D(E) rises rapidly with increasing energy and can be shown to have a near-exponential dependence near E = 0. Although this energy dependence is no longer exponential at energies as high as 4eV, a good order-of-magnitude estimate for the "average" transmission coefficient $\overline{D(\omega)}$ can be obtained by approximating D(E) by an exponential fit to the above two points. This yields $D(E) = 10^{-3}\, e^{\beta E}$, where $\beta = 1.5\text{eV}^{-1}$.

With the above approximations, for $\hbar\omega \simeq 4$eV we have

$$\overline{D(\omega)} = \frac{10^{-3}\int_0^4 e^{\beta E}\,\rho_2(E)\,\rho_2(E-4)\,dE}{\int_0^4 \rho_2(E)\,\rho_2(E-4)\,dE} = \frac{10^{-3}\cdot\left\{\int_0^{0.2}\ldots + \int_{0.2}^{4}\ldots\right\}}{\left\{\int_0^{0.2}\ldots + \int_{0.2}^{4}\ldots\right\}}$$

$$= \frac{10^{-3} \left\{ 0.262 + 16.6 \right\} \text{ atoms}^{-2}\text{eV}^{-1}}{\left\{ 0.225 + 0.237 \right\} \text{ atoms}^{-2}\text{eV}^{-1}} \approx 3.7 \times 10^{-2} \quad .$$

Finally assuming that the excitation factor $f_2(\alpha_2, L_2, t)$ is approximately 0.5, we have from Eq. (32):

$$J_{2F}(4\text{eV}) \approx (1.6 \times 10^{-19} \text{ Coul})(1.6 \times 10^{16}/\text{sec-cm}^2)(0.5)(4 \times 10^{-2})$$

$$\approx 50 \ \mu \text{ Amp/cm}^2$$

Since the zero-bias resistance of a 20 Å - thick oxide junction of area 10^{-2} cm^2 is typically[33] between 100 Ω and 1K Ω (i.e. Areal resistance ~ 1 Ω - cm^2 to 10 Ω - cm^2), the expected photo-induced voltage (neglecting the smaller contribution from the opposing J_{1F} term) will be of the order of $J_{2F} \cdot A \cdot R$ $\approx (5 \times 10^{-5}$ Amps/cm$^2)(10^{-2}$ cm$^2)$(200 Ω) i.e., approximately 100 μ-volts. Also since the tunneling current is relatively insensitive (decreases slowly) to the barrier thickness, whereas the resistance increases by a sharp exponential[34] with increasing barrier thickness, a much higher value of the photo-induced voltage is expected for thicker barriers. Finally, since $D_{2F}(E, V_b)$ increases rapidly with the bias voltage V_b (this fact was deliberately ignored above for simplicity), the "detected" or photo-induced voltage should increase further by an application of a bias voltage.

D.2 Collective electron excitations, oblique incidence:

As stated in Sect. II.C at frequencies close to the plasma frequency of metal 2, p-polarized radiation at oblique incidence (at angle θ) may be absorbed efficiently due to plasma excitations in the thin metallic film. Following the assumptions stated in Sec. III.C.1.b., the absorption due to excitation of antisymmetric coupled surface plasmons is[35]

$$A_p = 2\gamma_r\gamma_d \Big/ \left\{ \gamma_t^2 + 4(\omega-\omega_p)^2 \right\} \tag{33}$$

where $\gamma_d = 2\varepsilon_2/\varepsilon_1'(\omega_p)$, $\gamma_r = (\omega_p t/\varepsilon_1'(\omega_p)\, c)\, \sin\theta \tan\theta$

and $\gamma_t = \gamma_d + \gamma_r$. Note that $\gamma_r/\gamma_d = (\omega_p t/2\, \varepsilon_2 c)\, \sin\theta \tan\theta$, i.e. γ_r generally increases* with θ and so does the net plasma absorption $A_p(\omega)$; however this resonance gets broader and the peak value decreases for the larger angles as can be seen by the increase in the γ_t^2 term in the denominator. It is also easily seen that γ_r decreases with decreasing t, and so the peak value of A_p increases with decreasing t. (These results can also be seen by setting the partial derivations of A_p with respect to θ and t to zero).

---

* The expression given here for γ_r is more general than the one for the ideal free-electron gas case of Sec. II.6; for that particular case, $\varepsilon_1'(\omega_p) = 2/\omega_p$.

In order to get a well-defined plasma-resonance absorption with high peak absorptivity, while keeping in mind experimental limitations (and convenience), we will select $\theta = 60^{o}$ and a silver film of 200 $\mathring{A}$ thickness (t) for the following order-of-magnitude estimate of the peak current density and detected voltage. It can be easily seen (See Fig. 19(c) of Sec. II) that the peak absorptance in the present case is approximately $A_p\big|_{max} \sim 0.2$. Note that this value of absorptance is the net absorptance and the reflectance has already been accounted for.[45]

Because of the nature of the absorption of the optical radiation by resonant plasma excitations and its subsequent decay into single electron excitations, the following model conveniently describes the photon-assisted tunneling current for $\omega \simeq \omega_p$:

(a) absorption of the incident photon energy directly by the plasmons, with the net photon → plasmon conversion being given by A_p ;

(b) subsequent decay of these plasmons into single electron excitations uniformly throughout the thickness of the film; and

(c) the eventual tunneling of these excited electrons which have an energy distribution that is assumed to be similar to the one obtained in Sec. III.D.1 for direct photon → single electron excitations. Note that the transport of the electron to the tunneling barrier has been neglected merely for simplicity; it can be trivially shown that this transport factor is irrelevant for this order-of-magnitude estimate, especially if the plasmon → single electron decay is assumed to occur uniformly over the film thickness.

In support of the above model, it may be noted that evidence of plasmon → single electron decay[36] has been plentifully supplied in the past decade by photo-emission experiments,[37-40] done specifically to test this hypothesis. A peak in the photo-electric yield of Aℓ was observed and interpreted by Steinmann and coworkers[37,41] as due to plasmon → single electron decay via macroscopic Coulombic fields associated with the optically excited volume plasmons. Subsequently, Feuerbacher and Fitton[38] made careful measurements on the plasmon-enhanced photoemission yield for Cd,Zn and Mg; by taking accurate spectra of the enhanced photoemission for several different angles of incidence, they were able to calculate ω_p, γ_r and γ_d and thus use this technique to deduce accurately the volume plasmon energies and lifetimes in these metals. Subsequently, surface plasmon → single electron decay was observed and has been intensively studied in Aℓ, K and several other photoemissive materials.[39,40]

With the above photon → plasmon → single electron excitations model, we can easily calculate the expression for the tunneling current as follows. If n_{inc} is the incident photon flux the effective absorption of power/area is given by $\mathcal{E}_p(\omega) = (n_{inc} A_p(\omega))\hbar\omega$, and the total rate at which plasmons are created per unit area is given by $n_{p\ell}(\omega) = n_{inc} A_p(\omega)$. There are two predominant decay mechanisms for these plasmons: radiative (results in a peak in the reflectance spectrum) and non-radiative (the decay into single electron excitations), described by the rates γ_r and γ_d respectively. Thus, we would have to consider

a branching ratio for the channeling of the plasmon energy into single electron excitations. This is clearly given by $B = \gamma_d/(\gamma_d + \gamma_r) = \gamma_d/\gamma_t$. Clearly, as γ_r increases the branching ratio B decreases, and this effectively reduces the tunneling current. It is partly for this reason that one does not want to choose too large an angle for θ in the present calculations, and an 'optimum' value of 60^o was chosen. Thus the rate of single electron excitation per unit area is given by

$$n_s(\omega) = n_{p\ell}(\omega)B = n_{inc}\, A_p(\omega)(\gamma_d/\gamma_t).$$

If this excitation is assumed to have an energy distribution similar to the one involving direct interband transitions, the tunneling considerations will be identical to those of Sec. D.1 above. Thus, one can easily define an average transmission coefficient $\overline{D(\omega)}$ as described by Eq. (31), and the tunneling current density from metal 2 to metal 1 for $\omega \simeq \omega_p$ is given by:

$$J_{2p}(\omega) = e n_s(\omega)\, \overline{D(\omega)}$$

Thus,

$$J_{2p}(\omega) = e\, n_{inc}\, A_p(\omega)\, (\gamma_d/\gamma_t)\, \overline{D(\omega)} \qquad (34)$$

This gives the spectral dependence of $J_{2p}(\omega)$. Since in the above expression $A_p(\omega)$ is the quantity that varies most rapidly with frequency the spectral dependence of the tunneling current $J_{2p}(\omega)$ will essentially show the character of the plasma resonance $A_p(\omega)$.

The magnitude of the maximum value of the current density will occur at the peak of $A_p(\omega)$ and can be easily estimated. For the above conditions, $A_p\big|_{max} \simeq 0.20$, $\gamma_d \simeq 0.11$ eV, $\gamma_r \simeq 0.15$ eV (See Ref. 44 for γ_d, γ_r), and as before $\overline{D(\omega)} \simeq 3.7 \times 10^{-2}$, and the incident photon flux may be assumed to correspond to an optical power density of 1 Watt/cm^2 at 4eV yielding $n_{inc} = 1.6\text{x}10^{18}$/sec-cm^2. Then, from Eq. (34):

$$J_{2p}\Big|_{max} \simeq (1.6\text{x}10^{-19}\text{Coul})(1.6\text{x}10^{18}/\text{sec-cm}^2) \times (0.2)\left(\frac{0.11}{0.26}\right)(3.7\text{x}10^{-2})$$

$$\simeq 8\text{x}10^{-4} \text{ Amps/cm}^2.$$

This represents an enhancement of a factor of approximately 16 over the case when direct single electron excitation occur. Also, since the structure was assumed to be essentially the same as that used in D.1, the photo-induced voltage (assuming $R \simeq 200\ \Omega$) is approximately 1.6 mVolts compared to the 100 μVolts expected for the photo-induced voltage in the absence of plasmons. This enhancement is expected to be larger for smaller values of θ and t, although over a much narrower spectral range. Nevertheless, for a larger bandwidth of incident radiation centered around ω_p, a larger angle θ should generally result in a larger 'response'.

In Sec. III.C., it was noted that the collective electron oscillations will result in local electron density fluctuations at the barrier, thereby resulting in an effective Fermi-level modulation "voltage" at the barrier. The magnitude of such a

voltage v_o should be of the order of $v_o = \sqrt{\mathcal{E}_p}/R$, where $\mathcal{E}_p$ is the net energy/sec transferred to the plasma oscillations, described earlier as $\mathcal{E}_p(\omega) = n_{inc}\, A_p(\omega)\, \hbar\omega$. Here R is the effective junction impedance. Once such a Fermi-level modulation is assumed, the tunneling characteristics can be deduced in a manner similar to the work of Faris et. al.[3] Since this will contribute an additional current term the net photo-induced voltage will generally be larger than that deduced above. Interestingly, this increase can also be accounted for in the previous model by assuming a larger effective value of γ_d, attributed to the enhanced decay at the barrier due to tunneling. However, the finer details of the 'detection' characteristics vs. the bias and vs. the light intensity will still depend on the assumed form of this "photon → plasmon → tunneling electron" interaction.

III. E. EXPERIMENTAL DETAILS

The basic experimental set-up comprises an appropriate source of tunable ultra-violet radiation, and an appropriately fabricated metal-barrier-metal structure that will allow us to explore the different aspects of photon-assisted tunneling mentioned above. Specifically, it will be highly desirable to be able to observe the resonant enhancement of the optically-induced voltage, due to direct coupling of the radiation to collective electron modes. Since Ag is the only metal which has a conveniently accessible plasma frequency, it will be an essential metal in our M-B-M structure, and consequently the tunable ultra-violet source should cover the frequency spectrum around

3.85 eV or 3300 Å. Some of these factors have already been mentioned or implicitly stressed in the earlier sub-sections (Sec. III). However the principal considerations are repeated below in an organization consistent with the description of the experimental set-up.

1. The source of tunable ultra-violet radiation:

Because of its high spectral radiance, a doubled dye-laser covering the spectral range of approximately 3000 Å to 3500 Å is an ideal choice for a tunable ultra-violet source. Since the commercially available Chromatix 1050 dye laser can be made to cover the above spectral range by a proper choice of dyes and mirrors, it is a very useful source for attempting the present experiment. The nominal output of this laser includes a spectral range of 3000 Å to 3400 Å with the peak power per pulse being approximately 75 watts at 3000 Å (doubled Rhodamine B) and 20 watts at 3400 Å (doubled Kiton Red S), with pulse-widths of approximately 150 nsec at 75 pulses per second (the dye laser itself is pumped by a Q-switched 75 pps Chromatix model 1000 doubled Nd:YAG laser). Although this tuning range is sufficient to cover at least half the plasma resonance (including the peak), a full scan over the resonance should be obtainable by using Cresyl violet in the dye laser with appropriately modified optics.

2. The metal-barrier-metal structure:

The reasons for the choice of an Ag-$A\ell_2O_3$-$A\ell$ metal-barrier-metal structure, including the geometry and pertinent dimensions t,s have been adequately discussed in Sec. III.C. and III.D.

and will thus not be repeated here. However, a few additional points may be noted: (a) Aℓ is chosen primarily because of its near-ideal metallic behavior and the lack of any structure whatsoever in the spectral region around the Ag plasma resonance.

(b) The area of the junction should be kept small enough so that the RC time constant of the structure is of the order of 10^{-8} sec or less, because of the relatively short pulse-width of the excitation (~ 150 nsec). This implies that[24] (s) should be kept of the order of 20Å or less.* Since the inevitable non-uniformity of such a thin oxide barrier can easily result in conducting 'pin-holes' and ruin the tunneling characteristics of the junction, the area of the junction should be kept as small as reasonably possible to minimize the possibility of pinholes.

(c) Also because of the above reason, the oxide should be grown very slowly in a low-pressure oxygen plasma discharge, as adequately described in the literature;[46,47] this technique of slow plasma oxidation is well known to minimize 'pinhole' problems.

3. The experimental set-up:

The proposed experimental set-up is shown in Fig. 7. The doubled Nd-YAG pumped dye laser is intracavity doubled in the Chromatix 1050 resulting in a polarized ultra-violet output. This output passes through a polarization rotator and polarizer, so that both s- and p- polarizations can be irradiated at oblique incidence on the top Ag film. The s- polarized radiation should result in a response essentially due to direct single electron excitations, whereas the p- polarized radiation should result in a reasonably enhanced signal due to the plasma excitations in Ag.

*Note that the RC time constant is relatively independent of the junction area.

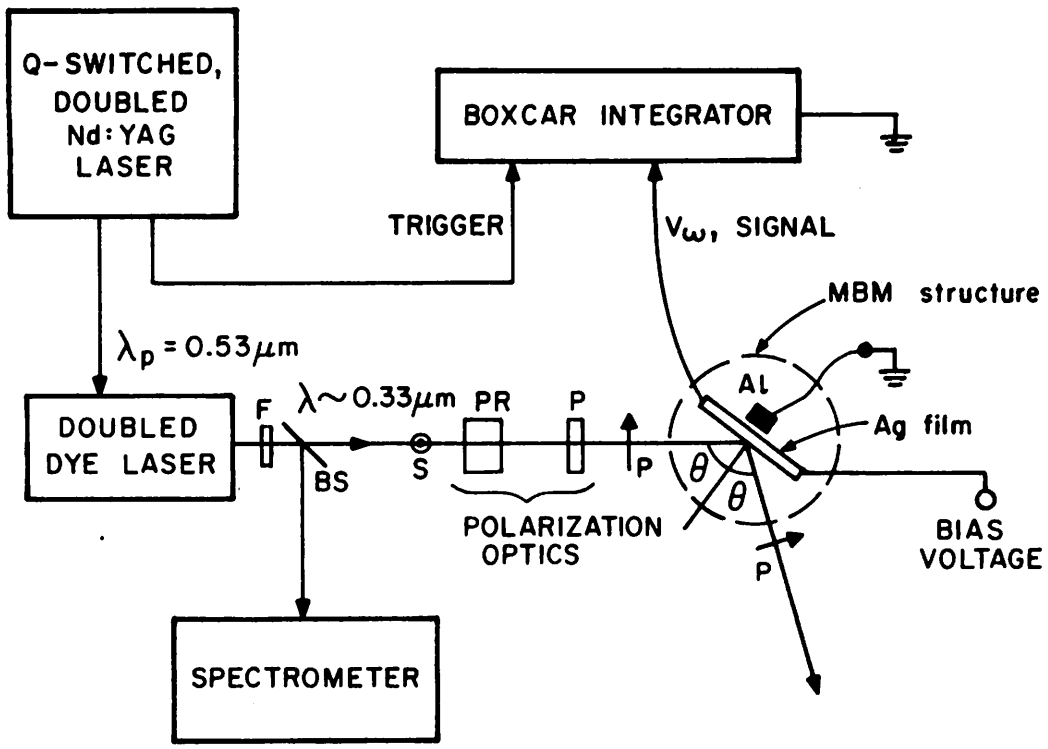

Fig. III-7 : Simplified schematic of experimental set-up. The optical elements F, BS, PR and P are a filter, beamsplitter, polarization rotator and polarizer respectively. The schematic is highly abbreviated. For instance, the spectrometer consists of a monochromator, photo-diode and scope assembly.

The detected signal is averaged in a PAR Model 162 box-car integrator to facilitate amplification of weak signals while eliminating signal/noise problems. The output of the box-car is connected to a strip-chart recorder to get a display of the spectral response, essentially described by $J_{2p}(\omega)$ or $A_p(\omega)$. The reasons for the use of the beam-splitters, filter, monochromator / spectrometer, photo-diodes and scope are obvious.

III.F. CONCLUSIONS

It is probably best to discuss here some of the potential applications of the resonantly enhanced tunneling. The most obvious applications stem from the similarity between the above phenomenon and photo-emission. Resonantly enhanced photoemission has been used for the study of plasma-resonances and also has been proposed as an efficient frequency-selective photodetector,[38,40] and it is precisely these two applications for which resonantly enhanced tunneling seems most suited for. However one essential difference exists between these two processes (or in the present context, techniques). Whereas photoemission will occur only if the plasmon energy (and consequently the excited single electron energy) $\hbar\omega_p$ is larger than the work function χ of the metal, this condition is not at all necessary for photo-assisted tunneling, since there is a significant 'escape' probability in the latter case, even for an excited electron whose final energy may be a few eV below the vacuum level. This is precisely the reason why the photoemission method cannot be used[38,46] to study one of the most interesting plasma resonances, that of pure Ag.[43]

The above-mentioned difference is <u>also</u> the basis of several advantages* of the present method over photo-emission. In particular, for a metal like Ag with $\hbar\omega < \chi$, this method seems ideal for the study of the plasma resonance. One of the main advantages is the proximity of the counter-electrode in the tunneling case, whereby the "photo-emission problems" of the spatial dispersion and of the solid angle collection of the emitted electrons no longer exist. As a matter of fact, once single electron excitations have occurred via the plasmon → single electron decay route, these excitations are virtually trapped in the thin film and can most easily escape into the other metal (which thus behaves as a counter-electrode or anode, especially if it is positively biased. Because of this very reason, this method is amenable to some sort of quantitative discussion, in sharp contrast with photo-emission, where factors like anode-cathode geometry and collection angle characteristics often make the quantitative discussion virtually hopeless. Finally, the proximity of the tunneling barrier to the actual excitation makes larger quantum yields (electrons/photon) possible than in photo-emission, thereby making the present method of particular interest in detection, and in light → electrical energy conversion of monochromatic light at the plasma frequency.

---

* Also, as in the photo-emission method, beam uniformity and absolute intensities of the light are not important, which are needed for the reflectance or transmittance methods of studying an 'optical plasma resonance.'

Also for the particular case of the study of the plasma resonance of Ag, the use of the narrow spectral bandwidth tunable laser should reveal the structure of the Tonks-Dattner resonances in the spectral detection characteristics, and thereby accurately provide the dispersion relation for Ag (See Sec. II.C for details).

Finally, the tunneling technique should be very useful in the study of the coupling of molecular fluorescence to surface plasmons.[48,49] In particular one may be able to use a structure with an RC time of the order of 10^{-10} sec or less, and make lifetime measurements on the fluorescence spectrum of the dye molecules, by looking at the tunneling response to short pulse excitation (say ~ 10^{-10} sec) as the frequency of the excitation is varied. Strong shortening of this detected response, indicative of a sharp reduction in the fluorescence lifetime would indicate both the inhomogeneous nature of the molecular transition,[49] and its strong coupling to the surface plasmons. Besides, an automatic consequence of the strong coupling of the molecular fluorescence to surface plasmons in itself would provide a technique for the efficient detection of shorter wavelengths of radiation (depending on the absorption spectrum of the dye) than λ_p.

In conclusion, we have proposed a model of photon-assisted tunneling to explain the detection properties of a particular metal-barrier-metal structure. A simple geometry was assumed, but the basic ideas can be extended to more complex geometries. In addition, we have predicted a resonant enhancement of the

detected signal near the plasma frequency of one of the metals. Finally, we have envisaged several applications of both the general technique of photon-assisted tunneling and of the resonant enhancement due to collective electron oscillations.

III. References

1. Exceptions might occur under special conditions. For instance, even at these low frequencies Fuchs, Kliewer and Jones (Ref. 75, Sec. II) have predicted an additional anomalous absorption due to single particle longitudinal excitations as seen by the wave-vector-dependent structure in the nonlocal longitudinal dielectric function.
2. It is assumed that the mean free path of the electrons is much shorter than the wavelength of the excitation.
3. Reference 6 of Section I (Faris et. al.)
4. References 7 and 8 of Section I.
5. (a) W.E. Spicer, in Optical Properties of Solids, ed. by F. Abelès (North-Holland Publ., Amsterdam, 1972), Chap. 10;
   (b) G. F. Derbenwick, D. T. Pierce and W. E. Spicer, in Methods of Experimental Physics (Vol. 11 - Solid State Physics, ed. by R. V. Coleman (Academic Press, New York, 1974), Chap. 3.
6. F. Wooten, Optical Properties of Solids (Academic Press, New York, 1972), p. 82.
7. (a) J. G. Simmons, in Tunneling Phenomena in Solids, ed. by E. Burstein and S. Lundquist (Plenum Press, New York, 1969), Chap. 10;
   (b) J. G. Simmons, J. Appl. Phys. 34, 1793 (1963);
   (c) J. G. Simmons, J. Appl. Phys. 35, 2472 (1964); as noted in this reference, a factor of 2 should be added to the terms involving effective dielectric constant K in Simmons' earlier work (including ref. 7(b) above).

III. References

(c) N. V. Smith, Phys. Rev. B3, 1862 (1971).

(d) N. E. Christensen, Phys. Stat. Sol. (b)54, 551 (1972);

(e) N. E. Christensen and B. Feuerbacher, Phys. Rev. B10, 2349 (1974).

8. W. E. Spicer, Phys. Rev. 112, 114 (1958).

9. (a) C. N. Berglund and W. E. Spicer, Phys. Rev. 136, A1030 (1964);

(b) W. F. Krolikowski and W. E. Spicer, Phys. Rev. B1, 478, (1970).

10. See Ref. 6, p. 110

11. For instance, see L. I. Schiff, Quantum Mechanics (McGraw-Hill, New York, 34d ed, 1968), p. 285.

12. W. E. Spicer and others have suggested that in cases where the non-direct model applies to crystalline solids, $\overline{k}$ might be conserved through many body effects. For instance, see: (a) W. E. Spicer, Phys. Rev. 154, 385 (1967); (b) W. E. Spicer and T. M. Donovan, J. Non-Crystalline Solids, 2, 66 (1970); (c) S. Doniach, Phys. Rev. 2, 3898 (1970).

13. See Refs. 61 and 62 of Sec. II. Also see: P. O. Nilsson, Appl. Opt. 7, 435 (1968).

14. (a) C. R. Crowell, W. G. Spitzer, L. E. Howarth and E. E. Lebate, Phys. Rev. 137, 2006 (1962). (b) C. R. Crowell, W. G. Spitzer, L. E. Howarth and E. E. Labate, Phys. Rev. Lett. 8, 57 (1962).

15. R. Stuart, F. Wooten and W. E. Spicer, Phys. Rev. 135, A495 (1964).

16. J. J. Quinn, Phys. Rev. 126, 1453 (1962).

III. References

17. B. R. Cooper, H. Ehrenreich and H. R. Philipp, Phys. Rev. 138 A494 (1965).

18. R. Rosei, C. H. Culp and J. H. Weaver, Phys. Rev. B10, 484 (1974).

19. The recent work of Rosei et. al., (Ref. 18 above) also conclusively establishes that the onset of the L_2, $\rightarrow L_1$ transition (~ 3.87eV) occurs before the onset of the $L_3 \rightarrow L_2$, transition (~ 4.03eV).

20. (a) H. Kanter, J. Appl. Phys. 34, 3629 (1963);
(b) H. Kanter, Phys. Rev. B1, 522 (1920).

21. R. N. Stuart and F. Wooten, Phys. Rev. 156, 364 (1967).

22. See Ref. 34 of Section II.

23. C. B. Duke, Tunneling in Solids, (Academic Press, New York, 1969).

24. C. A. Mead, in Tunneling Phenomena in Solids, Ed. by E. Burstein and S. Lundquist (Plenum Press, New York, 1969), Chapter 9.

25. Thus, insulators like KCℓ ($E_g \simeq 7.5$eV) and SiO_2 ($E_g \simeq 8.0$eV) would be ideal because of their large band gaps. However $A\ell_2 O_3$ will be used although it has a band gap of only ~ 4.5eV, because of the relative ease with which it can be grown in the present application.

26. See ref. 7(a) and 7(c). Due to the fact that metal 1 is on the left in these references, their barrier coordinate x corresponds to $(s-\xi)$ in this work. This explains the slight difference between the above and the present expression for ϕ_F and ϕ_R .

III. References

27. W. Franz, in Tunneling Phenomena in Solids, Ed. by E. Burstein and S. Lundquist (Plenum, New York, 1969), Chapter 2.

28. S. C. Miller, Jr., and R. M. Good, Jr., Phys. Rev. 91, 174 (1953).

29. A lot of the recent work on the density of states has been inspired by and directed towards the correlation of the experimental electron distribution curves in photo-emission to those predicted from the theoretical band structure of these metals. For instance see Ref. 9(c) for Ag, Au, and Cu; Ref. 9(d) for Ag; and Ref. 9(e) for W.

30. N. E. Christensen, see Ref. 9(d).

31. The values ϕ_1 and ϕ_2 assumed for this rough calculation obviously correspond to the work functions χ_1 and χ_2 of these metals. In practice ϕ_1 and ϕ_2 may be only about half as large as χ_1, because of the conduction band of the insulator. Fortunately this does not effect the present order-of-magnitude estimate of $\overline{D(\omega)}$ significantly. (It increases by less than a factor of 2 and is thus ignored for simplicity).

32. This bias is 'applied' so that occupancy of the Fermi-level states of metal 1 do not impose a restriction on the probability of tunneling (i.e., on the transmission coefficient).

33. These are the typical values obtained in our measurements and they agree with values quoted by Fisher and Giaever. (a) J. C. Fisher and I. Giaever, J. Appl. Phys. 32, 172 (1961). Note that values differing by an order-of-magnitude or more

from the above have also been quoted by other workers:

(b) D. McBride, G. Rochlin and P. Hansma, J. Appl. Phys. 45, 2305 (1974). These differences are explained partly by the different methods of sample preparation and partly by the fact that widely differing values of resistance can be obtained if different bias points are used to determine the low-voltage resistance (See Ref. 33(a)).

34. An exponential dependence of the low-bias resistance on oxide thickness was also observed, as has been already reported by several workers. For instance, see:

(a) Ref. 33(a).

(b) G. Lewicki and C. A. Mead, Phys. Rev. Lett. 16, 939 (1966).

35. This derivation has been published relatively recently in P. O. Nilsson, I. Lindau and S.B.M. Hagström, Phys. Rev. B1, 498 (1970); however the result was stated by McAlister and Stern in 1963 (See Ref. 51 of Sec. II).

36. The subject of plasmons decaying into interband transitions was first discussed theoretically by Nozières and Pines. See: P. Nozières and D. Pines, Phys. Rev. 109, 741 (1958).

37. W. Steinmann and M. Skibowski, Phys. Rev. Lett. 16, 989 (1966).

38. B. Feuerbacher and B. Fitton, Phys. Rev. Lett. 24, 499 (1970).

39. (a) J. G. Endriz and W. E. Spicer, Phys. Rev. Lett. 24, 64 (1970);

(b) J. G. Endriz and W. E. Spicer, Phys. Rev. B4, 4159 (1971);

(c) J. G. Endriz, Phys. Rev. B7, 3464 (1973);

(d) S. A. Flodstrom and J. G. Endriz, Phys.Rev.Lett. 31,893(1973).

40. J. G. Endriz, Appl. Phys. Lett. 25, 261 (1974). In this reference grating-tuned photoemissive cathodes have been used for application of the surface plasmon route photoemission to pre-selected frequency detectors.

41. J. Hofmann and W. Steinmann, Phys. Stat. Sol. 30, K 53 (1968).

42. See Table 2 of Section II for pertinent data on the plasma frequencies and work functions of several metals.

43. Cesiation of Ag to lower its work-function has been proposed, but the monolayer of Cesium hinders the study of what is essentially a surface mode. Cesiation of Ag has been successfully used to lower the work-function for the study of bulk photo-emission due to direct interband excitations. See Ref. 9(a).

44. P. O. Nilsson, et. al.,Ref. 35.

45. N. Matsudaira, J. Phys. Soc. Japan 18, 380 (1963). In this reference, some plots of the dependence of A_p on the angle θ are also given.

46. (a) J. L. Miles and P. H. Smith, J. Electrochem. Soc. 110, 1240 (1963); (b) W. Schroen, J. Appl. Phys. 39, 2671 (1968).

47. J. H. Greiner, J. Appl. Phys. 42, 5151 (1971).

48. (a) R. Chance, A. Prock and R. Silbey have recently (1975) studied experimentally the effects of resonant coupling of molecular excitations to surface plasmons (to be published).

(b) R. Chance, A. Prock and R. Silbey, J. Chem. Phys. 60, 2184 (1974).

49. H. Morawitz and M. R. Philpott, Phys. Rev. B10, 4863 (1974).